Theory of helical supramolecular polymers

Please check the document version of this publication:

Theory of Helical Supramolecular Polymers

PROEFSCHRIFT

ter verkrijging van de graad van doctor aan de
Technische Universiteit Eindhoven, op gezag van de
Rector Magnificus, prof.dr. R.A. van Santen, voor een
commissie aangewezen door het College voor
Promoties in het openbaar te verdedigen
op dinsdag 30 september 2003 om 16.00 uur

door

Jeroen Antonius Martinus van Gestel

geboren te Tilburg

Dit proefschrift is goedgekeurd door de promotoren:

prof.dr. M.A.J. Michels
en
prof.dr. E.W. Meijer

Copromotor:
dr.ir. P. van der Schoot

Contents

Chapter 1

Helical Ordering in Supramolecular Polymers

ABSTRACT

In this Chapter we present the subject of helical supramolecular polymers, and discuss how we can adapt and expand existing theories to describe this phenomenon and phenomena related to it. For this, we first give a general introduction to the helix-coil transition, chirality amplification, linear self-assembly and helical self-assembly. This is followed by a more detailed and somewhat more technical look at the theory of the helix-coil transition and that of linear self-assembly. We close the Chapter by giving the aim and outline of the thesis.
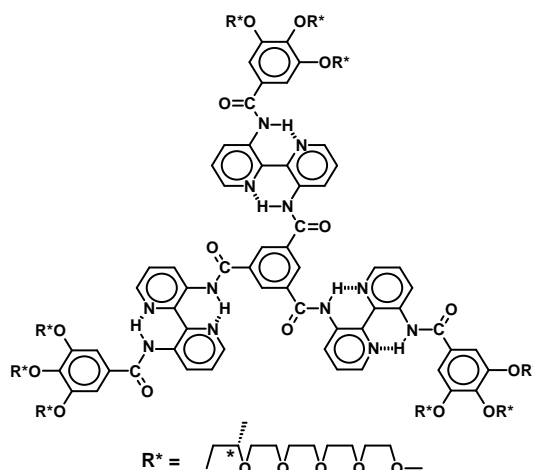
FIGURE 1.1:   Chemical formula of one of the chiral discotic molecules used by Brunsveld and co-workers.   The chemical name of the molecule is N,N',N"-tris{3[3'-(3,4,5-tris{(2S)−2-(2-{2-[2-(2-methoxyethoxy)-ethoxy]-ethoxy}-ethoxy)-propyloxy})-benzoylamino]-2,2'-bipyridyl}benzene-1,3,5-tricarboxamide. [9]

1.1   Helical Self-Assembly and Chirality Amplification

Depending upon their chemical architecture, biopolymers may undergo a transition between the entropically favorable random coil state and a more ordered helical state, under the influence of a change in, e.g., pH value or temperature. [1] That such a transition is not limited to conventional (covalently bound) biopolymers has been known for some time. Indeed, several supramolecular assemblies (being aggregates, the monomers of which are linked by reversible, physical bonds) that occur in biological systems, are believed to have a helical conformation under suitable external conditions. Examples include [2, 3] the protein actin [4, 5, 6] and tobacco mosaic virus (TMV). [7]

Recently, several types of synthetic molecule were shown to form helical supramolecular chains in solution. [8, 9, 10, 11, 12, 13, 14, 15, 16] In order to illustrate the richness of the behavior of these materials, we discuss one of these systems in some detail here, namely one of the discotics studied by Brunsveld et al. [9] (see Figure 1.1). These discotic, or disclike, molecules consist of a large aromatic core, surrounded by polar side chains. When they are dissolved in an apolar medium, such as chloroform, the molecules remain molecularly dissolved, and no evidence of aggregation is found. In a polar solvent (like water or n-butanol), however, the molecules self-assemble into disordered stacks at relatively high temperatures (around 310-330 K), dependent on the concentration. These stacks undergo a helical order-disorder transition as the temperature is lowered. [9]

Note that the monomers used in the experiments contain a stereocenter in each of the side chains. This causes the helix formation to be biased toward one of the screw senses, if all

(or at least most) of the side chains have the same enantiomeric form. The net fraction of helical bonds (the helicity) may be determined experimentally by, e.g., circular-dichroism spectroscopy. [9] If one were to use achiral monomers, one would not be able to measure any net helicity in this way, since an equal amount of right-handed and left-handed bonds would form. [17] Remarkably, when achiral and homochiral monomers are mixed and aggregates allowed to form, a disproportionately large optical effect is observed, [18, 19] a phenomenon which also occurs in conventional helical polymers, and which is known as *chirality amplification* (more specifically, chirality amplification of the sergeants-and-soldiers type). [17, 20]

Apart from being interesting due to their rich behavior and their link to biology, helical supramolecular polymers have several possible applications. They are potentially useful as novel gelators due to their strong growth (which we will discuss in detail in Chapters 3 and 7). [21] Furthermore, there is a possibility that disclike or ringlike monomers can aggregate to form molecular wires or channels. [22] The tunability of the properties of equilibrium polymers by external manipulation (e.g., a change in temperature) further makes them of interest from a material-technology point of view. Due to this, there now exists a need for a theory describing the coupling between the helical transition and self-assembly that goes beyond the simple all-or-nothing model of Oosawa and co-workers for the helical aggregation of actin [4, 23], and for a theory that describes the possibility of chirality-amplification effects in self-assembled systems. [18, 19] To these ends, we combine the theory of conformational transitions with a treatment of linear self-assembly. [24] This is the main focus of this thesis.

1.2   Model Description

1.2.1   The Helix-Coil Transition

To devise a theory for the helical transition in self-assembled aggregates, we first describe treatments of the helix-coil transition in (bio-)macromolecules and of the linear self-assembly, and then derive an expression for the free energy of a solution of self-assembled chains that display a helical transition (see Figure 1.2 and 1.3), which becomes the starting point of our description of helical self-assembly.

As already implied in section 1.1, the helix-coil transition came to prominence as a subject of study mainly due to its occurrence in such biologically important macromolecules as DNA and polypeptides (proteins). [1] The helical structures in these biopolymers are stabilized by physical bonds, e.g., ionic interactions, hydrogen bonds, or van der Waals interactions. [25, 26] The same types of interaction are used to create synthetic equivalents of helix-forming biologically important molecules. [27, 28] To synthesize a polymer that can indeed display a helical conformation, one must take into account the polymer architecture
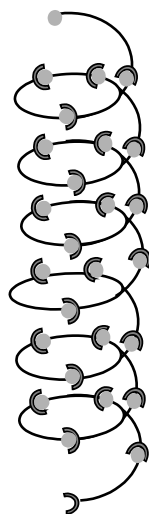
FIGURE 1.2:   Schematic depiction of a helical structure composed of bifunctional monomeric units.
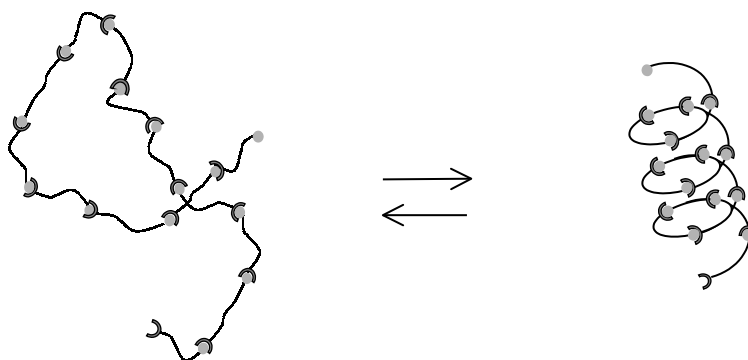
FIGURE 1.3:   Schematic depiction of the reversible coil-to-helix transition.

and the nature of the intramolecular (and sometimes also intermolecular) physical bonds which stabilize the helix, [25, 26] as well as the effect that the solvent composition can have on the polymer conformation. [29, 30]

Polymers that form a helix can do so under the influence of a change in, for instance, temperature. [1, 31] At high temperatures, they generally exist in the random-coil conformation, well-known as the most common conformational state of polymers. [32] Upon decreasing the temperature, they undergo a transition from this random structure to a helical one (see Figure 1.3). This process is reversible, and the reverse transition is often referred to in biology as denaturation. [33, 34] The helix-coil transition is generally believed not to be a phase transition in the true sense of the term, but rather a gradual order-disorder transition [1] (although Hansmann and co-workers claim to deduce from computer simulations on short polyalanine chains that it is a true phase transition, see

[35] and references cited therein). It turns out, however, that the helix formation is often remarkably sharp. As we shall see, this is due to the cooperativity of the process.

Despite the rather intricate picture of physical bonds linking groups and forming helical structures, it turns out that the conformation of helical polymers can be described with a remarkably simple model if we assume that these polymers can be treated as one-dimensional objects. [1, 36] Note that it is not a priori clear that this is allowed. Flexibility of the chain may, after all, cause the polymer to fold back onto itself and to interact with itself over large distances even when the direct interactions between monomers are short-ranged, something that is impossible in a strictly one-dimensional chain. These long-range intra-chain interactions can turn the (quasi) one-dimensional problem into a three-dimensional one, and in this case a true phase transition becomes a possibility. Intra-chain interactions can be ignored, however, when a sufficiently poor solvent is used, leading to so-called θ conditions, or when the polymer is sufficiently rigid. While the latter condition may not apply for all helical polymers, it is reasonable for the aggregates of discotic molecules described in section 1.1. For the same reason, we ignore in our work the formation of closed helical rings.

We define two types of bond along the one-dimensional chain, the helical type and the non-helical type. A polymer that contains N monomeric units (and therefore $N-1$ bonds) can then be in 2^{N-1} different states, since each bond can be either helical or non-helical. However, not all of these configurations are equally likely. The likelihood of each configuration depends on many factors, some of which are due to the properties of the monomers (such as the ease with which a helix is initiated and that with which it propagates), and some of which depend on the thermodynamic properties of the system (like the configurational entropy of the chain). The following model is an adaptation of the model of Zimm and Bragg for the helix-coil transition in polypeptides. [36] As we shall show in section 1.3, it can also be mapped onto the one-dimensional Ising model. [37]

We capture the properties which determine the state of the polymers in two free-energy parameters: that of the formation of a helical bond from a non-helical one, and that of the formation of an "interface" between a helical and a non-helical region along the chain. This description can be summarized in the following Hamiltonian, which, like all energies in this thesis, is given in units $k_B T$, with k_B Boltzmann's constant and T the absolute temperature. We have set the free energy for the formation of a non-helical bond equal to zero.

$$H = \frac{1}{2} R \sum_{j=1}^{N-2} \left(1 - s_j s_{j+1} \right) + \frac{1}{2} P \sum_{j=1}^{N-1} \left(1 + s_j \right) \tag{1.1}$$

Here, s_j gives the conformational state of the bond numbered j: non-helical ($s_j = -1$) or helical ($s_j = +1$). The quantities R and P represent the free energy of an interface between a non-helical and a helical region and the excess free energy of a helical bond over a non-helical one. The values of these parameters depend on the chemical architecture of the molecules, as well as on the solvent composition. As we shall see in section 1.3,
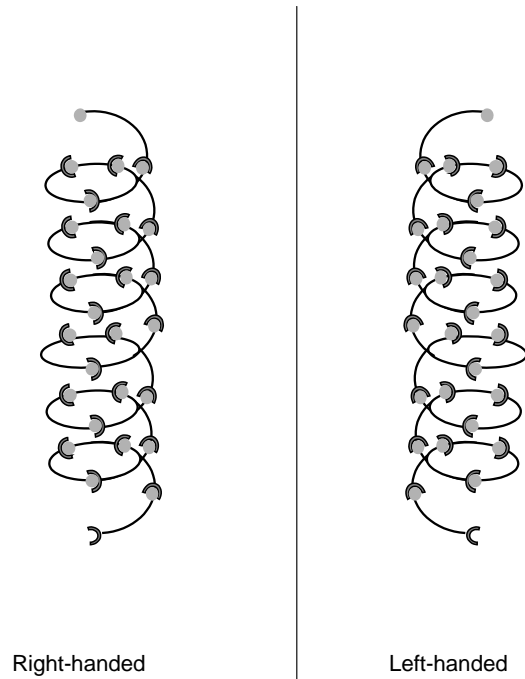
FIGURE 1.4: Schematic depiction of right-handed and left-handed helical polymeric structures.

the latter free-energy parameter functions as an external field that couples to the helical bonds, in that it attributes an additional free energy to the helical state, but not to the non-helical state. Note that, in eq (1.1), we have not specified the boundary conditions of the problems, i.e., the ends of the polymer. This we discuss in section 1.3.

The first term of the Hamiltonian eq (1.1) is only unequal to zero if a helical bond follows a non-helical one, or vice versa (i.e., when there is an interface between a helical and a non-helical region). The free-energy penalty on a helix-coil interface, R, can be seen as a cooperativity (or, as called in ref [36], nucleation) parameter. [36, 38] The larger it becomes, the less favorable the formation of helix-coil interfaces, and the larger the (mean) number of bonds that comprise a helical or non-helical region. An increase of this free-energy parameter causes the helix-coil transition to become sharper. An increase in the degree of polymerization of the chain can have the same effect. Note, however, that the helix-coil transition does not become infinitely sharp for an infinitely long polymer, and hence is not a phase transition for any finite R. The helix-coil transition can only become a true phase transition if both R and N go to infinity. [1]

1.2.2   Chirality Amplification

Helices can be constructed in two ways, with a right-handed or a left-handed screw sense. These two forms are mirror images of each other (see Figure 1.4), and one can therefore say that the formation of a single helix introduces a macromolecular chirality into a system, due to the fixed screw sense of the helix. [39] This chirality cannot usually be detected, since in a solution of polymers consisting of achiral monomers, equal amounts of right- and left-handed helical bonds are formed. As such, a solution of these polymers displays no net optical effect. [17] However, as already mentioned in the first part of this Chapter, the chiral nature of the helix can be demonstrated if one uses homochiral monomers as the building blocks of the polymer. In that case, symmetry is broken, one helical screw sense is preferentially formed, and an optical (Cotton) effect can be measured.[1] [9] It is well known that, even by mixing chiral and achiral monomers, or by using a non-racemic mixture of right-handed and left-handed chiral monomers, one can attain an optical effect. It turns out that the addition of a relatively small amount of chiral material or a relatively small enantiomeric excess may induce a disproportionately large optical effect. This phenomenon is known as chirality amplification, [17, 20] and its two forms are the *sergeants-and-soldiers principle* [40, 41, 42] (for mixtures of homochiral and achiral monomers) and the *majority-rules principle* [43, 44] (for non-racemic mixtures of left- and right-handed chiral monomers).

Chirality amplification in fully helical chains can (in principle) be described with a model in the same class as that of the helix-coil transition. After all, we still consider a system in which two types of bond are present (albeit left-handed helical and right-handed helical, rather than helical and non-helical) on a one-dimensional "lattice", and where a free-energy penalty on an interface between the two types of bond is imposed. However, the description of the chirality amplification is more complex due to the presence of two types of monomer, and the circumstance that the type of monomer under consideration influences which type of bond preferentially forms near it. A sensible model therefore makes use of a combination of two interwoven and interacting one-dimensional sublattices, one that describes the conformation of the bonds, and one that describes the composition of the chain. A detailed description is beyond the scope of this introduction and is given in the relevant Chapters (4-6).

In the context of polymers consisting of more than one type of monomeric unit (copolymers), a key difference between conventional polymers and equilibrium polymers manifests itself. In multi-component aggregates, [45, 46, 47] the composition of the aggregates and the order of the two types of monomer in a chain are equilibrium properties, whereas in conventional polymers these are fixed. These are examples of so-called annealed (equi-

---

[1]The conformational state of the polymers can be discerned most easily if an isolated monomer does not induce an optical effect, since in this case a measurement of the optical effect gives direct information about the net fraction of helical bonds of one screw sense. This is the case for the discotic molecules discussed in section 1.1.

librium) and quenched (fixed) disorder respectively, and the statistics describing the two are significantly different. [48, 49, 50] This means that treatments meant to describe multi-component aggregates are (at least, in principle) inaccurate for the description of copolymers, and vice versa (see also Chapters 4 and 5).

1.2.3   Linear Self-Assembly

As mentioned in Section 1.2.1, in the context of the helix-coil transition, intramolecular physical bonds are important in stabilizing a molecular conformation in (bio)polymers. However, as also already indicated, *inter*molecular physical bonds between monomeric units can play a vital role in nature as well. Through this type of bond, of which a large variety exists, [51] molecules can be linked without the use of covalent (chemical) bonds. Molecules that bind in this way are said to self-assemble into supramolecular structures. [8, 51, 52, 53, 54, 55, 56, 57, 58, 59] Examples of molecules that self-assemble are numerous, ranging from proteins [4] to asphaltenes [60] to dipolar fluid particles[61] to sulfur [57, 62, 63] to amphiphiles. [64] The variety of shapes of the aggregates is equally large, from spherical to cylindrical to bilayer-like structures. [58] Which shape is preferred depends strongly not only on the shape of the molecules, but also on external circumstances, such as the overall concentration of monomers. [58, 65]

In this thesis we focus on one particular class of aggregates, namely linear self-assembled aggregates. [57, 66, 67, 68] Linear self-assembly is the formation of quasi-one dimensional (chainlike) aggregates, also called equilibrium polymers or (in physics) living polymers (see Figure 1.5). In some ways, linear self-assembly resembles conventional polymerization, where monomeric building blocks are linked by covalent bonds. In both cases, chainlike compounds with a high degree of polymerization are formed in a propagation step, sometimes preceded by an initiation step. In regular polymerizations, there is often a termination step that fixes the length of the polymer. This step is absent in equilibrium polymerizations. [57] The reversibility of the propagation step, which characterizes equilibrium polymerization, causes the aggregates to constantly break up and recombine, shedding monomers and absorbing others, a process that makes the aggregates self-healing. [69] The reversibility, coupled to the fact that the physical bonds linking the monomers in these chains are generally weaker than covalent bonds, makes linear self-assembled polymers rather fragile objects. However, their equilibrium nature can also be considered one of their biggest advantages, as their properties (such as the mean aggregate size) can be controlled by changing the conditions of their surroundings, for instance the temperature or the monomer concentration.

The theoretical description of equilibrium polymers is far from trivial, as we shall discuss in section 1.4, and it proves necessary to invoke approximations. An often-used approximation, which we also use in this thesis, is the ideal-solution one, in which a dilute solution of polymers is described in terms of the chemical potential of the assembling monomers, a
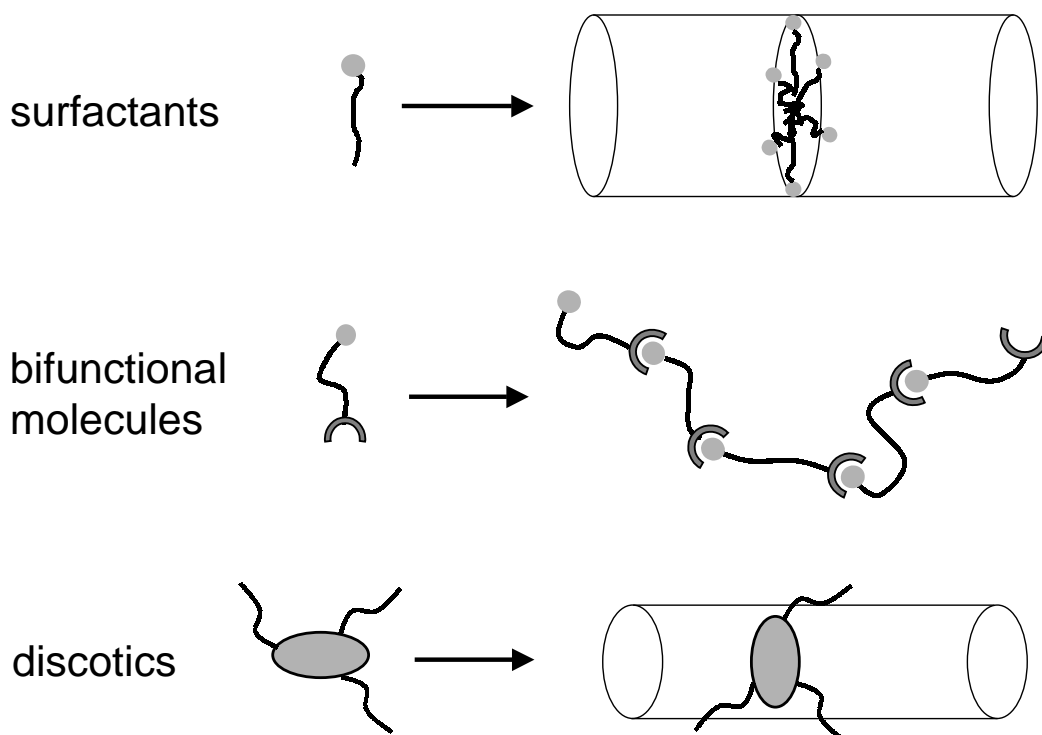
FIGURE 1.5:   Three examples of chainlike assemblies: a rod- or wormlike micelle, an aggregate formed from bifunctional monomeric units, and one formed from disc-shaped monomers with flexible side-chains.

free energy associated with breaking an aggregate in two (the so-called end-cap energy E), and a mixing entropy term. [24, 58, 66, 67] The free energy of a single aggregate is given by the free energy of a bond, $-E$, typically of the order of -10 to -20 k_BT or -20 to -50 kJ/mole, multiplied by the number of bonds, $N-1$. The free energy per unit volume F of a solution of self-assembled linear aggregates (made dimensionless with the volume of a monomer unit) can then be calculated by including a mixing-entropy term and performing the sum over all possible aggregate sizes. This gives

$$F = \sum_{N=1}^{\infty} \rho(N) \left[\ln \rho(N) - 1 - E(N-1) \right] \qquad (1.2)$$

with $\rho(N)$ the (as yet unknown) dimensionless number density of aggregates of degree of polymerization N. (Again, we give the free energies in units of the thermal free energy.) This rather simple equation is the end result of many approximations and simplifications, some of which are immediately apparent, such as the assumed independence of E on the size of the aggregate (which is reasonable if the aggregates are sufficiently long). Some others are briefly discussed in Section 1.4. Equation (1.2) is the starting point of a wide variety of studies, most notably in the field of so-called giant micelles. [66]

The size distribution of the self-assembled polymers can be determined from the free-energy density (eq (1.2)) by taking the functional derivative with regard to $\rho(N)$, while enforcing the law of conservation of mass

$$\phi \equiv \sum_{N=1}^{\infty} N\rho(N) \tag{1.3}$$

with ϕ the total volume fraction of aggregating material. This gives

$$\rho(N) = \exp\left[E(N-1) + \mu N\right] \tag{1.4}$$

Here, μ is a Lagrange parameter that takes the role of a chemical potential. The mean aggregate size $\langle N \rangle$ can be calculated from

$$\langle N \rangle \equiv \phi/\sum_{N=1}^{\infty} \rho(N) = \frac{1}{2} + \frac{1}{2}\sqrt{1 + 4\phi \exp E} \tag{1.5}$$

From eq (1.5) follow two different scaling laws. For $\phi \exp E \ll 1$, the mean size scales with $1 + \phi \exp E$, whereas for $\phi \exp E \gg 1$, it scales with $\sqrt{\phi \exp E}$.

It is immediately obvious from eq (1.4) that non-extensive contributions to the free energy play a major role in self-assembly, whereas extensive terms can simply be absorbed into the chemical potential. [66, 68] While, in polymer physics, non-extensive effects are often ignored altogether (see, e.g., the literature on the helix-coil transition), we cannot afford to neglect these effects here.

Another model, often used in chemistry to describe equilibrium polymerization, is the so-called ladder model. This model [64] is derived from reaction-kinetic theory, and assigns equilibrium constants analogous to the reaction constants of chemical-reaction theory to the propagation (and initiation) steps of the aggregation. [63] These equilibrium constants are related to the end-cap energy used in our model by $E = \ln K$ with K the equilibrium constant. Due to its mean-field nature, this model experiences difficulties when fluctuations become large. [57, 70]

1.2.4   Helical Self-Assembly

To combine the treatments of equilibrium polymerization and the helix-coil transition, we must include a free-energy term associated with the helical transition into eq (1.2) prior to minimization. This can be done by determining the canonical partition function $Q(N)$ of a single aggregate that can undergo a helical transition, since its free energy is given by $f = -\ln Q(N)$ in the canonical ensemble. This partition function contains, besides the end-cap energy, information about the conformational state of the bonds. The total dimensionless free energy density is now given by

$$F = \sum_{N=1}^{\infty} \rho(N)\left[\ln \rho(N) - 1 - \ln Q(N)\right] \tag{1.6}$$

In this equation, we sum again over all aggregate sizes, now taking into account the configurational state of each aggregate. Equation (1.6) is the starting point of our treatment of helical self-assembly, and will be expanded upon in Chapters 2 and 3. As we shall see, in our case, the free energy does not necessarily reduce to the general form of eq (1.2), not even in the limit $\langle N \rangle \gg 1$, as is often thought.

1.3 The Ising Model Applied to the Helix-Coil Transition

The basis of the model which we use to describe the helical transition (eq (1.1)) is the one-dimensional Ising model. [1, 36, 71, 72] This model is one from the class of magnetic n-component models, with $n = 1$. As we shall mention later, another model from this class, with $n \rightarrow 0$, can be used to describe (self-assembled) polymers. Although more elaborate models, as well as computer simulations, have been used in the past to describe the helix-coil transition, [73, 74, 75] the Ising model remains one of the more popular models to describe order-disorder transitions. The model is named after Ernst Ising, who solved it in one dimension in 1925 after Lenz suggested the model to him. [37, 76] Originally intended to describe phase transitions in ferromagnetic materials, [77] the Ising model has now become a prototype for many processes in diverse areas of science. Ising models have been used to describe, among others, gas-liquid condensation, [78, 79] adsorption on surfaces [80] and the helix-coil transition. [1]

The Ising model is a two-state lattice model, meaning that any lattice site has a property that can be in one of two states (e.g., "spin up" or "spin down"), and in its simplest form it presupposes a close-range, nearest-neighbor interaction between the spins that are present on the lattice sites. The Ising model in one dimension, which we use in this work, has the following dimensionless Hamiltonian (cf. eq (1.1)). [81]

$$H = -J \sum_{j=1}^{N-2} s_j s_{j+1} - h \sum_{j=1}^{N-1} s_j \tag{1.7}$$

where $N - 1$ is the number of lattice sites, and s_j corresponds to the spin at lattice site j. This spin variable can have a value of ± 1, where $+1$ indicates an "up spin", and -1 a "down spin". J is the dimensionless coupling constant between neighboring spins, and h the (dimensionless) strength of the external magnetic field. An informal mapping of the model for a helical polymer onto the Ising model is shown in Figure 1.6. The free-energy parameters translate as follows: J in the Ising model corresponds to $R/2$ in our model, whereas h corresponds to $-P/2$. Further, in our theory the reference free energy is shifted by an amount $(R + P)/2$. Note that in order to make this mapping we necessarily also assume that the interactions between monomers in the aggregate are short-ranged in
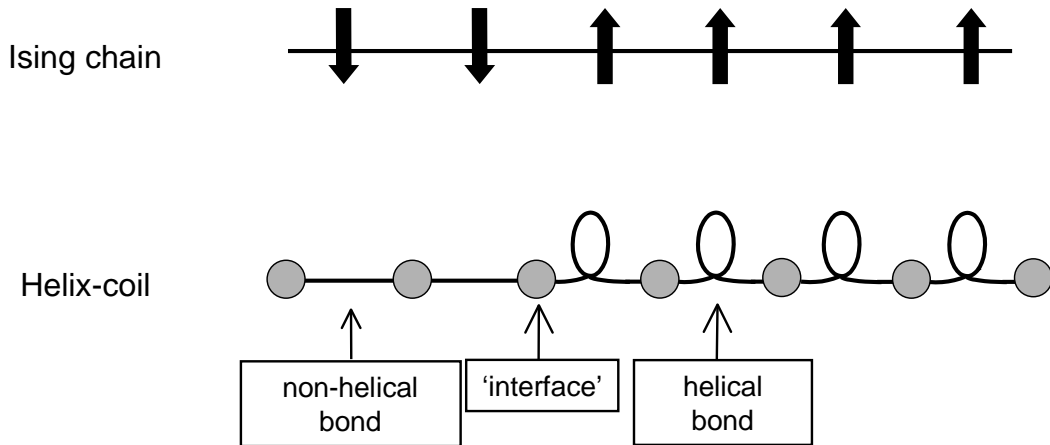
FIGURE 1.6: Comparison between a one-dimensional Ising chain and a partially helical polymer. The arrows in the top figure indicate the spins of the magnetic lattice, whereas the circles in the bottom figures represent the monomers, between which are the (helical and non-helical) bonds. Indicated are a helical bond, a non-helical one and an interface between a helical and a non-helical region.

nature. This is not always the case, as attractive forces of the van der Waals or ionic type generally extend beyond nearest neighbors. In the case of the discotic monomers, van der Waals interactions between the discs can be reasonably assumed to be largely responsible for the aggregate formation. However, it can be shown that the sum of the van der Waals interactions in a chain scales linearly with the size of the chain, and that as such, long-range interactions do not have a significant contribution.

In order to determine the thermodynamic properties of this system, the canonical partition function, defined as

$$Q(N-1) \equiv \sum_{s_1=\pm 1} \cdots \sum_{s_{N-1}=\pm 1} \exp(-H) \tag{1.8}$$

is calculated. In the absence of an external field ($h = 0$), the partition function is readily obtained and equals $Q(N-1) = 2^{N-1} \cosh^{N-1} J$ for the case where periodic boundary conditions apply, or, equivalently, for the case where an infinitely long chain is considered. [81, 82] Due to the difference between the Ising parameters and those in our model, this partition function has an added constant of proportionality in our model. If an external field is present, the partition function is usually obtained with the aid of the so-called transfer-matrix method pioneered by Kramers and Wannier, [83] which we also use throughout this thesis.

The transfer-matrix method is based on the statistical weights of the different types of spin following the preceding spin, e.g., the statistical weight of an "up" spin following an "up" spin or that of a "down" spin following an "up" spin. These statistical weights, which have the form of Boltzmann factors, are collected in a matrix, which provides a mathematically

simple way to calculate the partition function. In addition to the transfer matrix, the so-called end vectors are needed to complete the partition function. These vectors describe the state of the ends of the sequence of spins, and hence are only important for finite chains. By changing the end vectors, we can introduce different boundary conditions, which can correspond to different situations in biopolymers (see [84] for some examples). For a clear step-by-step description of the transfer-matrix method see [1], [85] or Chapter 2.

Besides the applications mentioned earlier, in polymer science a model that mathematically resembles the Ising chain is often used. This RIS (rotational isomeric state) model describes the conformational properties of ideal polymer chains. [86, 87, 88] In the RIS model, a polymer chain is represented by a collection of bonds of equal length, connected by junction points. At these junctions points, the angle between two bonds is approximated to take one of several discrete values. Usually three values for the angles are allowed (as in the case of the molecule n-butane), namely $0°$, in which the bond is a so-called trans bond, and approximately $\pm 120°$, known as the gauche$^+$ and gauche$^-$ bonds. [87] As such, the standard RIS model is a three-state model, and it formally corresponds to a three-state Potts model; [89] this is a model that resembles the Ising model but in which spins can be in any one of n states, with $n > 2$. However, for symmetrical polymers (e.g., polymers with identical side groups along the chain), the energies of the gauche$^+$ and gauche$^-$ states are equal, reducing the problem to one with only two possible energies for each bond. In this case, the theory becomes similar in form to that of the Ising chain, although because of its three-state character, the RIS model does describe more conformational states.

1.4   The Free Energy of a Linear Aggregate

When we attempt to write down an exact expression for the free energy of a self-assembling system, we soon encounter a problem: what exactly constitutes an aggregate? [90] In other words, when does a monomer belong to an aggregate, and when does it not? The theory of linear self-assembly requires a partition of the monomers into n_i aggregates of size $i = 1, ..., \infty$. This causes a paradox, since the monomers which were so far assumed indistinguishable, suddenly become distinguishable by their presence in an i-mer. This definition problem remains an unresolved complication in the field, and has been discussed in several contexts by many authors. [90, 91, 92] The root of the problem is that it is necessary to arbitrarily introduce a criterion to decide whether a monomer belongs to an aggregate, e.g., by defining that a monomer only belongs to an aggregate if it is less than a distance r away from the closest other monomer in that aggregate.

Even if we somehow manage to sidestep this conceptual problem, it is not a trivial matter to write down the exact partition function of a self-assembled aggregate. Strictly speaking, the partition function of an aggregate is given by the configurational integral over the

positions and momenta of all its constituent monomers. [58] To make a mapping from microscopic coordinates onto collective coordinates (this gives the $\rho \ln \rho$ term in eq (1.2)), the Jacobian must be known. This Jacobian is only known exactly in some highly idealized cases, namely in the dilute regime where fluctuations are Gaussian in nature.

It is not surprising, then, that a description of self-assembly necessarily hinges on many approximations. Many models have been put forward, at various levels of approximation. [58, 62, 63, 64, 70, 93, 94, 95, 96, 97, 98] Wheeler and co-workers, for instance, treat the aggregates in terms of a magnetic n-component model extrapolated to zero components, [57, 70] a view earlier proposed by de Gennes for conventional polymers, and later worked out by des Cloizeaux, and applied by Schäfer, in the context of equilibrium polymers. This $n \to 0$ model can include intra-aggregate interactions and accurately predicts the properties of self-assembled polymers. The mean-field version of this model corresponds mathematically to a model often used in chemistry, the so-called ladder model, which we described in section 1.2.3. [97]

In the model description we use (eq (1.6)), we approximate the total partition function of a collection of self-assembled chains by its maximum term for the size distribution. In other words, we only take into account the most likely size distribution and ignore the others. This is allowed when the size distribution is peaked around the mean aggregate size, which is the case when fluctuations (which become large for long aggregates) are small. Since the concentration of very long chains is small if the total amount of assembling material is constant, we expect that the maximum-term method is reasonable.

The maximum-term argument is not the only approximation inherent to the theory. We discuss four of the idealizations here: the neglect of the contribution of closed rings, the contribution of the molecular detail of the solvent, the role of the thermal wavelength, and the possibility of infinitely long chains in a finite system.

1) While, for sufficiently flexible chains, rings are always present, and in fact a ring-dominated regime has been theoretically predicted, [99, 100] they are believed to be unimportant for end-cap energies that are not exceedingly large, and for polymers with a large persistence length. [100] This is because for low end-cap energies, the closed rings will be unfavorable compared to open ones due to the entropy of the chains. Large persistence lengths render ring formation unimportant because the persistence length determines the optimal ring size. Wittmer et al. argue that rings shorter than approximately a persistence length are unfavorable, and ring formation is suppressed in favor of linear chain formation when the persistence length is large compared to a bond length. In any case, above the polymerization transition, rings merely deplete material from the system that would otherwise be available for linear chains. [100] If the end-cap energy goes to infinity, a phase transition between a state where the polymers are linear and one where they are ring-shaped can occur. However, an infinite end-cap energy implies that the aggregates become infinitely long, a point that is discussed later in this section. The role of rings is still hotly debated in the literature. [66, 100]

2) As usual in the field, we ignore the explicit contribution of the solvent molecules, since the discotics we shall mostly discuss are much larger than the solvent molecules. We treat the solvent as a structureless continuum that only changes the value of E (and R and P) in eq (1.1). However, see [94].

3) Equation (1.2) takes the entropy of a solution of aggregates into account by a mixing contribution, as well as through E. It has been argued that other degrees of freedom may have to be accounted for (see ref [68] and references cited therein). In many formal descriptions of equilibrium polymerization, quantum effects are included. [58, 67] Specifically, the thermal wavelengths of the vibrational and rotational degrees of freedom of the monomers (and solvent molecules) enter these descriptions. Since the thermal wavelength is much shorter than the smallest length scale we consider (the monomer size), we remove this wavelength from our description when we (implicity) coarse-grain out the solvent molecules. That this is justified follows from the circumstance that the theory without the quantum correction gives a scaling of the mean aggregate size with the square root of the overall concentration of monomers, [66, 67] a scaling that is also observed for dilute solutions in experiment. [66] Descriptions which retain the quantum-mechanical contributions give a different (much smaller) scaling exponent than produced by the classical theory. [101]

4) It may be seen in eq (1.2) that we sum over all aggregate sizes from unity to infinity. This, too, is an approximation, since in reality the size of the aggregates is limited by the container in which they are present, at least if the aggregates are rigid rods. If they are flexible, one has to include a free energy of chain compression in order to describe the state of the chains. Since the fraction of extremely large aggregates is small, our approximation is reasonable, unless the free energy needed to break an aggregate goes to infinity.

1.5   Aim and Outline of the Thesis

The aim of the thesis is to describe, using statistical-mechanical techniques, the coupling between self-assembly and the helical transition in linear supramolecular polymers, as well as the chirality amplification that may occur in mixed aggregates of this type, and to explore the effect of external fields and inter-aggregate interactions on the self-assembly and helical transition. In Chapter 2, we outline a treatment, expanding that of van der Schoot et al., [24] describing the helical transition in dilute solutions of supramolecular polymers, with special focus on the description of the aggregate ends. The results indicate that the helical transition and the growth are strongly coupled. In Chapter 3 we compare our theory with experiments, and find that only two of the sets of boundary conditions can quantitatively describe experiments on self-assembled disc-shaped molecules. In Chapters 4 and 5 we look at mixed aggregates of homochiral and achiral building blocks. As indicated earlier, such aggregates can display a form of chirality amplification known as the

sergeants-and-soldiers effect. In Chapter 4 we outline a theory for this phenomenon in the long-chain limit, which we expand in Chapter 5 to all chain lengths. In both Chapters, we provide a comparison with relevant experiments and find excellent agreement with measured values. In Chapter 6 we apply a similar theoretical treatment to the majority-rules type of chirality amplification, again valid in the long-chain limit, and provide a brief outlook on the modifications necessary to describe all chain lengths. Finally, in Chapter 7, we examine the effect of external fields and interaggregate interactions on the polymerization and helical transitions.

Chapter 2

Helical Aggregation: General Theory and the Role of End Effects

ABSTRACT

We outline a treatment for the helical-to-non-helical transition in self-assembled linear aggregates, emphasizing the role of end effects. In order to investigate this role in detail, we apply constraints to the first and last bonds of model linear aggregates that exhibit a helix-coil type configurational transition. Three different classes of behavior manifest themselves. These can be distinguished by the presence or absence of re-entrance of non-helical conformations with changing solute concentration, as well as by the dependence of the locations of the polymerization and helical transitions on the cooperativity of the helical transition. The helical transition and the polymerization are strongly coupled, as evidenced by a growth spurt of the aggregates below the helical-transition temperature.[1]

2.1   Introduction

The linear self-assembly of dissolved molecules into helical superstructures occurs not only in systems of biological interest, [2, 3, 4, 6, 7, 51] but has also been observed in solutions of synthetic molecules of quite diverse molecular weights. [9, 10, 11, 12, 13, 14, 15, 16, 102] Central to the current understanding of this helical self-assembly is the role played by cooperativity, in particular the strong coupling of the crossover between non-helical and helical aggregated states to the growth of the assemblies. [24]

As discussed in Chapter 1, many different theoretical treatments describing the equilibrium or 'living' polymerization have been presented. [58, 63, 64, 66, 70, 93, 95, 96, 103] From these works it becomes clear that linear self-assembly is strongly affected by non-extensive contributions to the free energy of an aggregate, since extensive contributions can simply be absorbed into the chemical potential. [66, 68] Non-extensive contributions derive from so-called end effects, i.e., from the differences between the local environment of a molecule at the end of an aggregate and that of one in the center. However, it is only in the case that the length of an aggregate greatly exceeds its intra-chain correlation length that such a separation in intensive and extensive contributions to the free energy can be formally made, and that one can truly speak of end effects instead of finite-size effects.

Much theoretical work has also been done on the helix-coil transition in conventional ('dead') polymers such as polypeptides and DNA. [1, 36, 73, 104] Finite-size effects are often ignored altogether as these theories usually consider the conformational properties in the long-chain limit. In this limit, the sharpness of the crossover from a fully non-helical to a fully helical polymer conformation is governed by the degree of cooperativity involved in the formation of the helical links, which are often stabilized by hydrogen bonds. In practice, the formation of these links can indeed be very cooperative, implying that the helical transition can be sharp and reminiscent of a phase transition.[2]

Van der Schoot et al. [24] devised an approximate theoretical model that was set up to describe helix-coil type transitions in solutions of self-assembled polymers, and concluded the transition to be remarkably cooperative. Here, we extend their theory to allow for a more accurate description of this transition, explicitly including deviations from the long-chain limit. As a result we are now able to present diagrams of states, indicating the existence of two ordering regimes: one where the polymerization transition and the helical transition coincide and one where they do not. In both cases there is a strong coupling between the growth of the aggregates and the helical transition. Our treatment implies that in the experiments of refs [9, 10] only a part of the possible aggregation behavior was explored and that by changing (for instance) the solvent conditions, a more complete picture of the physics of these systems may be obtained. Despite its apparent simplicity,

---

[2]The limit where the cooperativity becomes infinite formally corresponds to the limit of infinite coupling constant in an Ising chain. Hence, in this limit, and then only for infinitely long aggregates, does the helical transition become a true phase transition. [1]

the theory quantitatively accounts for experimental data obtained on solutions of certain chiral discotic molecules, [9] as we shall see in Chapter 3.

To investigate the influence of end effects, we vary the description of the aggregate ends. We can force either end to be helical, or non-helical, or choose not to constrain it, meaning there are nine possible pairs of boundary conditions. We find here that the theory is fairly sensitive to the boundary conditions set, and that varying the boundary conditions can lead to a radically altered behavior. This means that it is possible to determine from experiment the preferred state of the ends of the aggregates.[3]

The remainder of this Chapter is organized as follows. In section 2.2 we discuss the theory of linear self-assembly of unspecified molecular building blocks in solution. We focus on polymer-like aggregates that potentially exhibit a helical-type configurational transition, and specify the way the imposed boundary conditions are implemented. Next, in section 2.3, we discuss important quantities such as the mean helicity and the scission energy in the large-aggregate limit. Section 2.4 is devoted to a discussion of the impact of the boundary conditions on the various aggregation states. The Chapter concludes with a short discussion and conclusions in section 2.5, where we also make the connection with the well-known Oosawa-Kasai model for helical aggregation. [4, 23]

2.2   Formalism

We consider a dilute solution of molecules or particles that, under the appropriate conditions, form quasi one-dimensional, polymer-like aggregates. The driving force of the self-assembly need not be specified, but one may think of specific interactions, such as hydrogen bonding [105, 106] and ionic bonding, [55] or aspecific ones, such as those arising from the hydrophobic effect. [9, 56] Important is that the polymerization is reversible, so that the material in the monomeric and polymeric forms remains in thermodynamic equilibrium. The monomers are of an as yet undetermined shape and size (although large compared to the solvent molecules, allowing us to regard the solvent as a structureless continuum) but should display an order-disorder type transition in the aggregated state. Depending on whether the transition is enthalpy- or entropy-driven, the polymeric state appears either above or below a certain transition temperature which, due to the essentially one-dimensional nature of the aggregation, is not sharp. The same applies, at least in principle, to the appearance of the ordered state, or more specifically, the helical state. Without loss of generality and in keeping with the experimental findings, we assume the transitions

---

[3]Obviously, the energies of the first and last bonds of the aggregates can also be varied in a continuous way, rather than assigning discrete values to them. However, in order to avoid generating additional parameters in our model, we chose to fix the energies of the end bonds to either infinity or the appropriate energy of a helical or non-helical bond.

from monomers to aggregates and from disordered aggregates to helical aggregates to be enthalpy-driven, implying that these take place upon a lowering of the temperature.

The helical-aggregation theory [24] we use to study finite-size effects is a combination of the standard theory of linear self-assembly, and the Zimm-Bragg theory for the helix-coil transition. [36] The potential usefulness of the latter in equilibrium polymerization was first remarked upon by Oosawa and co-workers [23] in their description of the polymerization of actin. The Zimm-Bragg theory can be mapped onto an Ising chain with nearest-neighbor interactions between bonds. [1, 74, 84]

The free-energy density F of a dilute solution of self-assembled polymeric objects may, within a saddle-point approximation for the size distribution of the aggregates, be written as

$$F = \sum_{N=1}^{\infty} \rho(N)[\ln \rho(N) - 1 - \ln Q(N)] \tag{2.1}$$

with $\rho(N)$ an as yet unknown dimensionless number density of aggregates of size N, and $Q(N)$ the partition function of a single aggregate. F is given in units of the thermal energy $k_B T$, with k_B Boltzmann's constant and T the absolute temperature, as are all energies in this thesis (unless specifically indicated otherwise). In equilibrium $\rho(N)$ optimizes F, so we take the functional derivative of F with respect to $\rho(N)$ and equate that to zero, while enforcing the conservation of mass

$$\phi = \sum_{N=1}^{\infty} N\rho(N) \tag{2.2}$$

with ϕ the overall volume fraction of solute molecules. This gives

$$\rho(N) = Q(N) \exp \mu N \tag{2.3}$$

with $\mu < 0$ a Lagrange multiplier that may be interpreted as the (dimensionless) chemical potential of the solute molecules. It is immediately clear from eq (2.3) that, since the equilibrium size distribution is proportional to the partition function, the conformational state of the aggregates is directly coupled to their size distribution, i.e., to their growth.

To calculate the partition function, a model for the conformational states of the assemblies needs to be formulated. Our model is loosely based on that of Zimm and Bragg, [36] and characterized by two types of bond, namely helical and non-helical. Let $M < 0$ denote the free energy associated with the formation of a non-helical bond, and P the excess free energy of a helical bond, in addition to that of a non-helical one. If $P < 0$, a helical bond is more favorable than a non-helical one, and if $P > 0$, the reverse is true. The crossover from non-helical to helical aggregates takes place when P has a value close but not exactly equal to zero (see also below). We penalize interfaces between helical and non-helical regions along the chain with a free energy $R \geq 0$. For this model, the dimensionless

Hamiltonian H for an aggregate of $N > 2$ monomers [74, 84] reads

$$H = -\frac{1}{2}R\sum_{j=1}^{N-2}(s_j s_{j+1} - 1) + \frac{1}{2}P\sum_{j=1}^{N-1}(s_j + 1) + (N-1)M \qquad (2.4)$$

with $s_j = -1$ if the bond following the jth monomer is non-helical, and $s_j = +1$ if it is helical. The first term counts the number of unequal nearest-neighbor bond pairs, and penalizes these. This term is non-zero only if $s_j = -s_{j+1}$, and the jth bond is in a different conformational state than the $j + 1$st. The second term adds an excess free energy P for each helical bond along the chain, and the third one adds the non-helical (reference) free energy M for each bond. Monomers ($N = 1$) are not involved in bonded interactions so we put $H \equiv 0$, whereas for dimers ($N = 2$) a natural choice is $H = \frac{1}{2}P(s_1 + 1) + M$.

In the Hamiltonian of eq (2.4) the status of the first and last bonds has not yet been specified. Different boundary conditions can be implemented by fixing s_1 and s_{N-1} at predetermined values. For instance, if we set $s_1 = -1$ and $s_{N-1} = -1$, both ends are fixed to be non-helical by construction.

The partition function $Q(N)$ of a chain with *free* boundaries reads

$$Q(N) = \sum_{s_1=\pm 1} \cdots \sum_{s_{N-1}=\pm 1} \exp -H \qquad (2.5)$$

To alter the boundary conditions simply means setting s_1 and/or s_{N-1} to a fixed value, and ignoring the sums over these fixed ends. At this stage it turns out to be useful to factorize out the constant third term of the Hamiltonian, giving

$$Q(N) \equiv Q_h(N) \exp -M(N-1) \qquad (2.6)$$

with $Q_h(N)$ the partition function describing the conformational state of an aggregate of size $N > 2$ in terms of excess bond energies. For monomers, we obviously have $Q_h(1) \equiv 1$. For dimers, the choice of Q_h depends on the boundary conditions enforced, and is specified below.

A convenient way to calculate the partition function $Q_h(N)$ for $N > 2$ is by means of the transfer-matrix method, in which the sums of $Q_h(N)$ are recast into products of the so-called transfer matrix $\mathbf{M}$, consisting of the (unnormalized) transition probabilities between different types of bond

$$Q_h(N) = \mathbf{u} \cdot \mathbf{M}^{N-2} \cdot \mathbf{u}^+ \qquad (2.7)$$

The vectors $\mathbf{u}^+$ and $\mathbf{u}$ represent the a-priori statistical weights for the first and the last bond, and depend on the boundary conditions we wish to impose, see Table 2.1. The acronyms for the different boundary conditions are derived from the state of the aggregate ends: F stands for free, N for non-helical and H for helical.

acronym	description of ends	$\mathbf{u}$	$\mathbf{u}^+$
FF	both aggregate ends free to assume either conformation	(1,1)	(1,s)
NF	one end constrained to be non-helical	(1,1)	(1,0)
NN	both ends constrained to be non-helical	(1,0)	(1,0)
HF	one end constrained to be helical	(1,1)	(0,s)
HH	both ends constrained to be helical	(0,1)	(0,s)
HN	one end helical and one non-helical	(1,0)	(0,s)

TABLE 2.1:   Definition of the different sets of boundary conditions, with their associated vectors in the matrix representation of the partition function (eq (2.7)); $s \equiv \exp -P$ is the Boltzmann factor connected with the formation of a helical bond.

The transfer matrix consistent with the Hamiltonian, eq (2.4), may be put in the form

$$\mathbf{M} = \begin{pmatrix} 1 & \sqrt{\sigma} \\ \sqrt{\sigma}s & s \end{pmatrix} \tag{2.8}$$

with $s \equiv \exp -P$ and $\sigma \equiv \exp(-2R)$ the well-known Zimm-Bragg parameters. [36] The former represents the Boltzmann factor for the formation of a helical bond from a non-helical one. The latter parameter $0 \leq \sigma \leq 1$ is a measure of the cooperativity of the crossover from a non-helical to a helical conformation. The smaller the value of σ, the sharper this crossover, and the longer the mean length of stretches of all-helical bonds at fixed average degree of helical content.

Our transition matrix $\mathbf{M}$ differs slightly from that of Zimm and Bragg and is in fact identical to the one proposed by Grosberg and Khokhlov. [32] The differences between our matrix and that of Zimm and Bragg are unimportant and manifest themselves only if at least one of the aggregate ends is fixed to be helical. In our description such an end gets assigned a Boltzmann factor s, whilst in the original Zimm-Bragg theory it is assigned the product of Boltzmann factors $\sqrt{\sigma}s$.

The evaluation of eq (2.7) is simplified considerably by diagonalization of the transfer matrix,

$$\mathbf{M} = \mathbf{T} \cdot \mathbf{\Lambda} \cdot \mathbf{T}^{-1} \tag{2.9}$$

where $\mathbf{\Lambda}$ is a diagonal matrix containing the eigenvalues of the matrix $\mathbf{M}$, and $\mathbf{T}$ is the matrix of column eigenvectors. $\mathbf{T}^{-1}$ is the inverse of $\mathbf{T}$, so that $\mathbf{T}^{-1} \cdot \mathbf{T} = \mathbf{I}$ with $\mathbf{I}$ the unit matrix. Note that, since $\mathbf{M}$ is not Hermitian, the inverse of $\mathbf{T}$ is not equal to its transpose. For the eigenvalues of $\mathbf{M}$ we find

$$\lambda_{1,2} = \frac{1}{2} + \frac{1}{2}s \pm \frac{1}{2}\sqrt{(1-s)^2 + 4\sigma s} \tag{2.10}$$

where the $+$ sign defines λ_1 and the $-$ sign λ_2. These eigenvalues are identical to the ones found by Zimm and Bragg. [36] The eigenvectors are determined only to within an

boundary condition	x	y
FF	$\frac{(\lambda_1-1+\sqrt{\sigma})(1-\lambda_2+s\sqrt{\sigma})}{(\lambda_1-\lambda_2)\sqrt{\sigma}}$	$\frac{(\lambda_2-1+\sqrt{\sigma})(\lambda_1-1-s\sqrt{\sigma})}{(\lambda_1-\lambda_2)\sqrt{\sigma}}$
NF	$\frac{\lambda_1-s+s\sqrt{\sigma}}{\lambda_1-\lambda_2}$	$\frac{s-\lambda_2-s\sqrt{\sigma}}{\lambda_1-\lambda_2}$
NN	$\frac{\lambda_1-s}{\lambda_1-\lambda_2}$	$\frac{s-\lambda_2}{\lambda_1-\lambda_2}$
HF	$\frac{s\lambda_1-s+s\sqrt{\sigma}}{\lambda_1-\lambda_2}$	$\frac{s-s\lambda_2-s\sqrt{\sigma}}{\lambda_1-\lambda_2}$
HH	$\frac{s\lambda_1-s}{\lambda_1-\lambda_2}$	$\frac{s-s\lambda_2}{\lambda_1-\lambda_2}$
HN	$\frac{s\sqrt{\sigma}}{\lambda_1-\lambda_2}$	$\frac{-s\sqrt{\sigma}}{\lambda_1-\lambda_2}$

TABLE 2.2:   Weights associated with the larger and smaller eigenvalues in the partition function (eq (2.12)), for all boundary conditions.

arbitrary prefactor, which we fix at $\sqrt{\sigma}$. This prefactor turns out to be irrelevant to the final form of the partition function (as it should). With this choice of normalization, we obtain

$$\mathbf{T} = \begin{pmatrix} \sqrt{\sigma} & \sqrt{\sigma} \\ \lambda_1 - 1 & \lambda_2 - 1 \end{pmatrix} \tag{2.11}$$

The partition function $Q_h(N)$ can now be determined by combining the above equations, giving the exact result

$$Q_h(N) = x\lambda_1^{N-2} + y\lambda_2^{N-2} \tag{2.12}$$

for $N > 2$, where $\lambda_{1,2}$ are the eigenvalues of the transfer matrix $\mathbf{M}$, as found above. While the eigenvalues $\lambda_{1,2}$ are independent of the boundary conditions, the weights x and y are not. They are specified for each set of boundary conditions in Table 2.2.

This leaves us to specify $Q_h(2)$, the partition function of the dimers, which has to be fixed by the boundary conditions. For the cases where one or both ends are helical (cases denoted HF and HH) we assume all dimers to be helical too, so $Q_h(2) = s$. If one or both aggregate ends are constrained to be non-helical (cases NF and NN) we assume all dimers are non-helical and $Q_h(2) = 1$. In all other cases we allow the dimers to be either non-helical or helical, $Q_h(2) = 1 + s$. Clearly this treatment of dimers has some degree of arbitrariness, but it seems reasonable to suggest that the influence of a particular choice for $Q_h(2)$ on the helical transition should not be significant.

With the partition function known, quantities such as the mean fraction of helical bonds, the mean size of the aggregates and the fraction of material absorbed into aggregates can be readily calculated by standard methodology. [24] To calculate these quantities explicitly in terms of the concentration of dissolved material ϕ instead of the chemical potential μ, we insert eqs (2.3), (2.6) and (2.12) into eq (2.2), and perform the sum. This leads to a polynomial of order six in the fugacity $z \equiv \exp(\mu - M)$, which we solve numerically as a function of the system parameters M, P, R and ϕ. In order to determine which of the six solutions of this equation is the physically relevant one, the following considerations

were made. First, since μ and M are real numbers, the fugacity z is non-negative and real. Second, in order for the sum in eq (2.2) to converge, $z\lambda_1$ must be smaller than unity for all s, implying that $z < 1$, since $\lambda_1 \geq 1$. This leaves only one physically relevant solution for z in all cases investigated.

2.3 The Ground-State Approximation

Before presenting the results of our numerical calculations in section 2.4, it is instructive to show how the boundary conditions influence a quantity known in the field of giant worm-like micelles as the scission or end-cap energy.[66] The scission energy E is the free-energy cost of breaking an aggregate into two pieces, assumed to be independent of the point along the length of the aggregate where the break is introduced. The concept of a scission energy is sensible only if the (number-averaged) mean aggregate size $\langle N \rangle_n = \phi / \sum_{N=1}^{\infty} \rho(N)$ is very much larger than unity. In that case the larger eigenvalue λ_1 dominates the partition function $Q_h(N)$, allowing one to invoke the ground-state approximation [24] and write

$$\rho(N) \sim \left(1 - \frac{1}{\langle N \rangle_n}\right)^N \exp -E \sim \exp\left(-\frac{N}{\langle N \rangle_n} - E\right) \tag{2.13}$$

with

$$\langle N \rangle_n = \frac{1}{2} + \frac{1}{2}\sqrt{1 + 4\phi \exp E} \sim \sqrt{\phi \exp E} \gg 1 \tag{2.14}$$

the mean aggregate size and

$$E = -M - \ln x + 2\ln \lambda_1 \tag{2.15}$$

the aforementioned scission energy; x is the weight of the contribution of the largest eigenvalue λ_1 to the partition function (cf. eq (2.12)). From eq (2.15) we immediately read off how the properties of the ends of the aggregate affect the scission energy, namely through the weight x. Note that the larger E, the larger the mean size of the aggregates (see eq (2.14)).

In Table 2.3 we have collected the scission energies for high and low values of the Boltzmann factor s, as well as for $s = 1$, for all sets of boundary conditions. The scission energies in the low-s limit all share a non-helical bond strength $-M$, since for $s \ll 1$ helical bonds are less stable than non-helical ones and the aggregates are mostly non-helical. In the opposite limit $s \gg 1$, they share the overall strength of a helical bond, $-M - P$, for in this limit the assemblies are helical. At $s = 1$, where the helical and non-helical bond have the same energy, the factor $-M + 2\ln(1 + \sqrt{\sigma})$ is present in all cases, since in this case $\lambda_1 = 1 + \sqrt{\sigma}$.

Additional free-energy contributions, apart from these trivial ones, arise from the specific boundary conditions. Still, in both limits of stable and unstable helical bonds, as well as

boundary condition	$E(s \ll 1) + M$	$E(s = 1) + M + 2\ln(1 + \sqrt{\sigma})$	$E(s \gg 1) + M + P$
FF	0	$-\ln 2$	0
NF	0	0	$-P + R$
NN	0	$\ln 2$	$-2P + 2R$
HF	$P + R$	0	0
HH	$2P + 2R$	$\ln 2$	0
HN	$P + R$	$\ln 2$	$-P + R$

TABLE 2.3: Scission energies for $s \ll 1$, where a helical bond is less stable than a non-helical one, for $s = 1$, and for $s \gg 1$, for all boundary conditions. In all cases these energies are given without their trivial contribution.

for $s = 1$, boundary conditions can be grouped together that produce identical scission energies. For small s, the boundary conditions FF, NF and NN form such a group, as do HF and HN; the all-helical case HH has a scission energy distinct from these two. For $s = 1$, the cases HN, NN and HH form a group, as do HF and NF, and FF forms the third group. In the large-s limit, the boundary conditions FF, HF and HH form a group with identical scission energies as do the cases NF and HN; the case NN (with both ends non-helical) does not belong to either group. As may be easily verified for each of the boundary conditions, in the limits of stable and unstable helical bonds the results for the scission energy E given in Table 2.3 correspond exactly to the free-energy difference before and after the break in an aggregate that is fully non-helical (when $s \ll 1$) or fully helical (when $s \gg 1$), with possibly different end states if required by the imposed boundary conditions.

To illustrate the sensitivity of the scission energy to the boundary conditions, we plot in Figure 2.1 the quantity $E + M$ as a function of the excess helical-bond strength $-P$, for the highly cooperative case with $\sigma = 10^{-3}$. For reasons of clarity, only the results for the cases FF, NF and HF are shown. Obviously, the same trends can be distinguished as in Table 2.3. The cases with both ends either non-helical or helical NN and HH behave similar to the cases with one boundary fixed (NF and HF). The case with one end non-helical and the other end helical HN follows the case HF for $-P \ll 0$, and the case NF for high $-P \gg 0$, in accordance with Table 2.3. For all boundary conditions, except NN and NF (see Table 2.3), the scission energy of the aggregates first decreases with increasing $-P$ to rise again when $-P$ becomes positive, at least if σ is small enough. This means that for highly cooperative helical bonding the mean aggregate size is also a non-monotonous function of the helical-bond strength.

We now rationalize the somewhat counter-intuitive dependence of E on P for one of the boundary conditions, namely that with one end helical, HF. (For the other boundary conditions similar arguments hold.) In that case, each aggregate has at least one helical end, even in the regime where helical bonds are highly unfavorable (for $-P \ll 0$). Therefore, in
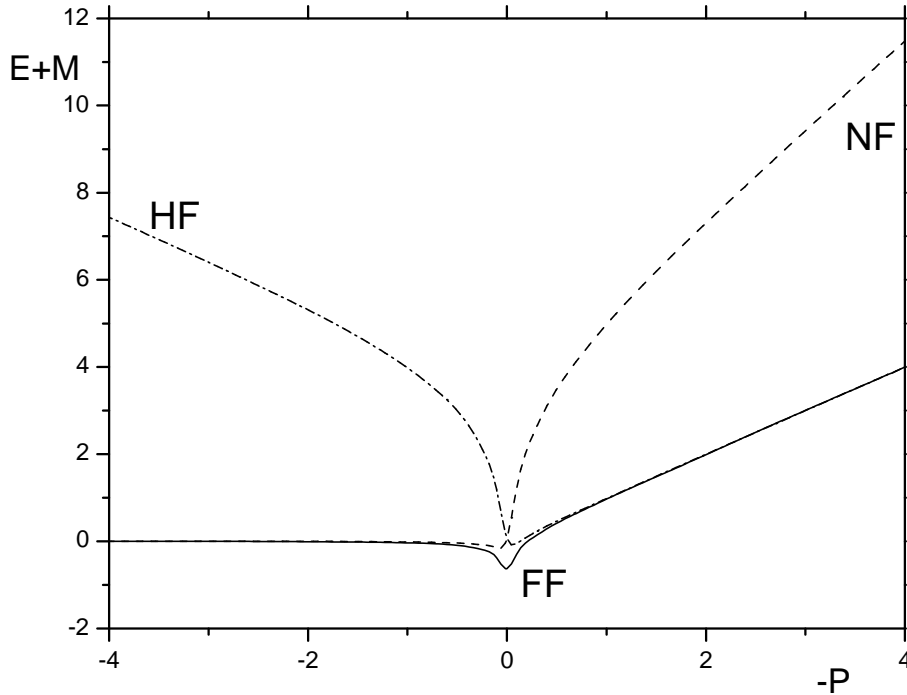
FIGURE 2.1: The shifted scission energy $E + M$ as a function of the helical-bond strength $-P$; M is the free energy of a non-helical bond and P is the excess free energy of a helical bond. The cooperativity parameter σ was fixed at a value of 10^{-3}. Results are shown for boundary conditions HF, FF and NF, as indicated.

this regime the system decreases the number of aggregate ends and the more so the larger P, which leads to an increase of the mean aggregate size; thus the scission energy also increases with increasing $P > 0$. For $-P > 0$, the scission energy increases with increasing $-P$ because helical bonds are now favorable and growth maximizes the total number of bonds.

The state of the assemblies is not only characterized by their mean size, but also by their mean helicity. (The former quantity is observable, e.g., with the aid of radiation-scattering techniques, and the latter by circular-dichroism spectroscopy.) A weight-averaged fraction of helical bonds may be given by [36][4]

$$\langle\theta\rangle_w \equiv -\frac{1}{\phi} \sum_{N=\alpha+1}^{\infty} \rho(N) \frac{N}{(N-\alpha)} \frac{\partial \ln Q(N)}{\partial P} \tag{2.16}$$

Here, the term $(N - \alpha)$ represents the maximum number of helical bonds allowed by the choice of boundary conditions in an aggregate of N monomers. For the boundary conditions

---

[4]Strictly speaking, the average helicity should contain a summation over the $(N - 1)$ bonds, rather than over the N molecules. However, this would require us to adjust the definition of ϕ in this context, and in practice the effect of this improvement is negligible.

FF, HF and HH, α equals unity, for NF and HN $\alpha = 2$, whilst for NN $\alpha = 3$. In this definition of the mean helicity we count the number of helical bonds, and compare it to the maximum number of helical bonds that could be present in the system. For monomers, and (depending on the boundary conditions) for some non-helical dimers and trimers, this definition may be somewhat confusing, since these species are obviously non-helical, yet also exhibit their maximum attainable helicity, namely zero. Here we choose to set the helicity of these small species equal to zero, hence the boundaries of the summation in eq (2.16). In our definition, the state of full helicity $\langle\theta\rangle_w = 1$ is reached only if the fractions of monomers and non-helical dimers and trimers approach zero, i.e., in the limit where $\langle N\rangle_n \to \infty$.

In the limit of large $\langle N\rangle_n$ the ground-state approximation is valid, and eq (2.16) reduces to [32]

$$\langle\theta\rangle_w = \frac{1}{2} + \frac{s-1}{2\sqrt{(s-1)^2 + 4s\sigma}} \tag{2.17}$$

If we (arbitrarily) define the helical transition to occur at the point when half the bonds are helical, it follows that in the limit $\langle N\rangle_n \gg 1$ this transition takes place when $s = 1$. It also follows that, in this limit, the helicity is apparently independent of the mean aggregate size. On the other hand, the mean size does depend on the conformational state of the aggregate through the scission energy (see eq (2.14)). This shows that, while instructive, the ground-state approximation cannot provide a full, internally consistent description of the helical aggregation. In the next section we therefore apply the full theory to examine the coupling between the size and the helical state of the aggregates, as well as the dependence of the diagrams of aggregated states on the choice of boundary conditions.

2.4 Solution beyond the Ground-State Approximation

We now discuss the diagrams of states presented in the Figures 2.2-2.4, which we calculated by numerically solving the pertinent equations for the boundary conditions FF (both ends free), NF (one end non-helical) and HF (one end helical). The state diagrams are parametrized in terms of the quantities $-P$ and $\Delta\mu \equiv \ln\phi - M$, the former being the excess helical bond energy (apart from its sign) while the latter can be loosely interpreted as the difference between the chemical potential of a monomer in free solution and one in an aggregate. Positive values of $\Delta\mu$ indicate a preference of the monomers to be present in the aggregated state, negative values indicate a preference for the free molecularly dissolved state. The bottom pair of drawn and dashed curves in the diagrams indicates the conditions for which the fraction of molecules in an aggregated state $\eta \equiv 1 - \rho(1)\phi^{-1}$ equals one-half, while the top pair indicates conditions for which the mean fraction of helical bonds $\langle\theta\rangle_w$ equals one-half. Clearly, the curves demarcate polymerized from non-polymerized states,
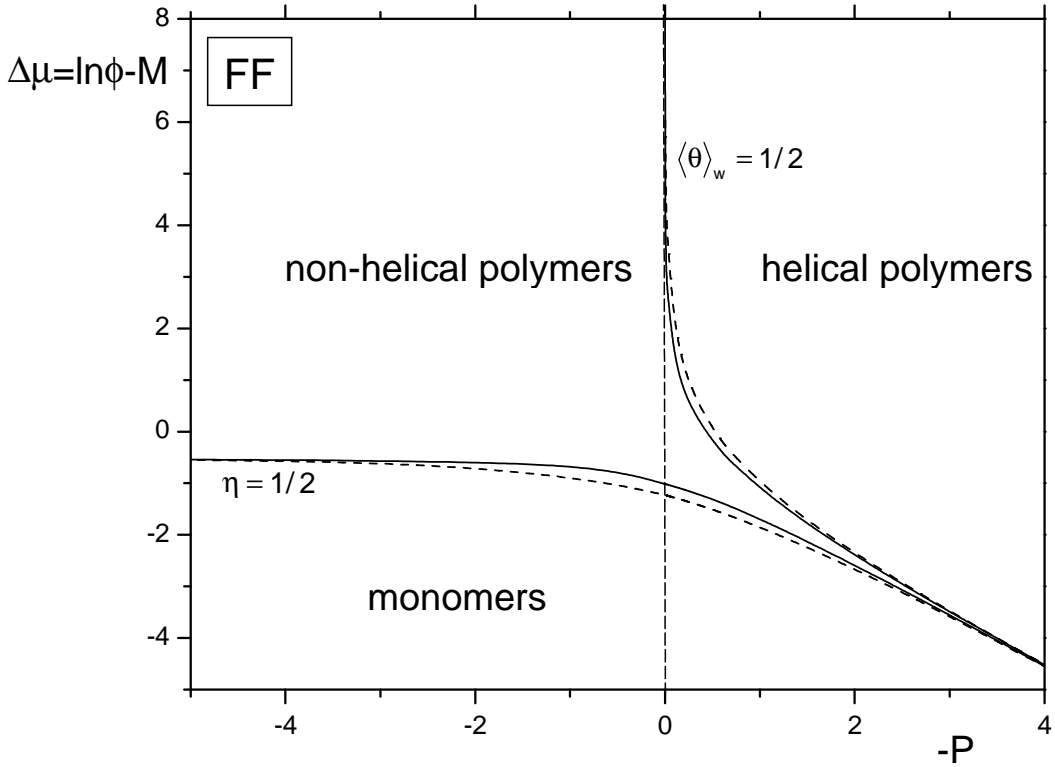
FIGURE 2.2: Theoretical diagram of states for the case with free boundary conditions (FF), for $\sigma = 1$ (dashed line) and $\sigma = 1.5 \cdot 10^{-3}$ (drawn line). Vertical axis: $\Delta\mu \equiv -M + \ln\phi$; horizontal axis: $-P = \ln s$. The top line is the helical transition line, where half the bonds are helical and $\langle\theta\rangle_w = 1/2$. The bottom line is the polymerization line, where half the material is in the aggregated state and $\eta = 1/2$.

and helical from non-helical states. Results are shown for two different values of σ, representing high and low cooperativity. Predictions for the cases with both ends non-helical (NN) or helical (HH) are not reproduced, because they are similar to those of the cases NF and HF. For similar reasons results for the boundary condition HN (one end helical, one non-helical) are not given; in fact, they display elements of both NF and HF.

For all boundary conditions, the diagrams show the presence of two regimes, one where the helical transition and the polymerization transition are widely separated, and one where they practically coincide. Also, for each case, the polymerization line approaches a constant value for $P \gg 1$, while the helical transition line approaches asymptotically the value $P = 0$ in the limit of large aggregates, i.e., for large values of $\Delta\mu$, as expected from the ground-state analysis. Furthermore, the coinciding polymerization- and helical-transition lines in the regime of negative $\Delta\mu$ and P clearly point at a scaling relation $\Delta\mu \sim P$, which may in fact be straightforwardly obtained within the ground-state approximation (e.g., from eq (2.2), (2.3), (2.10), (2.12), and (2.17)).
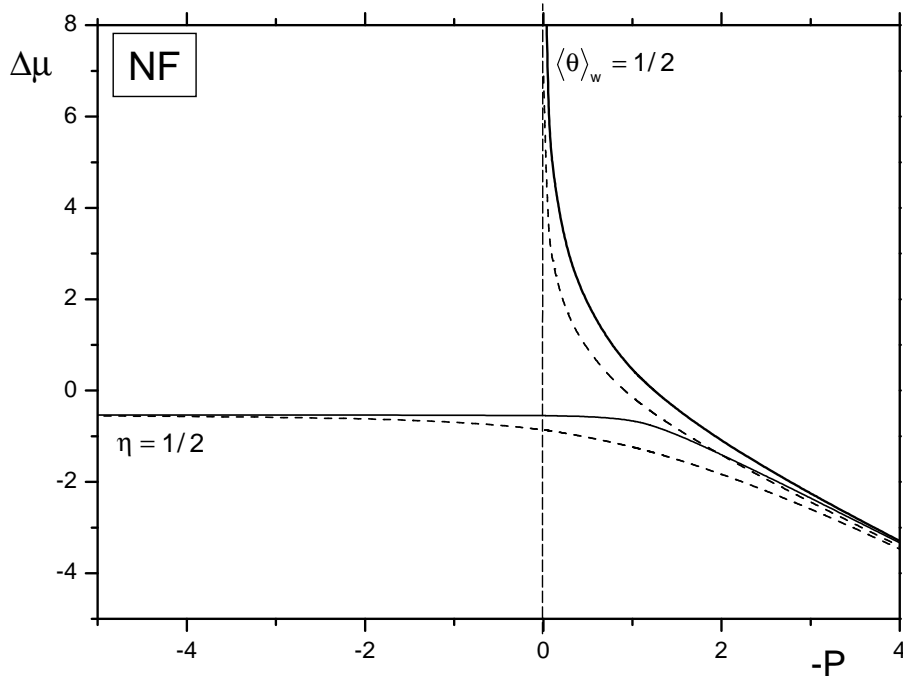
FIGURE 2.3:   As Figure 2.2, for the boundary condition with one end non-helical (NF).

The largest influence of the state of the aggregate ends is around $P = 0$ and $\Delta\mu = 0$, where the assemblies are still relatively short. Here the diagrams differ considerably. Focusing on these differences we, e.g., observe that the crossovers shift to larger values of $\Delta\mu$ and $-P$ when one compares the case where one end is non-helical (Figure 2.3) to that where both ends are free (Figure 2.2). In other words, fixing one end to be non-helical destabilizes the aggregated states. An explanation is that the helical transition and the growth of the assemblies both strongly depend on the ease with which the first helical bond is formed. Because for the NN and NF boundary conditions the first bond is non-helical, the formation of the first helical bond requires the formation of a helical-non-helical interface, at the cost of a free-energy penalty $R > 0$. This makes the formation of helical aggregated states always less favorable than in the model with the free boundaries FF.

A similar effect is seen when one compares Figure 2.4 (the case where one end is helical) to Figure 2.2 (with both ends free), albeit that here the ease of formation of the first non-helical bond is the deciding factor. For those cases where at least one bond is helical, HF and HH (the latter not shown), the helical state is stabilized by an increasing cooperativity (see Figure 2.4 for boundary conditions HF), while for aggregates with a non-helical end (Figure 2.3) an increase of the cooperativity favors the formation of non-helical bonds. This is as expected, since the appearance of bonds with a different configuration from that of the ends is inhibited by the interfacial free-energy penalty imposed.
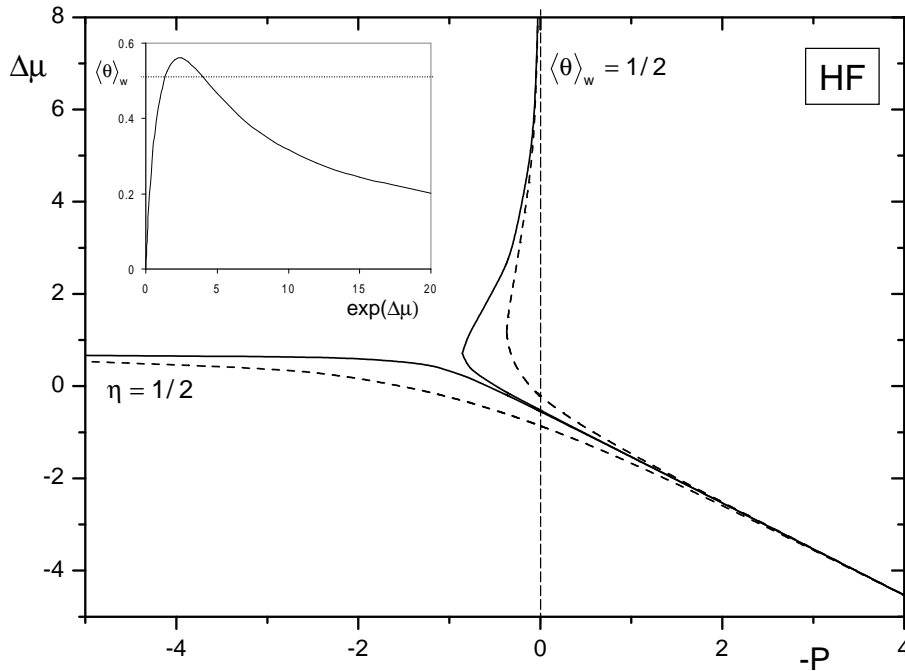
FIGURE 2.4:   As Figure 2.2 for the boundary condition with one end helical (HF). In the inset: a cross section of the diagram at $s = 0.5$ and $\sigma = 1.5 \cdot 10^{-3}$, showing the mean helicity as a function of $\Delta\mu$.

Another remarkable difference between the three diagrams of state is the sensitivity of the diagram on the degree of cooperativity, described by the parameter σ. While the diagram for the case with free boundary conditions FF (depicted in Figure 2.2) is quite insensitive to changes in σ, this is not so for all other boundary conditions, which do exhibit quite a strong dependence on σ (see Figures 2.3 and 2.4). The reason is that if the ends are free, aggregates can be helical or non-helical without the need to create helical-non-helical interfaces. Note that while the diagram of states for the case FF is relatively insensitive to σ, this does not necessarily extend to the actual crossovers, which do display a strong dependence on σ.

Perhaps the most striking feature we find is the re-entrance behavior of non-helical conformations for the cases with at least one helical bond, when $\Delta\mu$ is varied at constant P (see Figure 2.4 and inset). This is caused by the circumstance that for these boundary conditions small aggregates are helical even when the helical bond is unfavorable, so as to avoid paying the interfacial free energy penalty R. Increasing the value of $\Delta\mu$ at constant P causes non-helical bonds to become increasingly more favorable, leading to a decrease of the overall helicity, and eventually to re-entrance into the region of disordered aggregates. This effect is obviously stronger for the case HH than for the case HF, since the case HH has at least two helical bonds per aggregate as opposed to one in HF (results for HH not shown). Re-entrance behavior is also observed for the case HN (not shown).

FIGURE 2.5: The predicted fraction of molecules in the aggregated state and the mean fraction of molecules in the helical state, respectively η and $\langle\theta\rangle_w$, as a function of the effective density $\Phi \equiv \exp\Delta\mu$ for $\exp(-P) = s = 3$. The inset displays the mean aggregate size as a function of Φ. The arrows indicate the locations of the polymerization transition Φ_* and the helical transition Φ_{**}.

We shall see in Chapter 3 that only two of the boundary conditions (NF and NN) can describe measurements on aggregates of discotic molecules [9] adequately. Therefore, we feel it is instructive to take a somewhat more detailed look at the behavior of one of these sets of boundary conditions, namely NF.

We make the weight-averaged fraction of helical bonds $\langle\theta\rangle_w$ explicit for these boundary conditions. From equations (2.2), (2.3), (2.6), (2.12) and (2.16) with the boundary conditions NF from Table 2.2 inserted, we find

$$\langle\theta\rangle_w = \frac{\sum_{r=1}^{2}\left[(a_r - 2c_r)(d_r + e_r) + s\lambda_r' d_r \lambda_r^{-1}(2a_r + b_r) + d_r f_r(2c_r - a_r)\right]}{z\exp M + z^2\exp M + \sum_{r=1}^{2} d_r(2a_r + b_r)} \tag{2.18}$$

where

$$a_r \equiv \frac{z^3 \lambda_r}{(1 - z\lambda_r)}\exp M \qquad\qquad b_r \equiv \frac{a_r}{(1 - z\lambda_r)} \tag{2.19}$$

$$c_r \equiv z^2 \ln(1 - z\lambda_r)\exp M \qquad\qquad d_r \equiv \frac{s\sqrt{\sigma}(\lambda_r - 1) + \sigma s}{(\lambda_r - 1)^2 + \sigma s}$$
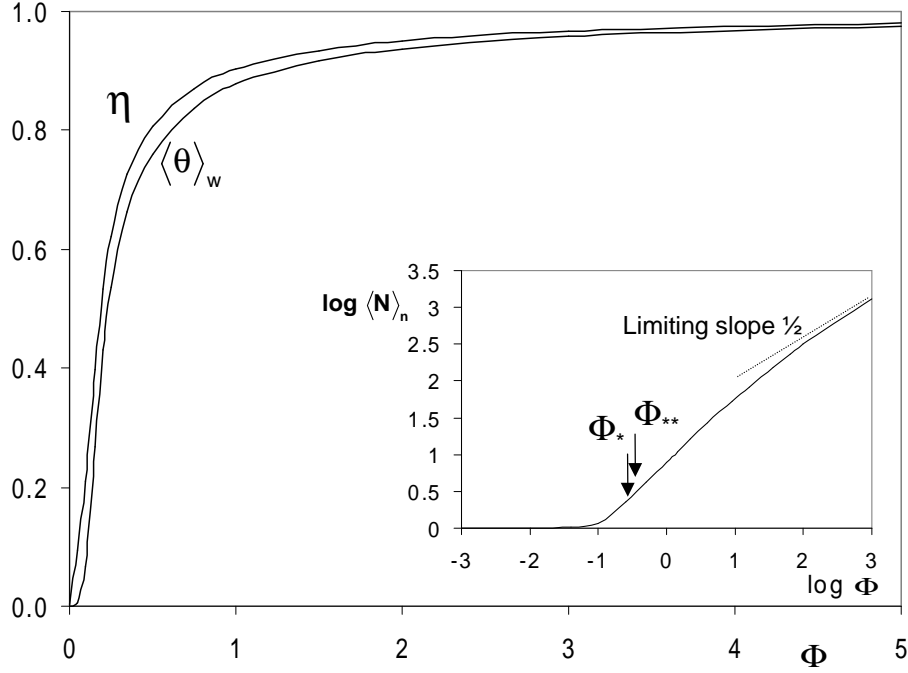
FIGURE 2.6:   As Figure 2.5, for $s = 10$.

$$e_r \equiv \frac{\lambda'_r s^2 \sqrt{\sigma}}{(\lambda_r - 1)^2 + \sigma s} \qquad f_r \equiv \frac{s[2(\lambda_r - 1)\lambda'_r + \sigma]}{(\lambda_r - 1)^2 + s\sigma}$$

and $\lambda'_r \equiv \partial\lambda_r/\partial s$. For the fraction η of material in aggregates of size $N > 1$, and the (number-averaged) mean aggregate size, $\langle N \rangle_n$, we obtain

$$\eta = \frac{2z^2 \exp M + \sum_{r=1}^{2}(2a_r d_r + b_r d_r)}{z \exp M + 2z^2 \exp M + \sum_{r=1}^{2}(2a_r d_r + b_r d_r)} \tag{2.20}$$

$$\langle N \rangle_n = \frac{z \exp M + 2z^2 \exp M + \sum_{r=1}^{2}(2a_r d_r + b_r d_r)}{z \exp M + z^2 \exp M + \sum_{r=1}^{2} a_r d_r} \tag{2.21}$$

To illustrate some of the salient features of the behavior of the system at hand, we take cuts through the diagram of states (Figure 2.3) and show how the fraction of helical bonds, the aggregation number and the fraction of aggregated material respond to changing conditions. In Figures 2.5 and 2.6 we take vertical cuts through the diagram of states at fixed $s \equiv \exp{-P} = 3$ and at fixed $s = 10$. Shown are η and $\langle\theta\rangle_w$ as a function of Φ, which may be seen as an effective density and is defined as $\Phi = \phi \exp{-M} \equiv \exp \Delta\mu$. The insets in these Figures give the dependence of $\langle N \rangle_n$ on Φ, where we have indicated with arrows the locations of the polymerization transition, Φ_*, for which $\eta = \frac{1}{2}$, and the helical transition, Φ_{**}, for which $\langle\theta\rangle_w = \frac{1}{2}$. Figures 2.5 and 2.6 illustrate the merging of the two transitions with increasing value of the parameter s, i.e., with increasing strength of the helical bond.
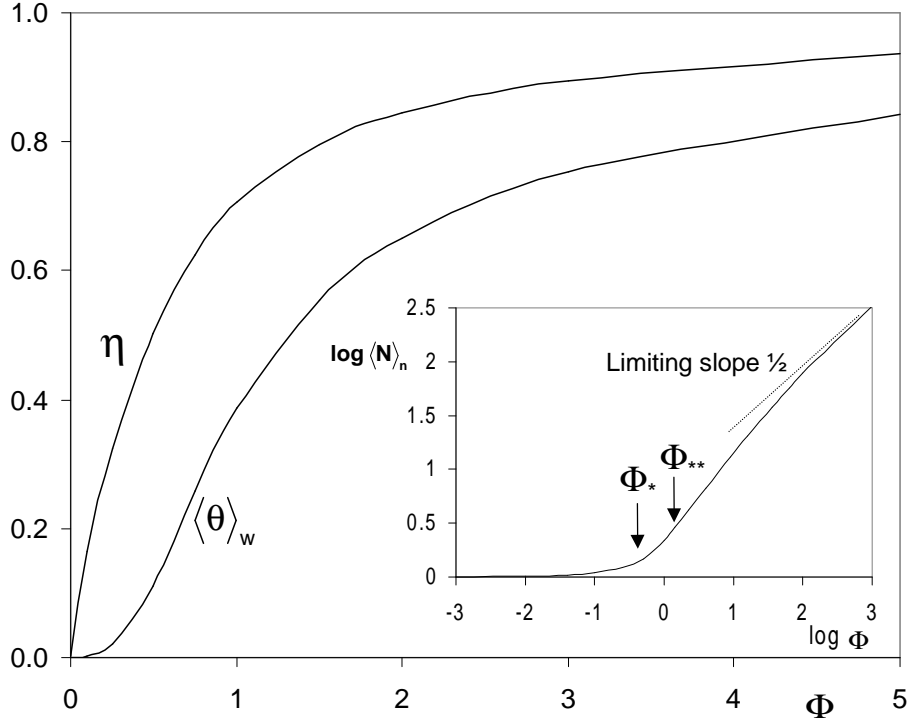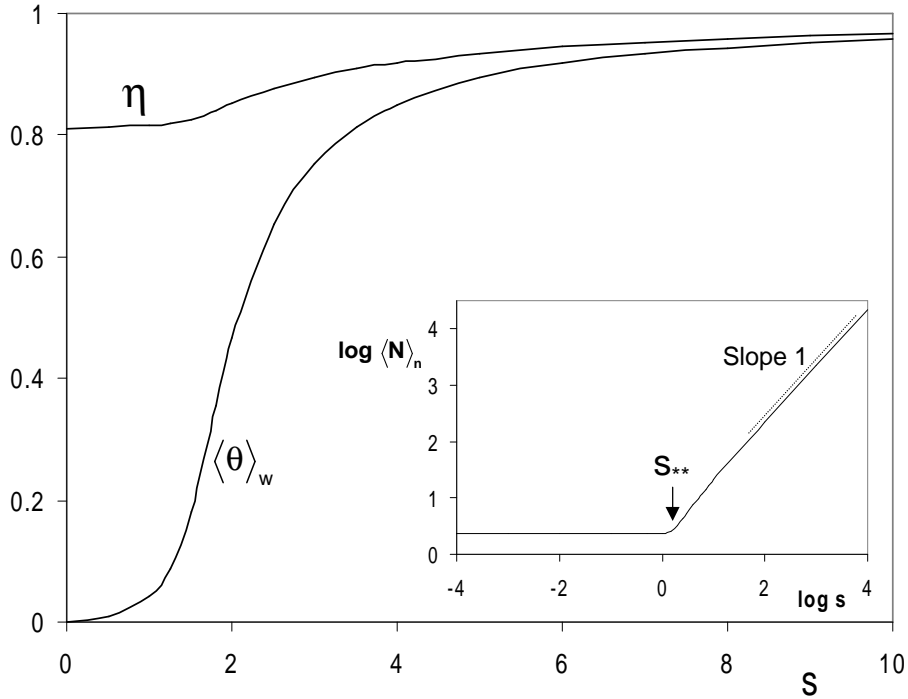
FIGURE 2.7: The predicted fraction of molecules in the aggregated state and the mean fraction of molecules in the helical state, respectively η and $\langle\theta\rangle_w$, as a function of s for $\Phi = 3$. The inset displays the mean aggregate size as a function of s. The arrow indicates the location of the helical transition.

In the limit of infinite helical-bond strength, the polymerization transition is completely dominated by the helical transition. Note the strongly enhanced growth for $\Phi \geq \Phi_{**}$; below Φ_{**}, the growth of the assemblies is a relatively weak function of Φ. In the absence of a helical transition $\langle N\rangle_n \sim 1 + \Phi$ if $\Phi \ll 1$ and $\langle N\rangle_n \sim \sqrt{\Phi}$ if $\Phi \gg 1$. [24, 67] The helical transition shifts the crossover from the weak- to the strong-growth regime to smaller values of Φ as it becomes more important, i.e., for larger values of s.

In Figure 2.7 we take a horizontal cut through the diagram of states of Figure 2.3 for fixed $\Phi = 3$. Illustrated in the main Figure are η and $\langle\theta\rangle_w$ as a function of the helical-bond strength s, and in the inset $\langle N\rangle_n$ versus s. For this choice of Φ, the polymerization and the helical transition are widely separated; the polymer fraction is already at a high 0.8 at the point where the fraction of helical bonds is still zero. The trend that was already visible in Figures 2.5 and 2.6 presents itself even more prominently in this Figure: for low values of s, where most of the bonds are in the non-helical state, the aggregates are in the mean relatively small and their size is fairly constant, while near the helical transition a sudden, accelerated growth sets in. Since in this case the polymerization line has long been passed this demonstrates that it is indeed the helical transition that causes this growth spurt. It

is easy to show that for large s, $\langle N \rangle_n \sim s$, [24] which is indeed observed in the Figure. Large assemblies are feasible below the helical transition, but only if $\Phi \gg 1$.

2.5   Discussion and Conclusions

The state of the aggregate ends has a large effect on the physical properties of self-assembled polymers with different conformational states, even when these polymers are not small. From a model that allows for restrictions on the state of the aggregate ends we have found that such restrictions lead to three different classes of behavior. These classes are distinguished by their dependence on the degree of cooperativity of the helical transformation, as well as by the emergence of a re-entrance of the non-helically aggregated state. We note in passing that a similar re-entrance behavior is observed in (rabbit muscle) actin in solution in the presence of $MgCl_2$ and varying concentrations of KCl, itself an example of a helically aggregating system. [107]

Although we have presented the, as far as we know, most complete theory of helical self-assembly, it is not the first. Oosawa and Kasai proposed a (much simpler) theory to describe the self-assembly in water of the globular protein actin into helical fibers. [4, 23] (A somewhat similar theory to that of Oosawa and Kasai was used by Niranjan et al. in their description of the polymerization of actin. [107]) That theory relies on a so-called all-or-nothing model, and assumes that all aggregates of degree of polymerization larger than two are either completely helical or completely non-helical; monomers and dimers are treated as inherently non-helical. Such an all-or-nothing model is sensible only if the average aggregate size is much smaller than the intra-aggregate correlation length and is therefore best suited to describe systems with a large cooperativity.

The (reduced) partition function of an aggregate in the Oosawa-Kasai model may be expressed as

$$Q_h(N) = 1 + \gamma s^{N-3} \qquad (2.22)$$

for $N \geq 3$, and $Q_h(N) = 1$ for $N = 1, 2$, with s its usual meaning and γ a Boltzmann factor expressing the ease with which a helical aggregate can be "nucleated". Equation (2.22) differs from the partition function we found in eq (2.12), irrespective of the boundary conditions. Nonetheless, the properties of the Oosawa-Kasai model are very similar to those of our model with free boundary conditions FF, albeit only at high cooperativity. In fact, the partition functions of the Oosawa-Kasai model and our model with free ends are identical in the limits $s \gg 1$ and $s \ll 1$ if we choose $\gamma = s^2$. Since the model with free boundary conditions poorly describes the experimental data of Brunsveld et al. (as we shall see in Chapter 3), it is not surprising that the Oosawa-Kasai theory also fails for that system. However, the Oosawa-Kasai theory does seem to provide a good description of the helical aggregation of actin in water, suggesting that different systems may be subject to different boundary conditions. [84]

The theory in its present form is believed to be suited for any system that undergoes self-assembly coupled with an ordering transition, provided the system is in the dilute regime. The theory is potentially unsuited for processes requiring an activation step, since we do not take the possibility of the presence of inactive monomers into account. Even without activation, despite the apparent accuracy in describing experimental data of our model, there is room for improvement. For instance, the possibility of ring closure has been neglected, as have excluded-volume-type interactions. For the discotic molecules discussed in section 1.1 at the considered concentrations these are presumably unimportant approximations. The reason ring formation can be neglected is that we found the aggregates to be relatively small for $T > T_{**}$. In the helical state, the aggregates do become long, but at the same time are expected to become more rigid than in the non-helical state, as the packing of the molecules is expected to be tighter. [9] Excluded-volume interactions can be neglected if the volume fraction $\phi \leq D/L$, with D the diameter of an aggregate and L its length. [108, 109] We describe the effect of this type of interaction in Chapter 7.

Chapter 3

Helical Assemblies in Solution: Comparison to Experiment

ABSTRACT

We compare the results of the treatment outlined in Chapter 2 to experimental results on dilute solutions of discotic molecules in n-butanol, obtained by a host of techniques. It turns out that only two sets of boundary conditions provide a quantitative description of the helical self-assembly of the discotic molecules, namely the boundary conditions in which one or both ends are fixed to be non-helical. It is in principle possible to distinguish further between these two boundary conditions, since they show a different dependence of the mean aggregate size on the temperature. However, currently available experimental results are insufficient to make this distinction.[1]

---

[1]Parts of this Chapter appeared in *Langmuir* **2003**, *19*, 1375. Most of it appeared in *J. Phys. Chem. B* **2001**, *105*, 10691.

3.1   Introduction

So far, we have discussed the predictions of the theory in terms of the "theoretical" control variables σ, s and $\Phi \equiv \exp \Delta\mu$, which describe the degree of cooperativity, the stability of the helical bond and the strength of the "mass action". In order to test the theory against experiment, we need to translate these control variables into experimentally accessible ones, such as the temperature, the concentration of dissolved material and the transition enthalpies. This we do in the next section, where we compare the theory for the different boundary conditions with the observations of Brunsveld et al. [9] As we shall see, only one of the three classes of behavior predicted in Chapter 2 describes the experimental data adequately.

The remainder of the Chapter is structured as follows. In section 3.2 we compare our theory to experimental data of Brunsveld et al. on a system of discotic molecules [9] for all classes of boundary conditions. It appears that the sets of boundary conditions in which one or both ends are constrained to be non-helical provide the best description of the experimental results. We provide an in-depth comparison to experiment for one of these boundary conditions (the one with one end non-helical) in section 3.3 and find quantitative agreement between theory and experiment. In section 3.4 we present a discussion and conclusions.

3.2   Comparison of Different Boundary Conditions

Before giving a full, quantitative translation of the theory into experimental parameters, we note that there is experimental evidence to support the presence of two regimes as seen in Figures 2.2-2.4. [9, 10] Hirschberg et al. [10] found for their bifunctional molecules a polymerization transition in one solvent and a combined polymerization and helical transition in another. Brunsveld and co-workers synthesized a chiral discotic molecule that in the solvent n-butanol self-assembles into stacks, which under the right conditions exhibit a helical transition. [9, 110] For these molecules, separate transitions were observed for their discotics in the solvents n-butanol and dodecane. [9, 111, 112] In dodecane, however, the two transitions were closer together for comparable concentrations. [112] This suggests that a change in the solvent quality can lead to the exploration of a different area of the diagram of states. As we have seen in Chapter 2, the distance between the transitions can also be tuned by varying the concentration of dissolved material.

In order to determine the quality of the theoretical model a comparison was made with experimental work on solutions of the so-called C_3 discotic of Brunsveld et al. [9, 110] in n-butanol. This molecule, like most discotics, [11, 13, 103, 113, 114, 115, 116] consists of an aromatic core, attached to which are (nine) side chains. In the work of Brunsveld et al. these side chains were chosen to be homochiral and of a polar nature (see Figure 1.1).

This combination of an apolar core with a polar rim causes the molecule to self-assemble in solution in order to shield the apolar core from the more polar solvent. The discotic molecules can also undergo a helical transition, which is presumably caused by an increased binding free energy of the helical aggregates when compared to the non-helical aggregates. A model relating the shape of the molecule to its ability to aggregate and form helices has been described in some detail earlier. [9, 24] The homochiral side chains bias the twist sense of the intrinsically helical columns, causing the formation of an excess of helices of a single handedness over the other, an example of molecular chirality inducing macromolecular chirality. [117] A host of experimental techniques were used to study dilute solutions of these molecules. [9] We concentrate on results from circular-dichroism spectroscopy (CD), time-resolved fluorescence spectroscopy and differential scanning calorimetry (DSC) experiments. Due to the large amount of experimental data that was gathered on this system, it turns out to be possible to fix all the control parameters of our theory.

Given that the molecular structure of the material does not appear to preclude or prescribe any state of the aggregate ends, it is not a priori clear which of the boundary conditions described in Chapter 2 provides the best description of the actual state of the system. We show below that one can in fact fairly accurately fix the boundary conditions by fitting to experiment. Note that different boundary conditions may correspond to different experimental systems. [84]

Following the procedure of van der Schoot in reference [24], we first make the temperature dependence of the non-helical and helical bond energies M and P explicit by means of a Taylor expansion around two reference temperature scales T_*^0 and T_{**}^∞ defined below:[24]

$$M(T) \approx M(T_*^0) + \left.\frac{\partial M}{\partial T}\right|_{T_*^0} (T - T_*^0) = \ln \frac{\phi}{2 - \sqrt{2}} - (\frac{T}{T_*^0} - 1)\frac{h_n}{k_B T_*^0} \qquad (3.1)$$

and

$$P(T) \approx P(T_{**}^\infty) + \left.\frac{\partial P}{\partial T}\right|_{T_{**}^\infty} (T - T_{**}^\infty) = (1 - \frac{T}{T_{**}^\infty})\frac{h_h}{k_B T_{**}^\infty} \qquad (3.2)$$

Here, we set $P(T_{**}^\infty) = 0$ by definition, and $M(T_*^0) = \ln \phi/(2 - \sqrt{2})$ follows from the theory of linear self-assembly when one inserts $\eta = 1/2$ (corresponding to $\langle N \rangle = \sqrt{2}$) into eq (2.14). In equations (3.1) and (3.2), h_n represents the enthalpy of the formation of a non-helical bond and h_h that of a helical bond from a non-helical one. T_*^0 represents the polymerization transition temperature in the hypothetical limit that no helical transition can take place, and T_{**}^∞ the helical-transition temperature of an infinitely long aggregate. We recall that, by definition, these transition temperatures demarcate conditions for which $\langle \theta \rangle_w = \frac{1}{2}$ and $\eta = \frac{1}{2}$.[2] From earlier work we know the values of h_n and T_*^0 to be model-independent. [9, 24]

---

[2]The mean helicity is defined slightly differently form that in Chapter 2, in order to better correspond to the interpretation of the CD data. While in eq (2.16) we took monomers and non-helical oligomers into consideration by dividing by ϕ, in the current $\langle \theta \rangle_w$ we neglect these, equating $\langle \theta \rangle_w = 1$ with the equilibrium state at low temperature, rather than the state where all conceivable bonds are helical.

The enthalpy of the helical transition h_h, -50 kJ/mol, was determined by differential scanning calorimetry (DSC), and corresponds to $-20k_BT$ per bond at the actual transition temperature T_{**}, independent of concentration in the regime 10^{-2} - 10^{-4} M covered by the experiments. We assume that this enthalpy is independent of the boundary conditions. While not strictly true, this approximation is sensible because the enthalpy was measured by integrating the measured heat capacity over a large temperature range, starting in the monomer regime and ending deep within the helical polymer regime. In this latter regime, the aggregates are so long that the state of the aggregate ends is expected to be unimportant. The concentration invariance of the enthalpy is also a strong indication that finite-size effects (and therefore the self-assembly process) have a negligible influence on the measured value of the enthalpy.

The enthalpy of the formation of a non-helical bond h_n was determined by means of fluorescence spectroscopy and found to be equal to $-27k_BT$ at the polymerization temperature $T_* \approx 316$ K for the concentration $\phi = 2.35 \cdot 10^{-6}$.[3] Values at other concentrations (where no data are available) were estimated from this value using the following extrapolation formula [24]

$$\frac{T_*^0(\phi_2)}{T_*^0(\phi_1)} \simeq 1 + \frac{k_B T_*^0(\phi_1)}{h_n} \ln \frac{\phi_1}{\phi_2} \qquad (3.3)$$

where we use the known experimental values $\phi_1 = 2.35 \cdot 10^{-6}$ and $T_*^0(\phi_1) = 316$ K as a reference, and Taylor expand around this temperature, assuming that the non-helical bond formation dominates at T_*^0. Since h_n and T_*^0 are connected only with the bare polymerization process, and h_h was determined directly from DSC measurements (i.e., without the intervention of a boundary condition-dependent theory), these parameters can be fixed without specifying the boundary conditions. Following ref [24] we assume R and therefore also σ to be temperature and concentration independent.

With h_n, h_h and T_*^0 fixed, the remaining unknowns are T_{**}^∞ and R, which we obtain by a two-parameter fitting procedure to the results of temperature-dependent circular-dichroism (CD) measurements. These measurements give direct information on the mean helical content of the supramolecular aggregates at five different concentrations ranging from 10^{-6} to 10^{-2} M, corresponding to volume fractions ϕ from $2.61 \cdot 10^{-6}$ to $2.43 \cdot 10^{-2}$. We reasonably assume that there is a constant proportionality between the fraction of helical bonds in the solution and the measured optical effect (expressed in mdeg at a wavelength of 337 nm). In order to obtain a meaningful comparison between theory and experiment, the experimental values of the mean helicity are normalized so that the highest measured helicity equals unity.

The fitting to the experimental helicity-temperature data is done as follows. First, T_{**}^∞ is fitted by hand to an experimental data point close to the midpoint of the transition. (For

---

[3]To calculate the volume fraction from the molar concentration, a density for the discotic molecule of 1.3 g mL^{-1} was used. We obtained this number from X-ray measurements in the solid state. The molecular weight of the discotic lies around 3400 g mol^{-1}.
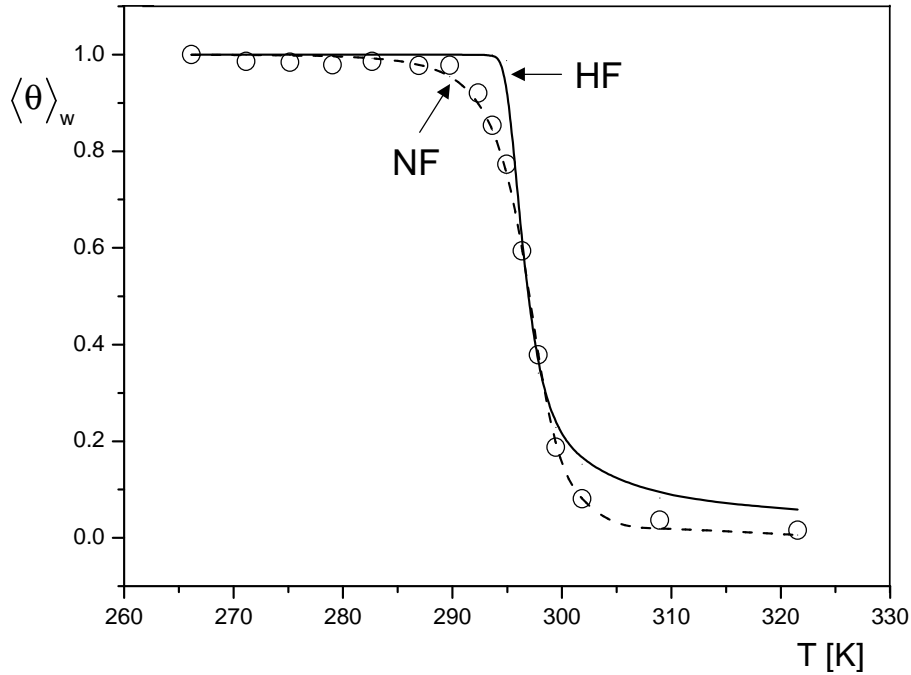
FIGURE 3.1: The mean helicity versus the temperature in K for the discotic molecules in n-butanol discussed in the main text, at a volume fraction $\phi = 2.55\cdot10^{-4}$. [9] The symbols represent experimentally found values, the dashed line gives the optimal numerical fit of the case NF with quality parameter $\varsigma = 0.15$, the drawn line that for case HF with quality parameter $\varsigma = 0.59$.

a typical set of experimental helicity-temperature data, see the symbols in Figure 3.1.) Then, σ is adjusted to give a good agreement at two points, slightly above and below the transition temperature but not in the regime where the helicity curve becomes horizontal. T_{**}^∞ and σ are varied until good agreement is found at all three points. To quantify the quality of the entire fit we number the experimental data points at different temperatures $i = 1, 2, ...$ Then we define as a measure of the quality

$$\varsigma^2 \equiv \sum_i \frac{(\langle\theta\rangle_{w,i} - \widehat{\theta}_i)^2}{\widehat{\theta}_i} \tag{3.4}$$

where the sum is over the experimental data points; $\widehat{\theta}_i$ is the mean helicity measured at these temperatures; $\langle\theta\rangle_{w,i}$ is the theoretical value of the mean helicity at the temperature corresponding to the data point i.

The quantity ς^2 is a weighted mean-square deviation and equals zero in the case of perfect agreement. Its form was chosen to attain a fit that is biased toward smaller values of the helicity, and as such takes relative errors, rather than absolute ones, into account. While a choice of $\widehat{\theta}_i^2$ in the denominator may seem more natural, this would overemphasize the

high-temperature part of the curve at the expense of the crossover region. Note that it is difficult to make a comparison between ς and standard quality parameters, since the value of ς can exceed unity for very poor fits. While the distinction between a good fit and a poor fit is rather arbitrary, based on our observations we define a poor fit to be any fit with $\varsigma > 0.3$ (see Figure 3.1 for examples of a good and a poor fit). The procedure of fitting and calculating the quality parameter was performed for all six cases, after which the values for the five experimental concentrations were averaged. The averaged values of T_{**}^{∞} and σ were used in the remainder of this chapter.

For the cases with helical ends (HH, HF and HN), a fit was first attempted for $\phi = 2.55 \cdot 10^{-4}$, but the helicity-temperature curves proved to be highly asymmetrical around the transition point $\langle \theta \rangle_w = \frac{1}{2}$ (see Figure 3.1), making it impossible to obtain a good agreement in both the high- and the low-temperature regimes. Typical values for the quality parameter fell between 0.55 and 0.60, indicating a poor curve fit. Due to the difficulty of these fits, we chose not to perform curve fits at other volume fractions, and we discarded these boundary conditions as candidates for good agreement with experiment.

Cases NF and NN gave good fits for all five concentrations (with $\varsigma = 0.13$ and $\varsigma = 0.16$ at $\phi = 2.55 \cdot 10^{-4}$) giving the average values $T_{**}^{\infty} = 300$ K and $\sigma = 1.5 \cdot 10^{-3}$, and $T_{**}^{\infty} = 301$ K and $\sigma = 9.3 \cdot 10^{-3}$, respectively. For the case FF it proved impossible to fit the $\langle \theta \rangle_w$ curve for all five concentrations, due to the insensitivity of this model to changes in σ (see Figure 2.2). To circumvent this problem a fixed value of σ of 10^{-3} was used and an attempt at a one-parameter fit was made, yielding the (rather low) average T_{**}^{∞} of 296 K. The quality parameter obtained for this fit was $\varsigma = 0.49$ from which we conclude that the FF boundary condition produces a poor agreement with the data (see also below).

For each set of boundary conditions we checked our manual fit with the help of a least-squares minimization procedure in Fortran 90 using the NAG library routine E04JYF, if only for a single concentration ($\phi = 2.55 \cdot 10^{-4}$). Routine C02AFF was used to determine the value of the fugacity z from the volume fraction. Note that this routine does not take into account the different weights given to the low- and high-temperature regime, i.e., in this procedure, all data points were treated equally. For the boundary conditions NN, HF, HH and HN, the routine suffered numerical difficulties, caused by the implicit nature of the dependence of the fugacity z on σ and T_{**}^{∞}, and the tendency of the algorithm to overshoot the upper bound of $z\lambda_+ < 1$. For the boundary condition NF the fitting procedure gave $\varsigma = 0.15$, which indicates that the manual fit and the numerical fit ($\varsigma = 0.13$) are close together. For the boundary condition FF, the least-squares algorithm showed similar difficulties in fixing σ as the manual procedure. The results for $\phi = 2.55 \cdot 10^{-4}$, $T_{**}^{\infty} = 297$ K and $\sigma = 10^{-8}$, yield a value for the quality parameter of $\varsigma = 0.36$, whereas the manual fit gave the value 0.49 (for $T_{**}^{\infty} = 297$ K and $\sigma = 10^{-3}$), indicating that a lower value for σ gives a somewhat better agreement, although neither approaches the quality of the curve provided by the boundary conditions NF and NN. See Figure 3.1 for a comparison between the manual fits for the cases NF ($\varsigma = 0.13$) and HF ($\varsigma = 0.59$) at the concentration $\phi = 2.55 \cdot 10^{-4}$.
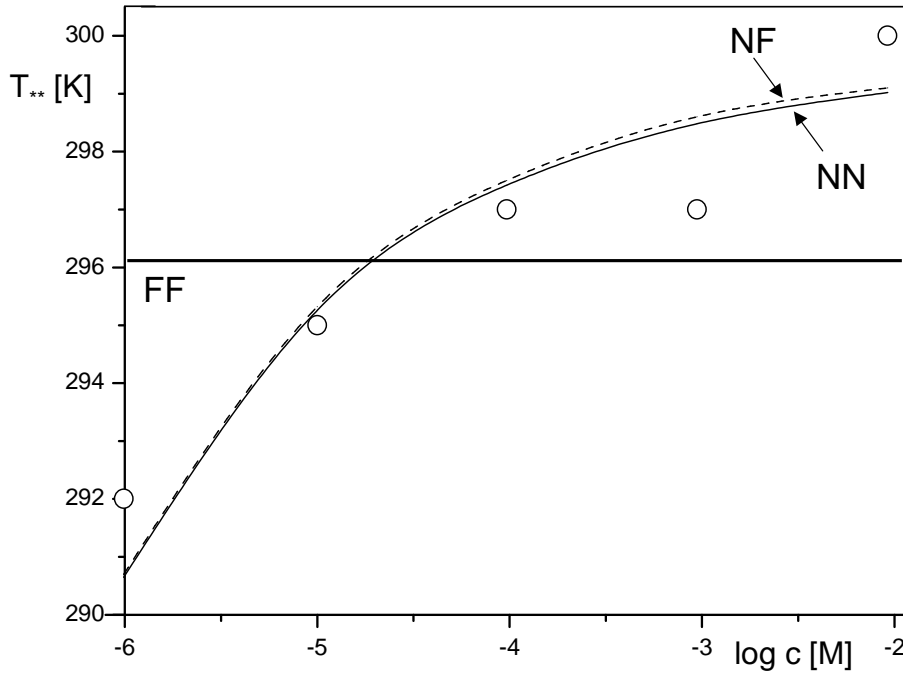
FIGURE 3.2: The helical transition temperature T_{**} in K versus the concentration in M of the discotic molecules in n-butanol. [9] The symbols represent the experimentally found values, the dashed line gives the results of the case NF, the drawn line that for case NN, and the thick line that for the case FF.

From the averaged values of T_{**}^{∞} and σ the concentration dependence of the helical transition temperature T_{**} was calculated. This we compared with experimental findings (see Figure 3.2). The agreement between theory and experiment for the case FF is poor, as the calculated helical-transition temperature for each concentration was found to be a constant $T_{**} = T_{**}^{\infty} = 296$ K. Both boundary conditions with non-helical ends (NF and NN) show quantitative agreement between theory and experiment, and any distinction between the two cases on these grounds is difficult. (The increase of the transition temperature with the concentration essentially shows that larger helical aggregates are more difficult to "melt" than smaller ones. A similar effect is seen in polymer crystals. [118]) Our fitting procedure has demonstrated that only these two boundary conditions can accurately describe the experimental measurements. Not only the $T_{**} - c$ curve (Figure 3.2) but also parameters such as η and $\langle \theta \rangle_w$, are insensitive to the change from model NF to NN. The only marked difference, as already expected from the scission energy, is in the predicted average size of the aggregates $\langle N \rangle_n$ shown in the inset to Figure 3.3, where the NN boundary condition predicts larger aggregates at low temperatures than does NF.

Unfortunately, the difference in aggregate size between the cases NF and NN is not large enough to distinguish between the two in a comparison with small-angle neutron scattering (SANS) data obtained on dilute solutions of the discotic molecules in n-butanol. [9, 119] See
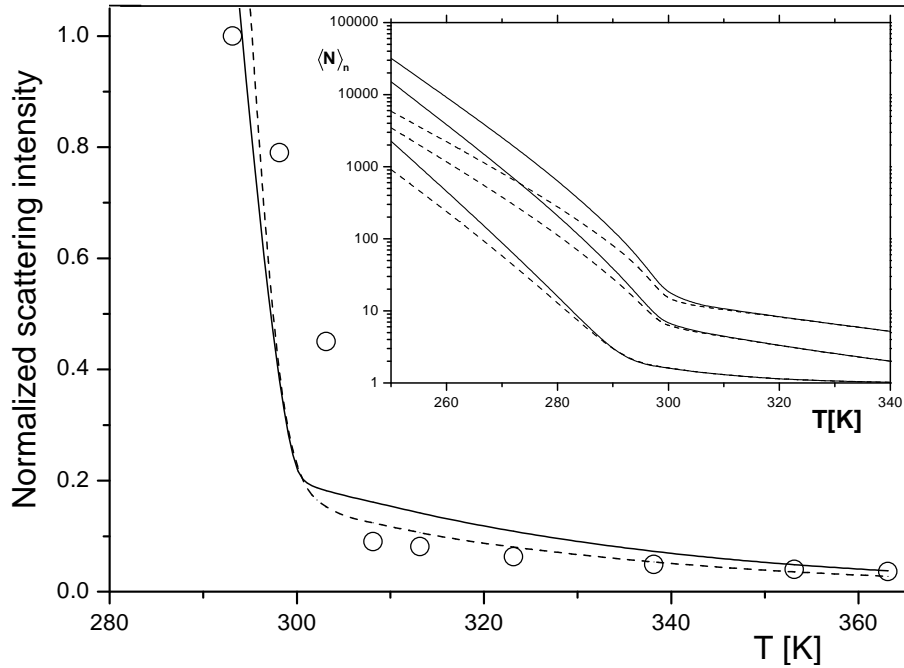
FIGURE 3.3:   Theoretical fits to the results of SANS measurements on the system of discotic molecules in n-butanol at a concentration of $2.39 \cdot 10^{-3}$ M. [119] On the vertical axis is the normalized scattering intensity, on the horizontal axis the temperature in K. The dashed line gives the weight-averaged aggregate size as a function of the temperature, rescaled to give the best possible fit, for the case NN. The drawn line gives the same for the case NF. In the inset: Theoretical values for the number-averaged aggregation number $\langle N \rangle_n$ as a function of the temperature in °C. The drawn line again indicates the case NN, the dashed line the case NF. The concentrations are $9.21 \cdot 10^{-3}$, $9.64 \cdot 10^{-5}$ and $9.89 \cdot 10^{-7}$ M, from top to bottom.

Figure 3.3. As a function of the temperature we show there a normalized SANS intensity divided by the volume fraction of dissolved material, known to be proportional to the weight-averaged aggregate size $\langle N \rangle_w = \phi^{-1} \sum_{N=1}^{\infty} N^2 \rho(N)$. Also shown are the predictions of this mean aggregate size for the two boundary conditions NN and NF as a function of temperature. For the theoretical curves shown in Figure 3.3 an unknown constant of proportionality between $\langle N \rangle_w$ and the normalized scattered intensity is adjusted to produce the best overlap with the data points. Both the theoretical predictions and the SANS data show a tendency of the aggregate size to steeply increase below T_{**}, indicating (as we also saw in Chapter 2) that the helical transition and the aggregate growth are indeed strongly coupled.
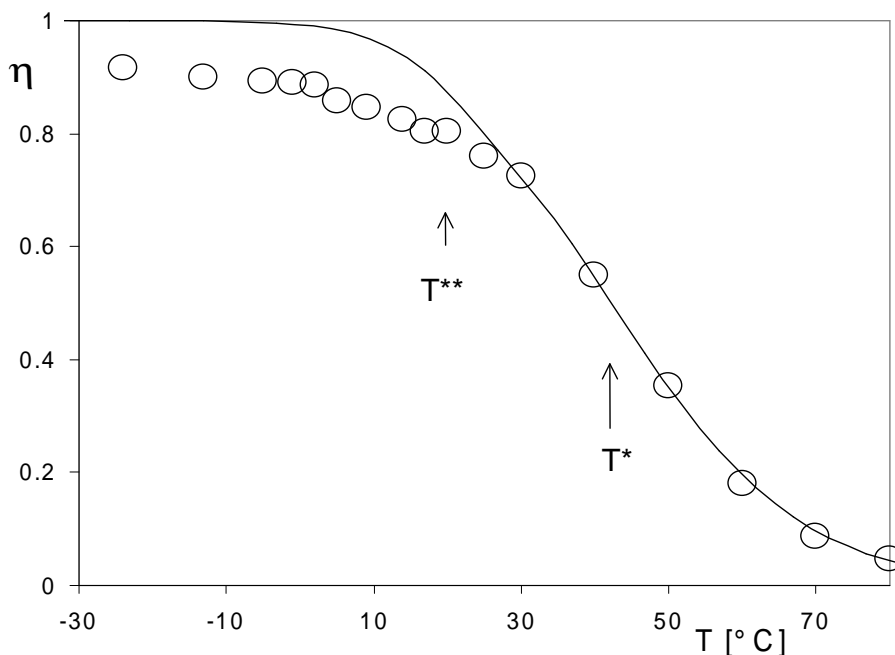
FIGURE 3.4: The fraction of molecules in the aggregated state as a function of the temperature T in degrees Celsius. The line gives the theoretical result, the symbols indicate the experimental data for the C_3 discotic in n-butanol at a concentration of $2.35 \cdot 10^{-6}$ M. [9] The arrows mark the helical-transition temperature T_{**} and the polymerization transition temperature T_*.

3.3 Comparison to Experiment of Boundary Condition NF

Since we have established that the models with boundary conditions NN and NF are the only ones that give an adequate description of the experiment, let us expand our comparison to experiment for one of these boundary conditions, being NF. We again use eqs (3.1)-(3.3) to make the temperature dependence explicit. For the values of the parameters T_{**}^{∞} and σ we used the manually fitted values of $T_{**}^{\infty} = 300.3$ K and $\sigma = 1.5 \cdot 10^{-3}$. These averaged values were inserted into eqs (3.2) and (2.18)-(2.21) to produce the theoretical curves for the various concentrations.

In Figure 3.4 we compare the measured temperature dependence of the fraction of aggregated material with what we find from the theory for the concentration of $2.35 \cdot 10^{-6}$ M. The fraction of aggregated material was deduced from time-resolved fluorescence spectroscopy. [9] Indicated in the Figure is the earlier-quoted polymerization temperature of $T_* \approx T_*^0 = 316$ K for the concentration $2.35 \cdot 10^{-6}$ M. For high temperatures the agreement between the theoretical and the experimental curves is excellent. Below $T_{**} \approx 292$ K, also
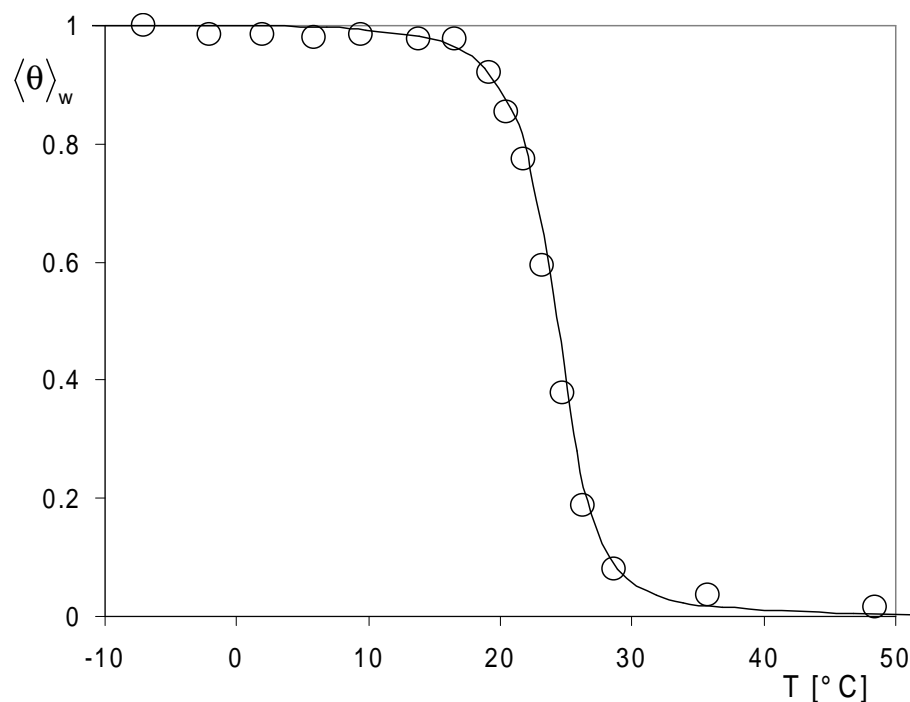
FIGURE 3.5:   Mean helicity as determined by circular-dichroism measurements as a function of temperature T for a concentration of $9.64 \cdot 10^{-5}$ M of the C_3 discotic in n-butanol. [9] The drawn line is the theoretical prediction, the symbols are the experimental results.

indicated in the Figure, theory and experiment appear to diverge. As was discussed already by van der Schoot and collaborators, [24] the divergence may be due to the interpretation of the experimental data, where the possible difference in electronic states of the molecules between a helical aggregate and a non-helical aggregate was not taken into account. [9] We therefore believe the apparent discrepancy at low temperatures to be unimportant.

Figure 3.5 gives the temperature dependence of the average fraction $\langle\theta\rangle_w$ of intermolecular bonds in the helical state for the concentration of $9.64 \cdot 10^{-5}$ M, as obtained by circular-dichroism (CD) spectroscopy. The reason the CD signal corresponds to a weight average, as opposed to a number average, is that both the weight average and the intensity of a CD signal are proportional to the number of helical bonds present in the system. Also indicated is the theoretical fit of $\langle\theta\rangle_w$, which was calculated in a slightly different manner than described earlier, in that monomers and dimers were ignored whereas earlier they were taken into account. The definition of the mean helicity in which we ignore monomers and dimers corresponds more closely to what is experimentally determined. In the interpretation of the experiments the maximum mean fraction of helical bonds, found at low temperatures, was set equal to unity. Thus, there is a difference between the experimental and theoretical maximum helicity: the experimental maximum helicity corresponds to the
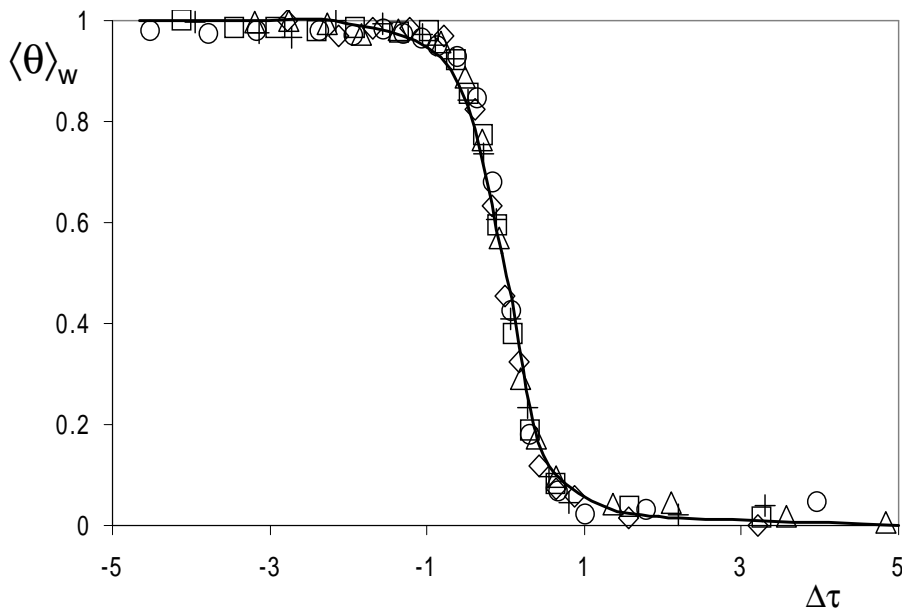
FIGURE 3.6: The calculated mean fraction of helical bonds of the C_3 discotic in n-butanol, $\langle\theta\rangle_w$, as a function of a reduced temperature $\Delta\tau \equiv -\left.\partial\langle\theta\rangle_w/\partial T\right|_{T_{**}}(T - T_{**})$, for concentrations ranging from 10^{-2} to 10^{-6} M. The thick line gives the theoretical master curve, whereas the symbols give experimental results for five concentrations.

situation at low temperatures (when there are still monomers and non-helical aggregates and parts of aggregates present), whereas the theoretical maximum helicity corresponds to the (unrealistic) situation where all molecules in solutions are present in helical aggregates. The agreement between theory and experiment is remarkably good for all concentrations in the range from 10^{-2} to 10^{-6} M (results not shown for all concentrations). Indeed, the theory provides a quantitative description of the experimental data.

As is shown in Figure 3.6, the theoretical helicity curves follow the same scaling as the experimental data (indicated with symbols) were found to obey [24]. Indeed, all predicted curves collapse onto a single master curve (indicated by the thick line) if we follow the same prescription as was used in the paper of van der Schoot et al. [24] and rescale the temperature such that $\Delta\tau \equiv -\left.\partial\langle\theta\rangle_w/\partial T\right|_{T_{**}}(T - T_{**})$, where we read off the slope of the helicity curve at T_{**} from the theoretical curves. The circumstance that the helicity curves conform to a simple scaling function implies that, for the material discussed, the difference in concentration merely shifts T_{**} - albeit in a non-trivial manner. In the ground-state approximation the shape of the curve is only a function of h_h and T_{**}; [24] apparently this remains true in our theory.

We summarize our comparison to experiment in Figure 3.7 by giving a diagram of states in terms of the concentration and temperature. Indicated are the theoretical predictions
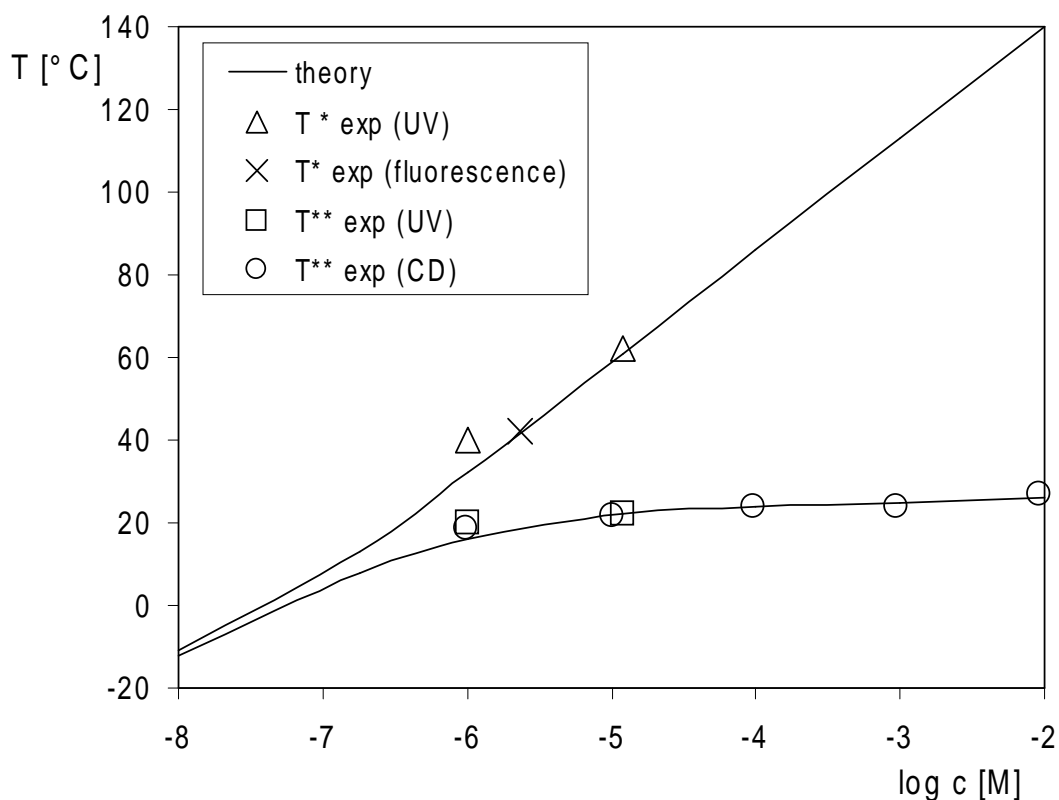
FIGURE 3.7:   Diagram of states in terms of the temperature in °C and solute concentration in M. The symbols indicate experimental results, as indicated, the lines indicate the conditions where the helical (bottom) and polymerization (top) transitions take place.

of the transition temperatures T_* and T_{**} as a function of the overall solute concentration. The advantage of this diagram is that we can now immediately compare the theory to the experimental results obtained with different techniques, including UV spectroscopy, circular-dichroism spectroscopy and time-resolved fluorescence spectroscopy. The agreement between experiment and theory is good, and the same two regimes as in Figure 2.3 can again be observed.

3.4   Discussion and Conclusions

The agreement between theory and experiment shows that our view of the linear self-assembly in dilute solution of a class of chiral materials exhibiting a potentially cooperative conformational transition is accurate. We can conclude that at high temperatures the molecules aggregate into short, polymeric assemblies in which they retain a relatively large amount of configurational freedom. Upon lowering the temperature, the aggregates

undergo the transition to a helical state of definite handedness; they, loosely speaking, "crystallize internally". The free-energy gain associated with the transition to the helical state causes a growth spurt of the aggregates at low temperatures which sets in around the helical-transition temperature (as is shown in Figure 3.3 and the insets of Figures 2.5-2.7). As it turns out, due to its strong cooperativity, the transition from the random to the helical state can occur over a very small temperature range. As a result of the coupling between growth and the helical transition, there exist two regimes. In one the helical transition and the polymerization are separated and in another they coincide.

Our theory gives for the co-operativity parameter σ of the C_3 discotic in n-butanol a value of $1.5 \cdot 10^{-3}$, more than ten times smaller than was found within the ground-state approximation. [24] This amounts to a doubling of the interfacial free energy between helical and non-helical stretches along a chain, from 1.6 $k_B T$ to 3.2 $k_B T$ per molecule. Apparently, the helical transition of the material is much more co-operative than previously thought, although still not as co-operative as the helix-coil transition of, for instance, the conventional polymer poly(γ-benzyl-L-glutamate), for which $\sigma \simeq 2.4 \cdot 10^{-4}$. [36]

Out of the six possible boundary conditions, only two describe the experimental data of Brunsveld and co-workers quantitatively. These two (imposing one or two non-helical ends) can, in principle, be distinguished by the growth of the assemblies with changing temperature. Unfortunately, while some SANS data is available for the low-temperature regime where the differences between the two boundary conditions are expected to be largest, interpretation of these results is difficult due to the impact of interactions between the assemblies on the scattered intensity for the low temperatures. [24] As a result, we are unable to distinguish between the two boundary conditions based on currently available experimental data. Since the diameter and height of the C_3 discs are approximately known, it is possible to determine for which values of ϕ and $\langle N \rangle_n$ there will be discrepancies between our theory and the experimental results. We find that interaggregate interactions will only play a role for concentrations exceeding 10^{-2} M, and then only at temperatures below approximately 0 °C. Obviously, there may be systems for which ring-closure and interaction are important. In those cases excluded-volume effects between randomly oriented stacks of discs can be included in a simple mean-field way for concentrations up to the close packing regime. [60] We deal with effects of this kind in Chapter 7.

Of the different boundary conditions that fail to describe the experimental data, the failure of the model with free ends FF is perhaps the most surprising. Its poor agreement with experiment stems from the circumstance that the model with free ends is able to generate both fully helical and non-helical aggregates, that is, to achieve any value of the mean helicity, without forming any helical-non-helical interfaces. This causes the equilibrium (lowest free energy) state to be one of separate helical and non-helical aggregates. The condition $\langle \theta \rangle_w = \frac{1}{2}$ then corresponds to a state of affairs where there is no preference for the formation of a helical or a non-helical bond, in other words, to $s = 1$. So, independent of concentration (contrary to experimental observation), the helical transition occurs when $s = 1$. From standard Zimm-Bragg theory we know that this corresponds to the case of

infinite aggregate length, so for free boundary conditions T_{**} equals T_{**}^{∞}, since finite-size effects have no impact on T_{**}. We conclude that the boundary condition FF is apparently not applicable to the system of Brunsveld et al.

Chapter 4

Amplification of Chirality in Helical Supramolecular Polymers: the Sergeants-and-soldiers Principle in Long Chains

ABSTRACT

We theoretically study the sergeants-and-soldiers principle of chirality amplification in self-assembled, *supramolecular* helical polymers, and show that a mapping is possible on a two-component Ising chain, in which one of the components has a spin of fixed orientation. The relative abundance of this component is regulated by a chemical potential. Our theory quantitatively describes recently published measurements of the optical activity of linear assemblies of certain discotic molecules in solution. We find that the strength of the chirality amplification depends strongly on the strength of the coupling between the spins, which translates into a free-energy penalty put on a helix reversal along the backbone of the self-assembled polymer.

4.1   Introduction

It is well known that the handedness of helical homopolymers is determined by chiral centers, present either in the backbone or in side groups. Polymers that contain no chiral centers can be helical too, but by symmetry cannot, in the mean, display a preferred handedness. [17] If sufficiently long, such polymers consist of left-handed and right-handed helical regions of variable length, which are in principle in dynamic equilibrium with each other. The mean length of these regions is determined by the free-energy cost of a helix reversal. [20] The larger this free-energy cost, the larger the (mean) distance between helix reversals.

In this context, it is perhaps not entirely surprising that the copolymerization of a small amount of homochiral monomeric units with achiral material can have a disproportionately large effect on the net handedness of a helical polymer. [17, 20, 42] This expresses itself in an optical activity of the polymer that increases highly non-linearly with the relative amount of homochiral material. Indeed, it is often seen that only a few percent of chiral material is necessary to attain the maximal Cotton effect, a phenomenon usually referred to as the 'sergeants-and-soldiers' principle. [40] The chiral monomers (the 'sergeants') direct the configuration of the achiral ones (the 'soldiers') near to them over a distance that is set by the free-energy penalty of a helix reversal. [41]

The sergeants-and-soldiers principle of copolymers as well as other types of chirality amplification have been the topic of much experimental [17, 40, 42, 120] and theoretical [20, 41, 121, 122] work. The theories, which make use of quite diverse theoretical tools, reproduce available experimental data often quantitatively, and confirm the important role of helix reversals. [20, 41] They also show that in the long-chain limit, chirality amplification becomes independent of the molecular weight of the polymer. [20, 121]

Recently, it has become evident that chirality amplification is not restricted to conventional polymers. Meijer and coworkers observed a large sergeants-and-soldiers effect in solutions of *supramolecular* polymers, [18, 19] i.e., polymer-like aggregates formed through the linear self-assembly of monomeric units. In our view, this is remarkable, because we would expect the monomer-monomer distance in these relatively weakly bound assemblies to be larger than in conventional polymers, and therefore any chiral interaction between them to be weak. In clear contrast to this naive expectation, we observe that the strength of the sergeants-and-soldiers effect in these aggregates is in fact quite high, and comparable to that in some conventional polymers.

Unfortunately, available theoretical methods aimed at describing the sergeants-and-soldiers effect in conventional polymers cannot be applied to supramolecular polymers (at least not in principle). The reason is that in supramolecular polymers the monomeric and polymeric states are in thermodynamic equilibrium, leading to an equilibrium distribution of the chiral and achiral components along the chains, whereas in conventional polymers this distribution is fixed. In this work we set up a minimal theory that specifically describes chi-

rality amplification of the sergeants-and-soldiers type in helical supramolecular polymers, and that is able to deal with this equilibrium distribution of chiral and achiral monomers.

As it turns out, the same physical principles regulate this type of chirality amplification in both types of polymer, provided they are long enough. The advantage of our theory is that it is analytical and exact in the infinite-chain limit, unlike current theories for conventional copolymers that either require input from numerical simulations or involve approximations to describe the chirality amplification. In addition, our theory also allows for a simple determination of the free energy associated with a helix reversal from experimental data.

The experiments of Meijer and co-workers [18, 19] point at the existence of two regimes, one where the sergeants-and-soldiers effect is virtually independent of the concentration and one where this is not so. According to the standard theory of linear self-assembly, the mean molecular weight of supramolecular polymers grows with the square root of the concentration. [24] This implies that in the former regime the sergeants-and-soldiers effect is independent of the molecular weight, and that the long-chain limit applies. For the latter regime, it follows that the sergeants-and-soldiers effect does depend on the mean length of the aggregates and that the self-assembly and chirality amplification are strongly coupled. For reasons of simplicity, we focus in this Chapter on the long-chain limit, where the self-assembly is enslaved by the configurational statistics of the aggregates. [24] The other limit, in which the self-assembly and the configurations of the chains are coupled, requires a much more elaborate theoretical description that we deal with in Chapter 5.

The remainder of the Chapter is structured as follows. In section 4.2 we outline our theory for the amplification of chirality in supramolecular polymers in terms of a one-dimensional, two-component Ising model. We present an implicit expression for the relative difference between the numbers of left- and right-handed helical bonds as a function of the fraction of chiral molecules in the chain and of the free energy of a helix reversal. Next, in section 4.3, we solve this implicit expression numerically and present the results of our calculations. The fraction of chiral material needed to almost completely suppress the handedness incompatible with the structure of the chiral monomers turns out to be roughly equal to the Boltzmann factor associated with a helix reversal. We confront our theory with experimental data of mixtures of chiral and achiral discotic molecules in water, obtained by means of circular-dichroism spectroscopy. [18] For comparison, we also fit our theory to optical-activity measurements on solutions of a conventional polymer. [40, 41] In both cases, we get excellent agreement, although our theory should not hold for conventional polymers. Finally, we present our conclusions in section 4.4.

4.2   Theory

We consider a dilute solution of helical supramolecular polymers, allowing us to disregard interaggregate interactions. The aggregates are thought to be sufficiently rigid to make long-range intra-aggregate interactions such as those of the excluded-volume type unimportant. They consist of two types of monomer, one chiral and one achiral. Presuming the direct interactions of monomers along the chain to be short-ranged, we can rely on a one-dimensional, two-component Ising model [123] to accurately describe the conformational properties of these aggregates. Note that similar models have been applied in the past to describe amplification of chirality in conventional polymers. [20, 41, 121] As we already briefly discussed in section 4.1, the difference with the earlier work is that for a supramolecular polymer the distribution of the two components over the one-dimensional lattice is not fixed, but is an equilibrium property. While the configurations of both types of polymer can (if only in principle) be described with the same model Hamiltonian, the methods of calculation of various average quantities are different. [82]

The model we use bears a close resemblance to mixed one-dimensional lattice fluids with Ising interactions. [34, 124, 125] In the work of Leung and co-workers [34] and that of Chiang and co-workers [125] both components can take the spin values ± 1. In the work of Kawatra and co-workers, [124] one component is spinless, while the other can again take the spin values ± 1. In contrast, the sergeants-and-soldiers experiment is most naturally described by letting one of the components have a spin of a fixed value equal to either $+1$ or to -1, and the other take both the values ± 1.

Let us for simplicity first deal with helical aggregates consisting only of achiral monomers, which we can treat with the simple (slightly modified) one-component Ising model. (Later on we introduce the second, chiral, component that acts like an instantaneous, localized magnetic field to which the first component couples.) In our description, we assign a spin of $+1$ to a helical bond of one handedness and a spin of -1 to one of the opposite handedness. For reasons to become clear below, we impose an external magnetic field that couples to the spins and shifts the balance between the "up" and "down" spins. Obviously, in zero magnetic field, both spins are equally probable, irrespective of any (finite) coupling between them. [82]

The dimensionless Hamiltonian of the model of an aggregate consisting of N monomers (linked by $N-1$ bonds) reads (see also eq (2.4))

$$H = \frac{1}{2}R\sum_{j=1}^{N-2}\left(-s_j s_{j+1} + 1\right) + \frac{1}{2}P\sum_{j=1}^{N-1}\left(s_j + 1\right) - E(N-1) \tag{4.1}$$

Here, $R \geq 0$ is the usual coupling constant between neighboring spins, representing the free-energy penalty on a helix reversal. P is the dimensionless magnetic-field strength, and corresponds to the excess free energy associated with a bond of one handedness over the other. The free energy of the reference bond we set equal to $-E$. The prefactors of

one-half in front of the first two terms in eq (4.1) are present to avoid the double counting of the contributions of the "up" spins and that of the interfaces between "up" and "down" spins.

From the Hamiltonian in eq (4.1), we determine the (canonical) partition function $Q(N)$ of an aggregate. This can be done exactly with the well-known transfer-matrix method. [1] In the large-aggregate regime, $N \gg 1$, $Q(N)$ can be simplified considerably by applying the so-called ground-state approximation, which retains only the largest eigenvalue of the transfer matrix. This gives [24, 32]

$$Q(N) = \sum_{s_1=\pm 1} \cdots \sum_{s_{N-1}=\pm 1} \exp(-H) \approx A(s,\sigma)\lambda^N \exp E(N-1) \qquad (4.2)$$

with $A(s,\sigma)$ a prefactor that we need not specify, containing contributions that are non-extensive in the aggregate size and that depend on the boundary conditions (see Chapter 2). [126] In equation (4.2), $\lambda = \frac{1}{2} + \frac{1}{2}s + \frac{1}{2}\sqrt{(s-1)^2 + 4\sigma s}$ is the largest eigenvalue of the transfer matrix with $s \equiv \exp -P$ the Boltzmann factor of an "up" spin and $\sigma \equiv \exp -2R$ the square of the Boltzmann factor of a helix (or spin) reversal. The latter functions as a cooperativity parameter: the smaller σ, the larger (in effect) the distance over which spins influence each other and the sharper the magnetization curve. The mean distance between helix reversals (a correlation length) is given by $N(1 - \partial \ln Q/\partial R)^{-1}$ and can be calculated from eq (4.2). Here the derivative $-\partial \ln Q/\partial R$ gives the number of helix reversals, so that the number of regions into which the helix reversals divide the aggregate is $1 - \partial \ln Q/\partial R$.

Note that by symmetry, the relevant case for a polymer consisting solely of achiral monomers is that where $s = 1$, since achiral monomers have no preference for either helical handedness. For this value and in the limit $N \gg \sigma^{-1/2}$, the distance between helix reversals is equal to $1 + \sigma^{-1/2}$, as follows by simple insertion. [32] It is easily seen that the distance between helix inversions becomes large for small σ.

Formally, the ground-state result of equation (4.2) is valid only for $N \gg 1$ (and exact in the limit $N \to \infty$), but it may be extrapolated down to $N > 2$. This is sensible as long as the mean aggregate size, $\langle N \rangle \simeq \sqrt{\phi A^{-1}(s,\sigma) \exp E}$, obtainable by inserting eq (4.2) into the standard theory of linear self-assembly, remains large. [24] Here, ϕ is the volume fraction of aggregating molecules and $E - \ln A(s,\sigma)$ assumes the role of an energy associated with two aggregate ends (the so-called end-cap or scission energy). See, e.g., reference [24] for a discussion of this energy. The prefactor $A(1,\sigma)$ for $s = 1$ becomes a constant equal to 2 if both aggregate ends are free to assume a right- or left-handed conformation. Since in the long-chain limit the mass distribution of the aggregates is peaked around $N = \langle N \rangle$, we need not explicitly deal with the self-assembly. Hence, from now on we imply the aggregation number N to represent its (concentration and temperature dependent) mean value $\langle N \rangle$.

In order to obtain the net magnetization (or net helicity, which we define as the difference between the fractions of right- and left-handed helical bonds), we first calculate the fraction

of "up" spins, $\theta_+ = -N^{-1} \partial \ln Q / \partial P$. We find

$$\theta_+ = 1 - \theta_- = \frac{1}{2} + \frac{s-1}{2\sqrt{(s-1)^2 + 4s\sigma}} \tag{4.3}$$

independent of $\langle N \rangle \gg 1$, with θ_- the fraction of "down" spins. The net magnetization per site η (or the net helicity per bond) is a measurable quantity (at least in principle) and is defined as the difference between the fractions of "up" and "down" spins,

$$\eta \equiv \theta_+ - \theta_- = 2\theta_+ - 1 \tag{4.4}$$

Obviously, for our achiral polymers, $s = 1$ so $\eta = 0$; η can only become larger than zero if we add chiral material. Note that this η is not the same parameter as studied in Chapters 2 and 3.

We now consider the case that there are two types of monomer present, chiral and achiral. This changes the above equations in a number of ways. First, based on the idea that chiral monomers have a distinct preference for a certain handedness and achiral ones do not, we arbitrarily define that a chiral monomer is always followed by an "up" spin, whereas an achiral monomer can be followed by either spin. Obviously, the free energy of a "down" spin following a chiral monomer can also have a finite value, rather than the infinite value we impose in our description. We choose to forbid such a "mismatch" configuration in order to avoid having to introduce another parameter in our model, thus keeping the number of model parameters to a bare minimum. In section 4.3, we discuss the impact of a finite free-energy penalty in some detail.

The dimensionless Hamiltonian H' for the copolymer becomes

$$H' = \frac{1}{4}R\sum_{j=1}^{N-2}\left(-\frac{n_j+1}{s_j+n_j} \cdot \frac{n_{j+1}+1}{s_{j+1}+n_{j+1}} + 1\right)^2 + \frac{1}{2}P\sum_{j=1}^{N-1}\left(\frac{n_j+1}{s_j+n_j} + 1\right) - E(N-1) \tag{4.5}$$

where $n_j = 1$ corresponds to a chiral particle, and $n_j = 0$ to an achiral one. It is easily checked that for an achiral aggregate, for which $n_j = 0$ for all j, eq (4.5) reduces to eq (4.1), because the equalities $s_j^{-1} = s_j$ and $s_j^2 = 1$ hold in our case. Here, we have assumed that the interaction parameters R and P (and therefore also the corresponding free energies) are identical for bonds following chiral and achiral molecules. Note that our Hamiltonian H' is constructed such that all configurations in which a "down" spin follows a chiral monomer are completely suppressed, giving a Boltzmann weight that is exactly zero.

Because the composition of an aggregate of N molecules can vary, it makes sense to invoke a quasi-grand canonical ensemble rather than the canonical ensemble we used for the single-component aggregate. The associated quasi-grand partition function $\Xi(N)$ can be written as

$$\Xi(N) = \sum_{s_1=\pm 1} \cdots \sum_{s_{N-1}=\pm 1} \sum_{n_1=0,1} \cdots \sum_{n_N=0,1} \exp\left(-H' + \mu\sum_{j=1}^{N} n_j + \mu_0 N\right) \tag{4.6}$$

Here, μ is a dimensionless excess chemical potential of the chiral component, and μ_0 is the reference chemical potential of all assembling monomers. Despite the apparent difference between the canonical and quasi-grand canonical partition functions, eqs (4.2) and (4.6), $\Xi(N)$ can be written in the same form as the earlier-discussed $Q(N)$. We only have to replace the Boltzmann factor s by an appropriately modified one, s', due to the presence of the chiral component. Using the Hamiltonian eq (4.5), we can formally derive an expression for this modified Boltzmann factor with the aid of the transfer-matrix method, giving exactly $s' = s(1 + \exp\mu)$, where s retains its previous meaning as the Boltzmann factor of an "up" spin over a "down" spin.

That we merely need to replace s by $s(1 + \exp\mu)$ can also be seen from the following simple probability considerations. One has to realize that the quantity s' may be seen as the (unnormalized) probability that a randomly chosen spin along the chain is in an "up" conformation. For the mixed system, this probability is equal to the sum of the probability of an "up" conformation following a chiral monomer (which occurs with a probability dependent on its chemical potential), and that of an "up" conformation following an achiral monomer.[1] Whence, the total unnormalized probability for a random spin to have an "up" configuration must indeed be $s' = s(1 + \exp\mu)$.

We now impose, as discussed earlier, the condition that achiral molecules should have no preference for spin "up" or spin "down", by putting $s = 1$ (or $P = 0$). In other words, $s' = 1 + z$ with $z \equiv \exp\mu$ a fugacity that determines the fraction of chiral monomers in the chain. Replacing s by s' in eqs (4.3) and (4.4) we conclude that the net magnetization per site must equal

$$\eta = \frac{z}{\sqrt{z^2 + 4(z+1)\sigma}} \tag{4.7}$$

For aggregates composed entirely of achiral monomers, $z \to 0$ so $\eta \to 0$; "up" and "down" conformations are then equally likely. For fully chiral aggregates, $z \to \infty$ and $\eta \to 1$. In the ground-state approximation, the mean aggregate size $\langle N \rangle$ is enslaved by quantities such as z and η that describe the conformational state, and is only very weakly dependent on them. In this case the conformational transition and the aggregate growth are virtually independent, so we need not discuss this issue any further.

The fraction of chiral material in the aggregates, x, can be calculated directly from eq (4.6). From standard statistical mechanics we know that $x = N^{-1}\partial \ln \Xi(N)/\partial\mu$. This gives

$$x = \frac{(\eta + 1)z}{2(1 + z)} \tag{4.8}$$

which is exact in the limit of infinite aggregates. Substituting eq (4.7) into eq (4.8) we deduce that x can be expressed as a function only of z and σ. We can eliminate z, and

---

[1]This argument does not apply to conventional polymers. Since the order of their monomers is fixed, the probability of the presence of a chiral monomer is not dictated only by its excess chemical potential.

obtain an implicit expression for η as a function of x,

$$x = (\eta + 1)\frac{\sigma\eta^2 + \eta^2\sqrt{\sigma\eta^{-2} + \sigma^2 - \sigma}}{1 - \eta^2 + 2\sigma\eta^2 + 2\eta^2\sqrt{\sigma\eta^{-2} + \sigma^2 - \sigma}} \qquad (4.9)$$

It turns out to be useful to define a quantity x_* as the fraction chiral material needed to induce one-half of the maximum attainable helicity, $\eta = 1/2$. From eq (4.9) we find that

$$x_* = \frac{3}{2}\frac{\sigma + \sqrt{3\sigma + \sigma^2}}{3 + 2\sigma + 2\sqrt{3\sigma + \sigma^2}} \approx \frac{1}{2}\sqrt{3\sigma} \qquad (4.10)$$

for $\sigma \ll 1$. Equation (4.10) provides an convenient way to directly obtain the free energy of a helix reversal from experiment.

In experiment one measures an optical effect that depends on the total amount of helical material in a probe volume. This in turn depends, e.g., on the optical path length, the concentration of dissolved material and the optical properties of the molecules. To account for this we introduce a constant of proportionality α that links the theoretical and experimental optical effects. Furthermore, the contributions to the optical effect from the two types of monomer in a helical aggregate may be unequal in magnitude, and we also need to account for that. We do this by defining the ratio γ between these contributions for a chiral and an achiral monomer, and assigning this weight to each bond that follows a chiral monomer, the fraction of which is $z(z+1)^{-1}$. The fraction of bonds that follow an achiral monomer equals $(z+1)^{-1}$, and to these we assign the weight 1. The measured net helicity denoted by η' is thus in our description given by a linear superposition of the two weights, and may be expressed as

$$\eta' = \alpha\eta\left[1 + (\gamma - 1)\frac{z}{z+1}\right] \qquad (4.11)$$

The roles of σ and γ are discussed in the next section, where we also make a comparison to experimental data.

4.3   Results and Discussion

To illustrate how cooperativity influences the amount of chiral material needed to (almost) completely suppress left- or right-handed helical configurations in initially achiral supramolecular chains, we have plotted eq (4.11) in Figure 4.1 for $\alpha = \gamma = 1$. It clearly shows that the smaller σ is, the less chiral material is needed to achieve the same net helicity. This can in fact also be deduced directly from eq (4.10) that gives x_* as a function of σ. Note that in the limit $\sigma \to 1$ there is no amplification of chirality, and chiral and achiral monomers behave as a simple mixture with $\eta = x$.
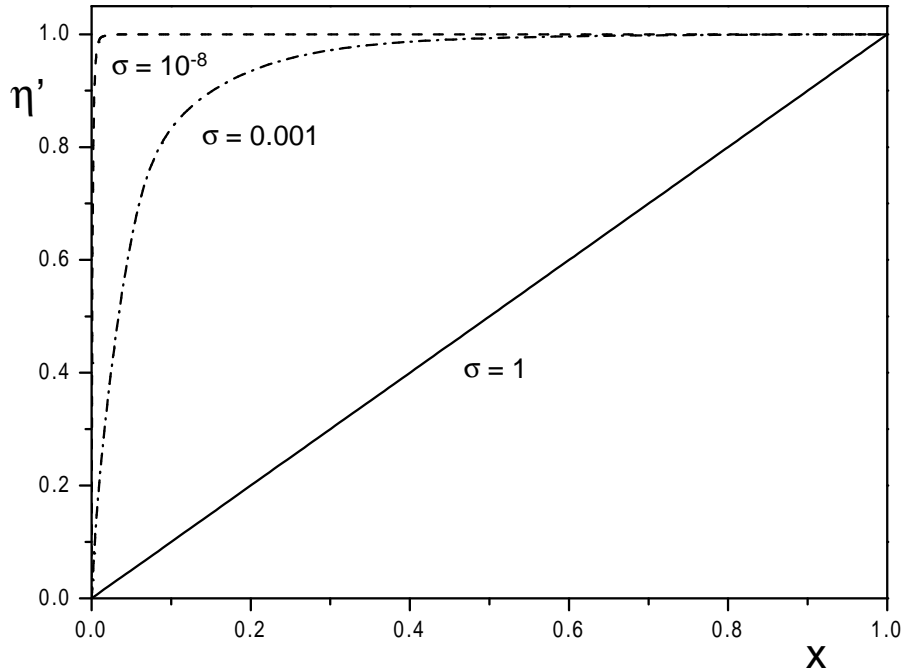
FIGURE 4.1: The net helicity η' as a function of the fraction of chiral material x, for $\alpha = \gamma = 1$ and three values of the cooperativity parameter: $\sigma = 1$ (solid line), $\sigma = 10^{-3}$ (dot-dash line) and $\sigma = 10^{-8}$ (dashed line).

Note further that, in our model, a fully chiral aggregate cannot exhibit helix reversals, so $\eta \to 1$ for $x \to 1$ for all values of σ. This, obviously, is an approximation. To allow for mismatches, i.e., configurations in which a "down" spin follows a chiral monomer, we can include a finite free-energy penalty U. If we do this, however, we find that $\sigma \to \sigma/(1-u)^2$, with $u \equiv \exp -U$ the Boltzmann weight of the mismatch energy, at least for conditions where U exceeds the helix reversal penalty, and $\sigma \ll 1$ (this being the limit most interesting from an experimental perspective). In other words, the mismatch energy only renormalizes the free energy of a helix reversal in this case. This means that the value of σ that we obtain from fits to experiment is the actual value of $\exp -2R$ only if $u \ll 1$, and an effective one otherwise. It does not seem possible to disentangle u and σ experimentally, and obtain the actual σ from the effective one. However, if we estimate that $-U$ is of the order of the bond energy (which is typically between -10 and -20 $k_B T$ for this type of system [24]), u is indeed much smaller than unity, and the value of σ we obtain will be close to the actual helix-reversal penalty.

The effect of the optical parameter γ on the net helicity is shown in Figure 4.2, for the case where $\alpha = 1$. While for low fractions of chiral material η' is insensitive to γ, for high fractions it displays a maximum if $\gamma < 1$. This is because chiral molecules have a lower contribution to the overall optical effect than do achiral ones if $\gamma < 1$. At fixed α, a further decrease of γ decreases the height of this maximum and moves it to lower x. For $\gamma > 1$
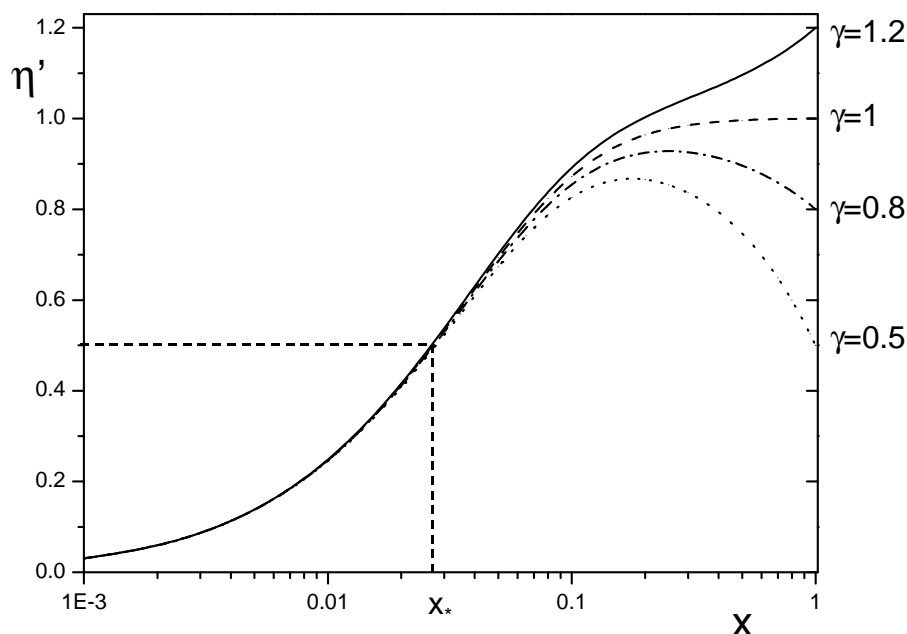
FIGURE 4.2:   The net helicity η' as a function of the fraction of chiral material x at $\sigma = 10^{-3}$, for four values of the ratio γ between the contributions to the helicity of the chiral and achiral components. The solid line gives $\gamma = 1.2$, the dashed line $\gamma = 1$, the dot-dash line $\gamma = 0.8$, and the dotted line $\gamma = 0.5$. The fraction chiral material giving a net helicity of half its maximum value x_* is indicated for $\gamma = 1$.

(when chiral molecules have a larger contribution to the optical signal than achiral ones) the curve continues to rise, even when the bare helicity has saturated at $x < 1$. This could lead to difficulties if interpreting experimental results, since one could erroneously draw the conclusion that the maximum helicity has not yet been reached, when in fact it has. Note that the approximate equation (4.10) can still be used to fix the cooperativity parameter σ even if $\gamma \neq 1$, since x_* is insensitive to the precise value of γ if the cooperativity is sufficiently large.

We now confront the prediction of our theory with experimental data [18] on a certain type of discotic molecule that we refer to for brevity as 'C$_3$ discotic', dissolved in water. These molecules have a molecular weight of about 3400 gmol^{-1} and consist of aromatic cores, surrounded by nine polar side chains. [9] They self-assemble into helical aggregates in polar solvents under suitable conditions. Brunsveld et al. [18] synthesized versions of the discotic molecules with chiral and achiral side chains (see Figure 1.1 for the structure of the chiral version of the discotic), and performed circular-dichroism measurements on mixtures of these components at the overall concentrations of 10^{-4} M and 10^{-5} M in water at 5 °C. They observed a large sergeants-and-soldiers effect, remarkable not only due to the fairly weak bonds between monomers discussed earlier, but also because the chiral groups
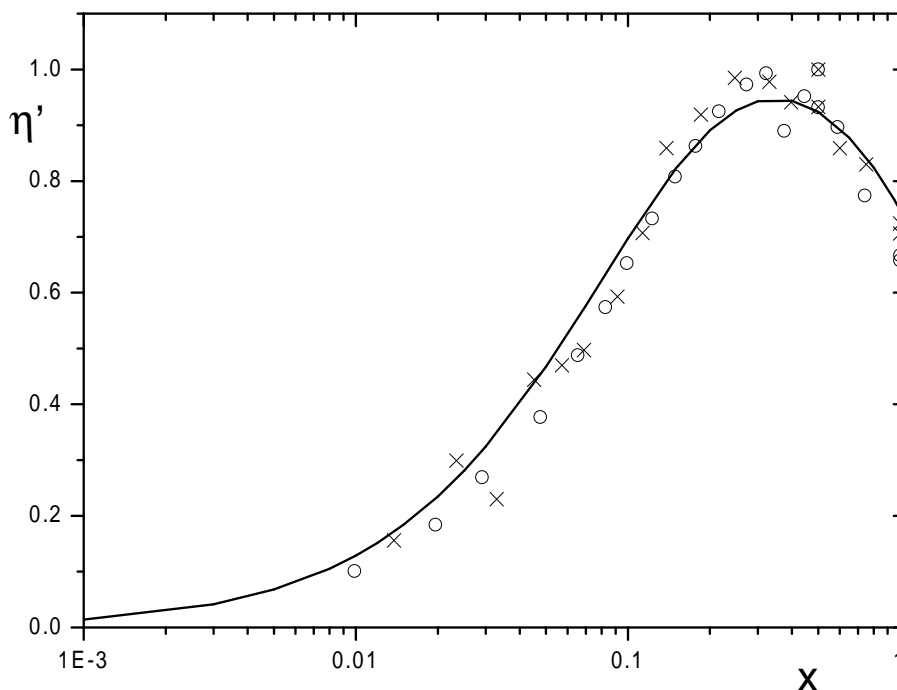
FIGURE 4.3:   The net helicity η' versus the fraction of chiral material x (line). Symbols: experimental data of Brunsveld et al. at two concentrations. (Circles: 10^{-5} M, crosses 10^{-4} M). Line: fitted curve with the optimal fitting parameters $\sigma = 6.4 \cdot 10^{-3}$, $\gamma = 0.65$, $\alpha = 1.15$.

are located in the flexible side chains of the molecules, far from the core which is the main interacting part of the molecule.

Brunsveld et al. [18] observed that the chirality amplification in water was concentration independent, at least for the two concentrations at which they performed the measurements. As explained in section 4.1, this implies that finite-size effects should not play a role and that our ground-state theory may be used to describe their data. Furthermore, the differences between the chiral and achiral molecules are so small, being a single methyl group on each side chain of the discotic molecules, that we expect that our assumption of equal binding strengths of the chiral and achiral units is justified. It was also observed that the maximum Cotton effect occurs at a fraction chiral material $x < 1$, suggesting that γ must be smaller than unity. This occurrence of a maximum was attributed in reference [18] to a difference in packing between the chiral and achiral molecules due to the presence of the methyl groups in the side chains of the chiral molecules.

In our comparison with the experimental data we fit our theory to the intensity of the Cotton effect at a wavelength of 336-341 nm, divided by the absorption, as a function of the fraction of chiral component. We set the maximum in the measured value of this quantity equal to unity, and use the net helicity η' as defined in eq (4.11) as its theoretical

equivalent. The fitting procedure requires the fixing of the cooperativity parameter σ, the parameter α introduced in eq (4.11), and the ratio of the contributions to the helicity of chiral and achiral monomers γ. One of these we determine independently from the other two. In the small-x regime, the helicity is virtually independent of γ, and we fit this part of the curve with a single parameter, namely σ. To this end, we locate the experimental value for x_*, and fix the value of σ (with $\gamma = \alpha = 1$) at $\sigma = 6.4 \cdot 10^{-3}$. Using this value, we are able to describe the low-x part of the curve, but not the maximum that occurs in the high-x regime. We fit this part with the two remaining parameters γ and α, and find good agreement between theory and experiment if we set $\alpha = 1.15$ and $\gamma = 0.65$ (see Figure 4.3).

The value of σ we find corresponds to a helix-reversal energy of 2.5 $k_B T$, indicating a high degree of cooperativity. This free-energy penalty for a helix reversal is in fact of the same order of magnitude as those found in certain classes of polyisocyanates discussed in the next paragraph. It is also similar to the interfacial penalty between helical and non-helical regions in aggregates of the chiral C_3 discotic in a different solvent that we found in a previous study (see Chapter 2). [127] As discussed earlier, we indeed find that a value of $\gamma < 1$ is necessary to describe the maximum found in experiment. This lends support to the suggestion of Brunsveld et al. that packing effects cause this maximum. [18]

For comparison, we also fit our theory to optical-activity measurements of copolymers of (R)-2,6-dimethylheptyl isocyanate and *n*-hexyl isocyanate in chloroform at temperatures of -20 and $+20$ °C, [40, 41] although, as mentioned in section 4.1, our theory is strictly not applicable to this type of (conventional polymeric) system. Again we rescale the experimental data (given as the specific rotation versus the mole fraction of chiral monomers) to give unity at the maximum in the curve, and again we determine σ from x_*. We now find $\sigma = 3.1 \cdot 10^{-4}$ for $T = -20$ °C and $\sigma = 1.2 \cdot 10^{-3}$ for $T = 20$ °C. Because the maxima in the curves for the isocyanate copolymers occur at relatively high x, quantitative agreement is found already in this regime for a one-parameter fit involving only γ, where α is kept at a value of unity. The curve fit shown in Figure 4.4 uses the values $\gamma = 0.94$ for $T = -20$ °C and $\gamma = 0.96$ for $T = 20$ °C.

The values of σ we find are in close agreement with values Selinger and Selinger[2] obtained from a fit of both their approximate theory and computer simulation to the same optical-activity measurements on the polyisocyanate system. It seems that $\sigma = \exp -2R$ is temperature dependent, which is what we expect if the dimensionless helix reversal free energy R were enthalpy dominated. Is that the case, then from thermodynamics it follows that the ratio of the values of R taken at temperatures T_1 and T_2 obeys $R_2/R_1 \simeq T_1/T_2$, which relation is indeed obeyed for the values of R found here.

The reason why our theory is able to describe the polyisocyanate experiments is difficult to understand and deserves further study. Naively, one could speculate that the distribution

---

[2] Selinger et al. [41] used a helix reversal energy of 4.2 $k_B T$ for their best fit to experiment. We find 4.0 $k_B T$ for $T = 253$ K and 3.4 $k_B T$ for $T = 293$ K, which values correspond well to that used by Selinger.
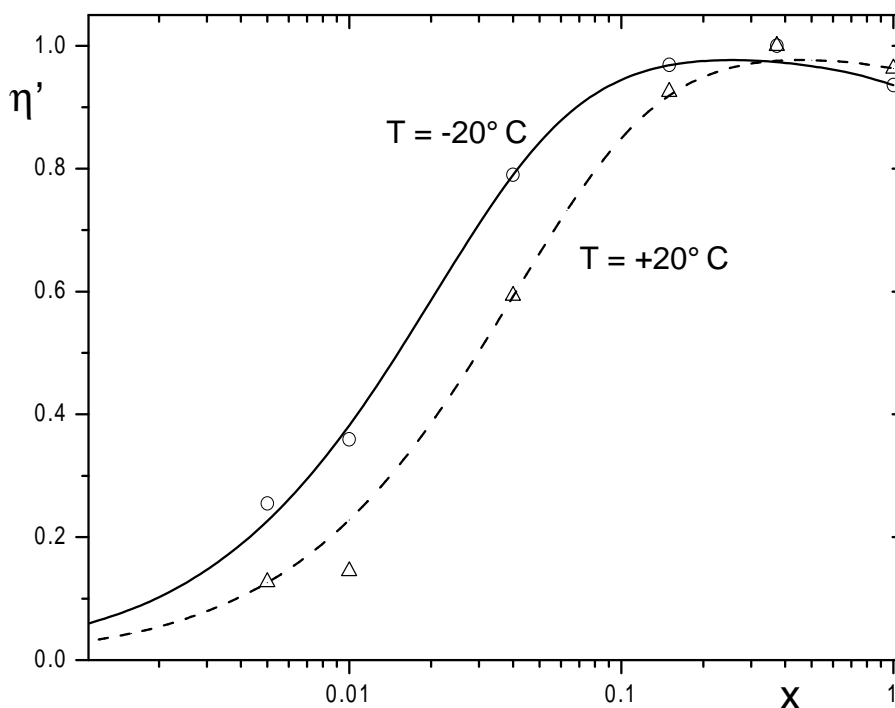
FIGURE 4.4:   Fit of the theoretical net helicity η' versus x (line) to experimental data of Green et al. at two temperatures. Dashed line (theory) and triangles (experiment): $T = 20\ °C$, with fitting parameters $\sigma = 1.2 \cdot 10^{-3}$ and $\gamma = 0.96$. Solid line (theory) and circles (experiment): $T = -20\ °C$, with fitting parameters $\sigma = 3.1 \cdot 10^{-4}$ and $\gamma = 0.94$.

of chiral monomers in the aggregates is similar to that in conventional random copolymers when their fraction is small (i.e., very much smaller than one per bare correlation length). In this case the locations of the chiral monomers within an aggregate are uncorrelated, and truly random. However, this can no longer be the case when the fraction of chiral monomers is not small, and we should therefore expect to see a marked difference between the results for fixed and equilibrium randomness outside of the small-x limit. It may well be that the agreement we observe is merely coincidental. However, we find that our theory is also able to quantitatively fit experimental measurements of the optical activity of a whole range of other copolymers. [42, 120, 128] In addition to giving experimental results, the authors of reference [128] used the approximate theory of Selinger and Selinger [41] to fit two sets of optical-activity measurements. Our values of R show a reasonable agreement with those obtainable from these fits.

It appears that for the problem studied here, the distinction between an equilibrium type of disorder and a fixed type of disorder is not as large as often thought. From a pragmatic point of view, one may perhaps use our theory even for conventional copolymers,

since it gives good agreement with measurements on such polymers, and it is perhaps less cumbersome in its application than existing theories. [20]

4.4   Conclusions

The two-component Ising model outlined here provides a quantitative description for the sergeants-and-soldiers principle in self-assembled ("living") polymers, provided they are long enough so that the self-assembly is enslaved by the conformational statistics of the chains. We find that the free-energy penalty associated with a helix reversal is central to the description of the chirality amplification. In this our findings resemble earlier work on conventional ("dead") copolymers. [20, 41] Our analytical theory is exact in the infinite-chain limit, and quantitatively describes the Cotton effect as measured by circular dichroism spectroscopy in dilute aqueous solutions of the molecules we refer to as the C_3 discotic, for two concentrations that differ by a factor of ten. We are able to reproduce the experimentally observed maximum in the Cotton effect versus chiral content by following up a suggestion of Brunsveld et al., [18] and assuming a different contribution to the measured helicity of the chiral and achiral monomers. For reasons unclear at this point, our theory also quantitatively describes the sergeants-and-soldiers effect in several conventional copolymers.

Chapter 5

The Sergeants-and-Soldiers Principle in Chains of any Length

ABSTRACT

The optical activity of helical homopolymers devoid of chiral centers increases drastically when a small amount of homochiral monomers is incorporated into them. We study this so-called sergeants-and-soldiers effect of chirality amplification in solutions of helical supramolecular polymers with a theoretical model that bears a strong resemblance to a one-dimensional, two-component Ising model. We showed in the last Chapter that, in the limit of very long self-assembled helical polymers, the strength of the sergeants-and-soldiers effect depends strongly on the free energy of a helix reversal, and less so on the concentration of aggregating material. In this Chapter we study the chirality amplification outside the long-chain limit, and find the reverse, that is, a strong concentration dependence and a weak dependence on the helix-reversal energy. Our theory quantitatively describes recently published circular-dichroism measurements on mixed aggregates of some discotic molecule in the solvents water and n-butanol, at two different overall concentrations.

5.1   Introduction

Many biological and synthetic molecules polymerize into helical chains. [1] In mixtures of homochiral and achiral versions of such materials, the polymers formed typically display a larger Cotton effect than one may expect from the fraction of chiral material they contain. [17, 20] This so-called sergeants-and-soldiers type of chirality amplification [40] is due to a cooperative shift in the balance between the numbers of right-handed and left-handed helical bonds, caused by the influence the chiral monomers have on the conformation of nearby achiral monomers. This effect has been observed both in conventional polymers, [17, 40, 42, 120, 129] which have a fixed length and composition, and in supramolecular polymers, [18, 19, 111] for which the length and composition are equilibrium properties. That a strong sergeants-and-soldiers effect is indeed observed in the latter system is quite remarkable because supramolecular polymers are in a way fragile, involving relatively weak, reversible bonds.

The sergeants-and-soldiers principle in conventional polymers has been studied theoretically by several authors. [41, 121, 122] (For a recent review paper on this topic, see [20].) From these treatments it becomes clear that the strength of the chirality amplification depends strongly on the free-energy penalty of a helix reversal and on the degree of polymerization. In the long-chain limit the dependence on the chain length disappears, [20, 121] and the strength of the chirality amplification depends only on the free energy of the helix reversal. The larger this free-energy penalty, the larger the number of achiral monomers that are affected by the insertion of a single homochiral monomer, and the stronger the chirality amplification.

The sergeants-and-soldiers effect has only recently been discovered in supramolecular polymers, [18, 19, 111] and attempts to describe it theoretically have been few in number. [111] The usefulness of these treatments is limited, however, as they are either valid only in the long-chain regime (see the previous Chapter), or invoke a mean-field approximation that is difficult to justify due to the essentially one-dimensional character of the problem. [111] In this Chapter we outline an approach that improves upon the earlier work by describing the sergeants-and-soldiers principle in supramolecular polymers beyond the long-chain limit and outside of the mean-field approximation as regards the configurational statistics of the chains. We find, in accordance with recent experimental measurements, [18, 19] and contrary to what is known for conventional polymers, that there are (at least) two regimes: one where the chirality amplification depends on the overall monomer concentration, and one where this is not so. We argue that, because the mean degree of polymerization of supramolecular polymers is roughly proportional to the square root of the solute concentration, [24, 58, 66, 67] the concentration dependence of the chirality amplification in this type of polymer is actually a chain-length dependence similar to that found in conventional polymers. The problem in hand should therefore be accurately described by combining the usual theory of equilibrium polymerization with a non-mean-field description of the con-

formational state of the polymers. Comparison with experimental results shows that our treatment is indeed a sensible one. For the long-chain limit, we recover the result obtained in Chapter 4, and we predict that outside of this limit the sergeants-and-soldiers effect becomes more strongly dependent on the concentration and less so on the free-energy cost of a helix reversal.

The remainder of this Chapter is organized as follows. In section 5.2 we outline a model that describes chirality amplification in a helical chain, based on the two-component Ising chain, and calculate the partition function of such a chain. In section 5.3, we apply this partition function in the classical theory of equilibrium polymerization, and derive a formal expression for the average difference between the number of right-handed and left-handed helical bonds per unit mass (the so-called mean net helicity) as a function of the overall concentration of solute molecules, the free energy of aggregation, the fraction of homochiral monomers, and the free-energy cost of a helix reversal. Next, in section 5.4, we show how the mean net helicity responds to changes in these parameters, and discuss the various regimes and trends that appear. Here, we focus on the dependence of the net helicity on the solute concentration and on the free-energy penalty of a helix reversal. In section 5.5, we compare our results to those obtained from circular-dichroism measurements on mixtures of chiral and achiral discotic molecules in the solvents n-butanol and water. [18, 19] The agreement between our theory and these experiments is quite good. Finally, in section 5.6, we present our conclusions.

5.2   The Single-Aggregate Partition Function

We again consider a dilute solution of polydisperse aggregates that we presume rodlike, so that we may ignore both interaggregate and long-ranged intra-aggregate interactions. The aggregates consist of two types of monomer, homochiral and achiral. If we assume that the direct interactions along the main axis of an aggregate are short-ranged, we can describe the conformational state of this aggregate with a one-dimensional, two-component Ising model. [34, 123, 124, 125] We treat the bonds between monomers as spins that can have a value of ± 1, corresponding to a right- or left-handed screw sense. Given the strong preference of chiral molecules for a certain helical handedness, we force any bond following a chiral molecule to have a fixed spin value of $+1$.

Obviously, the free-energy penalty of a "down" spin (with a spin value of -1) following a chiral monomer can also be given a finite value, rather than being fixed at infinity as we do here. However, this would introduce an additional parameter in our model that somehow needs to be fixed in any comparison to experiment. This is problematic for a number of reasons (see Chapter 4), the most important one being that it can be shown that the introduction of this additional parameter merely renormalizes other parameters

we already use in our description, at least in the double limit where the cooperativity is high and moreover the additional energetic parameter exceeds the free energy of a helix reversal, which is the most interesting regime. As we argued in Chapter 4, it suffices to fix the bond type following a chiral molecule to describe the essential physics of the problem. In effect, we ignore helix reversals in all-chiral aggregates.

Let N denote the number of monomers that comprise the aggregate. In accordance with the above arguments, our model Hamiltonian reads (cf. eq (4.5))

$$H = \frac{1}{4} R \sum_{i=1}^{N-2} \left(-\frac{n_i+1}{s_i+n_i} \cdot \frac{n_{i+1}+1}{s_{i+1}+n_{i+1}} + 1 \right)^2 + \frac{1}{2} P \sum_{i=1}^{N-1} \left(\frac{n_i+1}{s_i+n_i} + 1 \right) - E(N-1) \quad (5.1)$$

provided $N \geq 3$. For $N = 1$, we have $H \equiv 0$, whereas $H = \frac{1}{2} P \left(\frac{n_1+1}{s_1+n_1} + 1 \right) - E$ for $N = 2$. In eq (5.1), $s_i = \pm 1$ gives the state of the ith spin along the chain, and n_i describes the chirality of the ith monomer, with $n_i = 0$ for an achiral monomer, and $n_i = 1$ for a chiral one. The parameter $R \geq 0$ is the usual coupling constant between neighboring spins, which corresponds to the free-energy penalty on a helix reversal between achiral monomers. The quantity P is, in Ising terms, the dimensionless magnetic-field strength, and represents the excess free energy associated with a bond of one handedness over the other. The bare energy of a bond we set equal to $-E$; it determines the a priori propensity of the monomers to form aggregates. (These free energies, and indeed all energies in this Chapter, are again given in units $k_B T$.) Note that the Hamiltonian eq (5.1) is constructed in such a way that any configuration that contains a spin i with a value of $s_i = -1$ following a chiral molecule $(n_i = 1)$ is completely suppressed.

From the Hamiltonian eq (5.1) we can formally write down the quasi-grand partition function of an aggregate, in which the composition of the aggregate can change but its total length is fixed at N monomers, as

$$\begin{aligned}
\Xi(N) &= \left(\prod_{k=1}^{N} \sum_{n_k=0,1} \right) \exp \left[\mu_0 \left(N - \sum_{i=1}^{N} n_i \right) + \mu_1 \sum_{i=1}^{N} n_i \right] \\
&\quad \times \left(\prod_{j=1}^{N-1} \sum_{s_j=\pm 1} \right) \exp -H
\end{aligned} \quad (5.2)$$

Here, the two bracketed terms in front of the exponentials denote repeated sums, and μ_0 and μ_1 in the exponential are the chemical potentials of the achiral and chiral molecules. The transfer matrix method presents an elegant way to simplify the partition function eq

(5.2), [1] giving

$$
\begin{aligned}
\Xi(N) \;=\; & \left(\prod_{k=1}^{N} \sum_{n_k=0,1} \right) \exp\left[\mu_0 \left(N - \sum_{i=1}^{N} n_i \right) + \mu_1 \sum_{i=1}^{N} n_i \right] \\
& \times \left(\mathbf{u} \cdot \prod_{i=2}^{N-1} \mathbf{M}_{n_i} \cdot \mathbf{u}^+ \right) \exp E(N-1)
\end{aligned}
\tag{5.3}
$$

The matrix $\mathbf{M}_{n_i}$ contains the (unnormalized) probabilities that a particular type of bond follows another bond along the chain. For our two-component system, we define two matrices, $\mathbf{M}_0$ and $\mathbf{M}_1$, one to describe the statistical weights for a bond following an achiral monomer and one to describe those for a bond following a chiral one. Note that the first bond of the aggregate is not included in the matrix multiplication, as it does not follow a preceding bond. This bond is instead described by the end vector $\mathbf{u}^+$, while $\mathbf{u}$ describes the other aggregate end; $\mathbf{u}^+$ and $\mathbf{u}$ depend on the boundary conditions imposed (see Chapter 2). [126]

The statistical weights for the matrices $\mathbf{M}_0$ and $\mathbf{M}_1$ can be obtained from eq (5.1) by standard methodology. [82] They read

$$
\mathbf{M}_0 = \begin{pmatrix} 1 & \sqrt{\sigma} \\ \sqrt{\sigma}s & s \end{pmatrix} \text{ and } \mathbf{M}_1 = \begin{pmatrix} 0 & 0 \\ \sqrt{\sigma}s & s \end{pmatrix}
\tag{5.4}
$$

Here, $s \equiv \exp{-P}$ is the Boltzmann factor of a spin with value $+1$ over one with a value -1, and $\sigma \equiv \exp{-2R}$ is the square of the Boltzmann factor of a spin (or helix) reversal; these factors are taken to be independent of the type of monomer present. (Note that the quantities s and σ have similar meanings as in the well-known theory of Zimm and Bragg for the helix-coil transition in polymers. [36])

Further simplification is possible, if we define an excess chemical potential $\mu \equiv \mu_1 - \mu_0$ that couples to the chiral content, and a reference chemical potential μ_0 that couples to the total mass incorporated into assemblies. Eq (5.3) then simplifies to

$$
\Xi(N) = \exp\left[\mu_0 N + E(N-1) \right] \tilde{\mathbf{u}} \cdot \mathbf{M}^{N-2} \cdot \tilde{\mathbf{u}}^+,
\tag{5.5}
$$

which can be obtained by absorbing the excess-chemical-potential term into $\mathbf{M}_{n_i}$, factorizing the summations and evaluating each term separately. $\mathbf{M}$ is the sum of the contributions of chiral and achiral monomers, and reads

$$
\mathbf{M} = \mathbf{M}_0 + z\mathbf{M}_1 = \begin{pmatrix} 1 & \sqrt{\sigma} \\ \sqrt{\sigma}s(1+z) & s(1+z) \end{pmatrix} \equiv \begin{pmatrix} 1 & \sqrt{\sigma} \\ \sqrt{\sigma}s' & s' \end{pmatrix}
\tag{5.6}
$$

where $z \equiv \exp\mu$ is a fugacity linked to the total amount of chiral material in the solution and $s' \equiv (1+z)s$ can be loosely labeled as the overall preference for one handedness over the other in a mixed aggregate. For the end vectors $\tilde{\mathbf{u}}$ and $\tilde{\mathbf{u}}^+$ we write

$$
\tilde{\mathbf{u}} = \begin{pmatrix} 1+z, & 1+z \end{pmatrix} \text{ and } \tilde{\mathbf{u}}^+ = \begin{pmatrix} 1 \\ s' \end{pmatrix}
\tag{5.7}
$$

assuming free ends; we do not enforce a restriction to a particular conformation for the aggregate ends, because there is no reason to assume that either aggregate end will prefer a right- or left-handed helical conformation. Note also that, upon going from $\mathbf{u}^+$ to $\tilde{\mathbf{u}}^+$ (and $\mathbf{u}$ to $\tilde{\mathbf{u}}$), we have absorbed the term from eq (5.3) describing the chemical potential of the first and last monomers of the chain into the end vectors.

The partition function can now be calculated by matrix multiplication, and takes the form

$$\Xi(N) = \frac{z_0^N(1+z)\exp{-E}}{(\lambda_1-\lambda_2)\sqrt{\sigma}}[(\lambda_1-1+\sqrt{\sigma})(1-\lambda_2+s'\sqrt{\sigma})\lambda_1^{N-2}$$
$$+(\lambda_2-1+\sqrt{\sigma})(\lambda_1-1-s'\sqrt{\sigma})\lambda_2^{N-2}] \tag{5.8}$$

Here, $z_0 \equiv \exp[\mu_0 + E]$ is again a fugacity, and $\lambda_{1,2} = \frac{1}{2} + \frac{1}{2}s' \pm \frac{1}{2}\sqrt{(s'-1)^2 + 4\sigma s'}$ are the eigenvalues of the transfer matrix (with λ_1 defined by the $+$ sign, and λ_2 by the $-$ sign). Strictly speaking, this partition function is only valid for $N > 2$, however, inserting $N = 2$ gives the correct result, $\Xi(2) = z_0^2 \exp{-E}(1+z)(1+s')$. For $N = 1$, we put $\Xi(1) \equiv z_0(1+z)\exp{-E}$. In Chapter 4, we discarded the contribution proportional to λ_2^{N-2}, and in doing so neglected finite-size effects; this reduces the partition function to a single term, which greatly facilitates further calculations. Here we keep both terms, since we are interested in the influence of finite-size effects on the chirality amplification. We may simplify eq (5.8) by noting that, by symmetry, a right-handed and left-handed bond are equally likely for the achiral species, and set $s = 1$, and thus $s' = 1 + z$. However, for reasons to become clear shortly, we choose not to do this yet.

Note that the model we use is not symmetrical, i.e., that a bond following a chiral monomer is treated differently from one preceding the same monomer. We feel it is justified to use this model, however, since a helix is inherently directional and is, therefore, an asymmetrical structure. Nonetheless, it is easy to adapt our model to enforce symmetry between bonds preceding and following a chiral monomer: instead of forbidding only "down" spins following a chiral monomer, we then also forbid the occurrence of a helix reversal at this monomer. In that case both the bonds before and after the chiral monomer must be in the same configurational state, i.e., "up". This changes the transfer matrix $\mathbf{M}$ to

$$\mathbf{M} = \begin{pmatrix} 1 & \sqrt{\sigma} \\ \sqrt{\sigma}s & s \end{pmatrix} + z\begin{pmatrix} 0 & 0 \\ 0 & s \end{pmatrix} = \begin{pmatrix} 1 & \sqrt{\sigma} \\ \sqrt{\sigma}s & s(1+z) \end{pmatrix} \tag{5.9}$$

This adjustment of the theory turns out not to give any significant change in the results for the chirality amplification, at least for small σ. Since the small-σ regime is of the most interest to us, we consider it justified to use the theory as outlined above.

5.3 The Mean Net Helicity of a Solution of Aggregates

Now that we have established the partition function of a single aggregate, let us investigate how this affects the mean net helicity of a solution of polydisperse, self-assembled aggregates. In experiment, this net helicity expresses itself as an optical activity.

From the theory of equilibrium polymerization [58, 66, 67] we can find that, within a saddle-point approximation for the size distribution of the aggregates, the grand potential per unit volume of a solution of self-assembled polymers reads

$$\Delta\Omega = \sum_{N=1}^{\infty} \rho(N)[\ln \rho(N) - 1 - \ln \Xi(N)]. \tag{5.10}$$

Here, $\rho(N)$ is the dimensionless number density of aggregates of size N. The equilibrium size distribution can be calculated by minimizing $\Delta\Omega$ with respect to $\rho(N)$. This gives

$$\rho(N) = \Xi(N) \tag{5.11}$$

Using the equilibrium size distribution, we can calculate the mean net helicity, defined as the difference between the number of right- and left-handed helical bonds averaged over all monomers present in the aggregated state,

$$\langle\eta\rangle \equiv -1 + \frac{2}{\phi - \rho(1)} \sum_{N=2}^{\infty} \rho(N) \frac{N}{(N-1)} \frac{\partial \ln \Xi(N)}{\partial \ln s'} \tag{5.12}$$

with ϕ the total volume fraction of aggregating molecules

$$\phi \equiv \sum_{N=1}^{\infty} N\rho(N), \tag{5.13}$$

which we keep constant. Note that monomers are not taken into account in the definition (5.12), because they contain no bonds. The overall fraction of chiral monomers in the solution can be calculated from

$$x \equiv \frac{1}{\phi} \sum_{N=1}^{\infty} \rho(N) \frac{\partial \ln \Xi(N)}{\partial \ln z} \tag{5.14}$$

and the mean aggregate size is again defined as

$$\langle N \rangle \equiv \frac{\phi}{\sum\limits_{N=1}^{\infty} \rho(N)} \tag{5.15}$$

We now plausibly assume, as discussed earlier, that achiral monomers have no preference for a left- or right-handed conformation and set $s' = 1 + z$, i.e., $s = 1$. This reduces the eigenvalues of the transfer matrix $\mathbf{M}$ to

$$\lambda_{1,2} = 1 + \frac{1}{2}z \pm \frac{1}{2}\sqrt{z^2 + 4\sigma(1 + z)}. \tag{5.16}$$

After this substitution is made, we can express the mean net helicity in terms of z, σ, ϕ, E and μ_0 using eq (5.8) and eqs (5.10-5.12).

To determine the mean net helicity as a function of the fraction of chiral material, we fix z and numerically determine the value of the fugacity z_0 by inserting eqs (5.8) and (5.10) into eq (5.12), performing the sum and solving the resulting equation for a fixed value of the dimensionless quantity $\phi \exp E$. Here, ϕ is the overall volume fraction of aggregating molecules, and $-E$ and is the earlier-introduced bare bond energy. This gives six possible solutions for z_0. To determine which is the physically relevant one, we take into account the following. First, since μ_0 and E are real numbers, z_0 must be non-negative and real. Second, for the sum in eq (5.12) to converge, $z_0\lambda_1$ must be smaller than 1 for all compositions of the polymers. This means that $z_0 < 1$, since $\lambda_1 \geq 1$. In all the cases we investigated, this reduces the number of physically relevant solutions to one. With σ, z_0 and z known, we can now calculate the mean net helicity and the corresponding fraction of chiral material by simple insertion. The entire "magnetization" or helicity diagram, giving $\langle \eta \rangle$ as a function of the fraction of chiral material x, can be obtained by using different values of z and repeating the calculation.

5.4   Results

In the previous Chapter, we showed that, provided the supramolecular polymers are very long, the strength of the sergeants-and-soldiers effect is strongly dependent on the value of the cooperativity parameter σ (and hence on the free energy of a helix reversal), and independent of the concentration of assembling molecules. As we show next, for chains that are not very long, the reverse is true, and the net helicity does become a function of the overall volume fraction of assembling monomers ϕ.

We identify three regimes, one where the chains are long, one where the chains are in some sense short, and a monomeric regime where the concept of chirality amplification becomes meaningless. It turns out that a natural way to quantify and distinguish these regimes is by considering not the mean aggregation number $\langle N \rangle$, but one scaled to a correlation length, so that one counts the number of correlation lengths in an aggregate, rather than the number of monomers.

Let ξ_0 denote the "bare" correlation length, i.e., the mean distance between helix reversals in an infinite aggregate that does not contain any chiral material. (Obviously,

the actual correlation length depends on the aggregation number and the chiral content of the chain.) This bare correlation length is given by $\xi_0 \equiv (-\partial \ln \lambda_1 / \partial R)^{-1}$, with $\lambda_1 = 1 + \frac{1}{2}z + \frac{1}{2}\sqrt{z^2 + 4\sigma(1+z)}$ the largest eigenvalue of the transfer matrix, cf. eqs (5.8) and (5.16). We find $\xi_0 = 1 + \sigma^{-1/2}$, which reduces to $\xi_0 \approx \sigma^{-1/2}$ if $\sigma \ll 1$, i.e., if the cooperativity is high. The relevant control parameter determining the relative size of the assemblies is now $\xi_0^{-2}\phi \exp E$, since the "bare" degree of polymerization obeys $\langle N \rangle_0 = \frac{1}{2} + \frac{1}{2}\sqrt{1 + 4\phi \exp E} \sim \sqrt{\phi \exp E}$, at least for $\langle N \rangle \gg 1$. [24] Here, the bare degree of polymerization is defined as the mean number of monomers of an all-chiral aggregate. As we shall see below, $\langle N \rangle \approx \langle N \rangle_0$, i.e., the actual degree of polymerization is quite close to the bare one, meaning that the presence of a second type of monomer does not significantly affect the mean aggregate size.

In the top graph of Figure 5.1 we plot curves of constant mean net helicity $\langle \eta \rangle = 0.1$, 0.3, 0.5, 0.7 and 0.9 as a function of the control parameter $\xi_0^{-2}\phi \exp E$ and the fraction of chiral material x, for a fixed degree of cooperativity $\sigma = 10^{-3}$. Three regimes can be distinguished, indicated with Roman numerals in the Figure. These are (I) the "long-chain regime", where $\phi \exp E \geq \xi_0^2$, (II) the "short-chain regime", where $1 \leq \phi \exp E \leq \xi_0^2$, and (III) the "monomer regime", for which $\phi \exp E \leq 1$. In the long-chain regime the sergeants-and-soldiers effect is (virtually) independent of the concentration: the curves become vertical in this regime. In the short-chain regime there is a strong decrease in the chirality amplification as the concentration decreases, because the relative amount of chiral material needed to attain a given net helicity increases with decreasing concentration. The monomeric regime, where the curves become vertical again (indicating concentration independence) is uninteresting, for in this regime we cannot speak of a polymerized state.[1] It follows from Figure 5.1 that in experiment the values of certain parameters cannot be obtained from the chirality amplification in all three regimes. In the long-chain regime for instance, one cannot determine $\langle N \rangle$ from the measured net helicity, whereas the shorter the chains become (regimes II and III), the more difficult it becomes to fix σ. It is therefore necessary to obtain results for the relationship between $\langle \eta \rangle$ and x in at least two regimes to determine both parameters, or to fix $\langle N \rangle$ in an independent experiment (e.g., in a light-scattering experiment).

The impact of the degree of cooperativity (that is a function of the free-energy cost of a helix reversal) on the strength of the chirality amplification is shown in the bottom part of Figure 5.1. Here we have indicated the fraction of chiral material needed to induce a net helicity of half its maximum value, defined as x_*, for values of σ ranging from 10^{-8} to 1. (For reasons of clarity, we now plot $\phi \exp E$ on the vertical axis, rather than $\xi_0^{-2}\phi \exp E$.) Our results confirm that the chirality amplification does indeed increase with increasing cooperativity, i.e., that x_* decreases with decreasing values of σ. It is also obvious, however, that the effects of mass action and cooperativity are not independent: in the monomeric regime (III) the value of σ does not influence the strength of the sergeants-and-soldiers

---

[1]As a result of our definition of $\langle \eta \rangle$, eq (5.12), which does not include free monomers, we get non-zero values for $\langle \eta \rangle$ even if almost all the material is present in monomeric form.
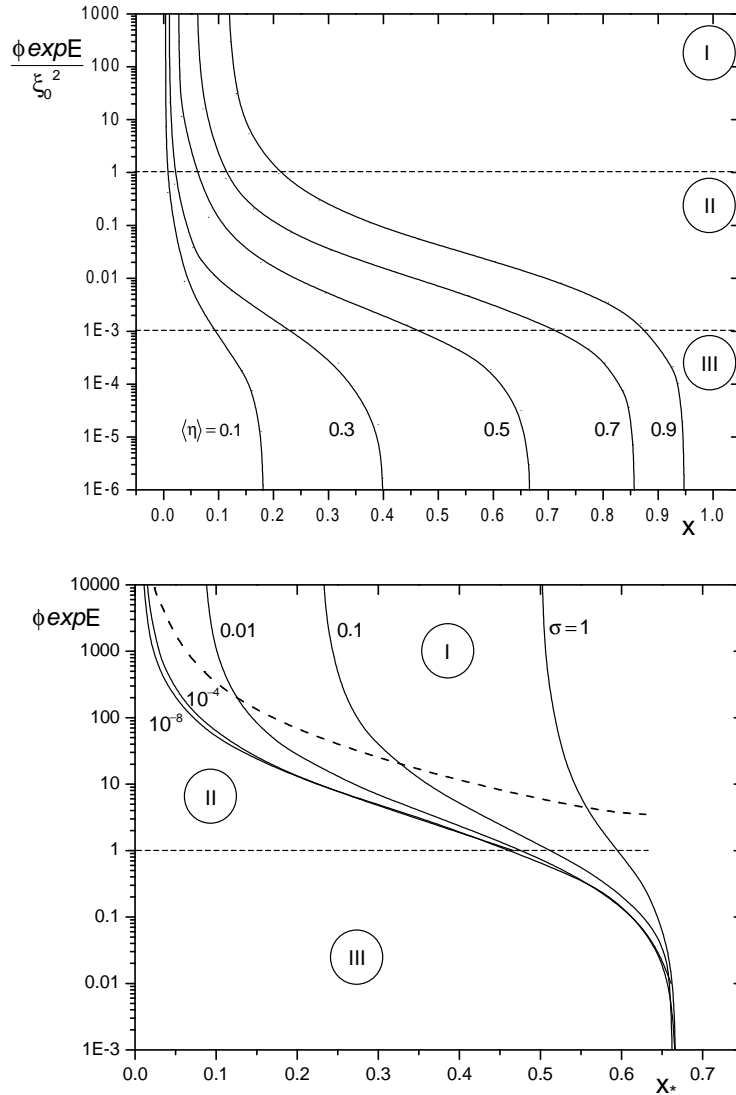
FIGURE 5.1: **top:** The mass action parameter $\xi_0^{-2}\phi\exp E$ versus the fraction of chiral material x, for $\sigma = 10^{-3}$. The lines indicate those values of x and $\xi_0^{-2}\phi\exp E$ that produce values of a net mean helicity of $\langle\eta\rangle = 0.1, 0.3, 0.5, 0.7$ and 0.9, as indicated. The Roman numbers I, II and III indicate the long-chain regime, the short-chain regime and the monomer regime, separated by dashed lines. **bottom:** $\phi\exp E$ as a function of the fraction of chiral material corresponding to a net helicity of one-half its maximum value, x_*. The lines indicate the values of x_* and $\phi\exp E$ for different values of σ, as indicated. The Roman numbers and dashed lines again indicate the regimes, as in the top Figure.

effect (since the chains will be on average too short to allow for a helix reversal) and all curves coincide, whereas in the long-chain regime (I) the effect of σ is strongest. We further note that for sufficiently low values of σ, all curves lie quite close together when plotted

on a linear scale. This implies that an increase in the cooperativity in this regime may not lead to a noticeable change in the amount of chiral material needed to obtain a fixed net helicity, except when placed on a logarithmic scale.

It may seem surprising that, even in the absence of any cooperativity or chirality amplification with $\sigma = 1$, a fraction of chiral monomers of x that equals one-half does not always lead to a mean net helicity $\langle \eta \rangle$ of one-half. The bottom graph of Figure 5.1 shows that in fact more chiral material is necessary to get this fixed net helicity when the overall concentration (and thus the mean size) decreases. This is a consequence of our assumption that a bond is only influenced by a chiral monomer if it follows this monomer. The shorter the aggregates, the larger the probability that a chiral monomer turns out to be the last molecule of the chain, and as such does not change the conformation of any bond.

In the long-chain limit $\phi \exp E \to \infty$, x_* approaches a universal value x_*^∞ that depends only on σ (see Chapter 4):

$$x_*^\infty = \frac{3\sigma + 3\sqrt{3\sigma + \sigma^2}}{6 + 4\sigma + 4\sqrt{3\sigma + \sigma^2}} \qquad (5.17)$$

It makes sense, then, to rescale $x_* \to x_*/x_*^\infty$. This produces a universal curve for conditions in the long-chain regime, as shown in the top part of Figure 5.2. The Figure again demonstrates the influence of finite-size effects, which is to reduce the degree of chirality amplification.

In a similar vein we can produce a universal curve for the short-chain regime by noting that, in this regime, the size of the aggregates lies between unity and, say, a bare correlation length. In that case a single chiral monomer is sufficient to change the conformation of an entire aggregate of size $\langle N \rangle \approx \langle N \rangle_0$, implying that only very few chiral monomers are needed to induce a large net helicity if $\langle N \rangle \gg 1$. As a consequence, the probability of finding two chiral monomers in a single aggregate approaches zero if x is not very much larger than x_*. The number of aggregates (per unit volume) whose conformation is changed by the presence of a chiral agent must be approximately equal to the number of chiral monomers $x\phi$. The net helicity per unit volume is then given by the number of such aggregates divided by the total number of aggregates, $\phi \langle N \rangle_0^{-1}$, and equals $x \langle N \rangle_0$. We therefore rescale $x_* \to x_*/x_*^0$, with $x_*^0 = \langle N \rangle_0^{-1}$.

As can be seen in the bottom graph of Figure 5.2, the rescaling produces a set of curves that nearly overlap for all concentrations, not just in the short-chain regime. In the long-chain regime universal scaling can be observed, since x_*/x_*^0 scales as $x_*^\infty \langle N \rangle_0$ while $\xi_0^{-2} \phi \exp E$ scales as $\xi_0^{-2} \langle N \rangle_0^2$ and both x_*^∞ and ξ_0 are functions of σ only. On the other hand, in the monomer regime, the overlap of the curves occurs, since $\langle N \rangle_0$ approaches the value unity, and $x_*/x_*^0 = x_* \langle N \rangle_0 \to x_*$ for all σ. Small deviations from the universal curve arise because we use $\langle N \rangle_0$ rather than $\langle N \rangle$ to rescale the curves.

In contrast to the "bare" aggregate size $\langle N \rangle_0$, the actual mean size $\langle N \rangle$ depends not only on the overall concentration of aggregating molecules and the strength of the physical
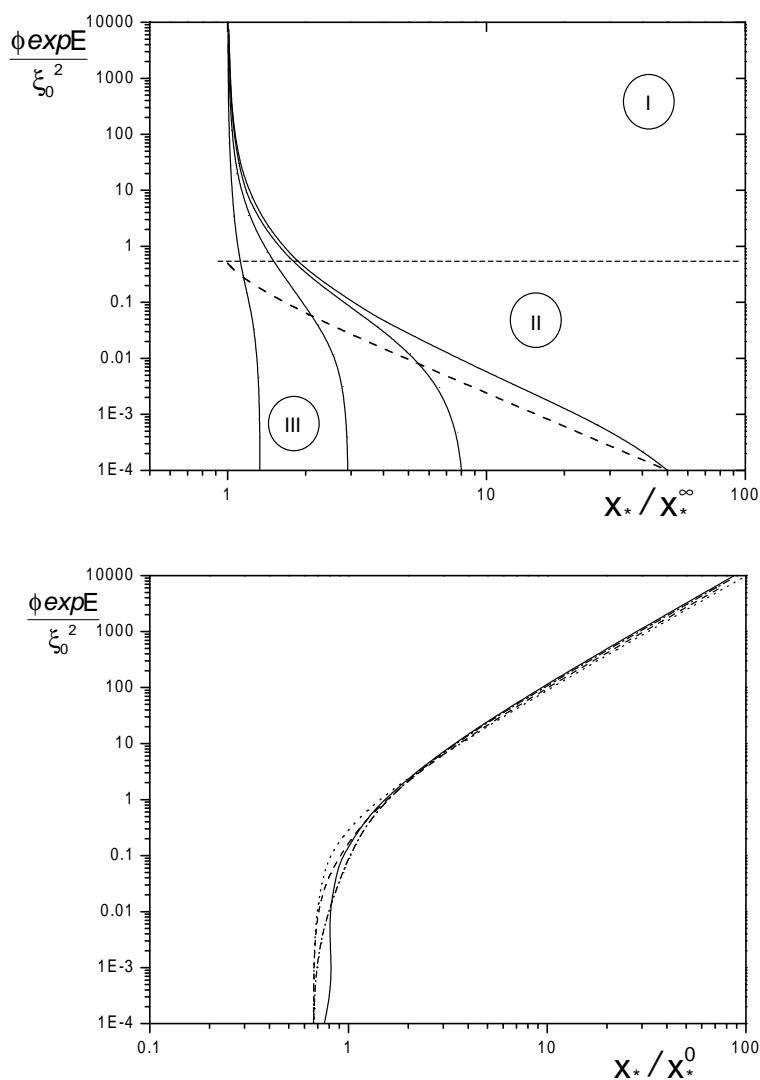
FIGURE 5.2: **top:** $\xi_0^{-2}\phi\exp E$ versus x_*/x_*^∞, for different values of the cooperativity parameter σ. From left to right: $\sigma = 1$, $\sigma = 0.1$, $\sigma = 10^{-2}$ and $\sigma = 10^{-4}$. The Roman numbers and dashed lines indicate the regimes, as in Figure 5.1. **bottom:** $\xi_0^{-2}\phi\exp E$ as a function of x_*/x_*^0, for different values of the cooperativity parameter σ. Drawn line: $\sigma = 10^{-4}$, dot-dash line: $\sigma = 10^{-2}$, dashed line: $\sigma = 0.1$, dotted line: $\sigma = 1$. Lines indicating the regimes are omitted for clarity.

bonds, but also on the composition of the aggregates, albeit only weakly so. The reason for this dependence is that the chiral content influences the number of helix reversals in an aggregate, and the aggregate may respond to the presence of helix reversals by changing its size. The influence of the composition on the mean size of the aggregates is shown in Figure 5.3 for the limits of small (the top Figure) and large (the bottom one) degrees of polymerization. We have plotted here $\langle N \rangle / \langle N \rangle_0$ against x for different values of σ (being
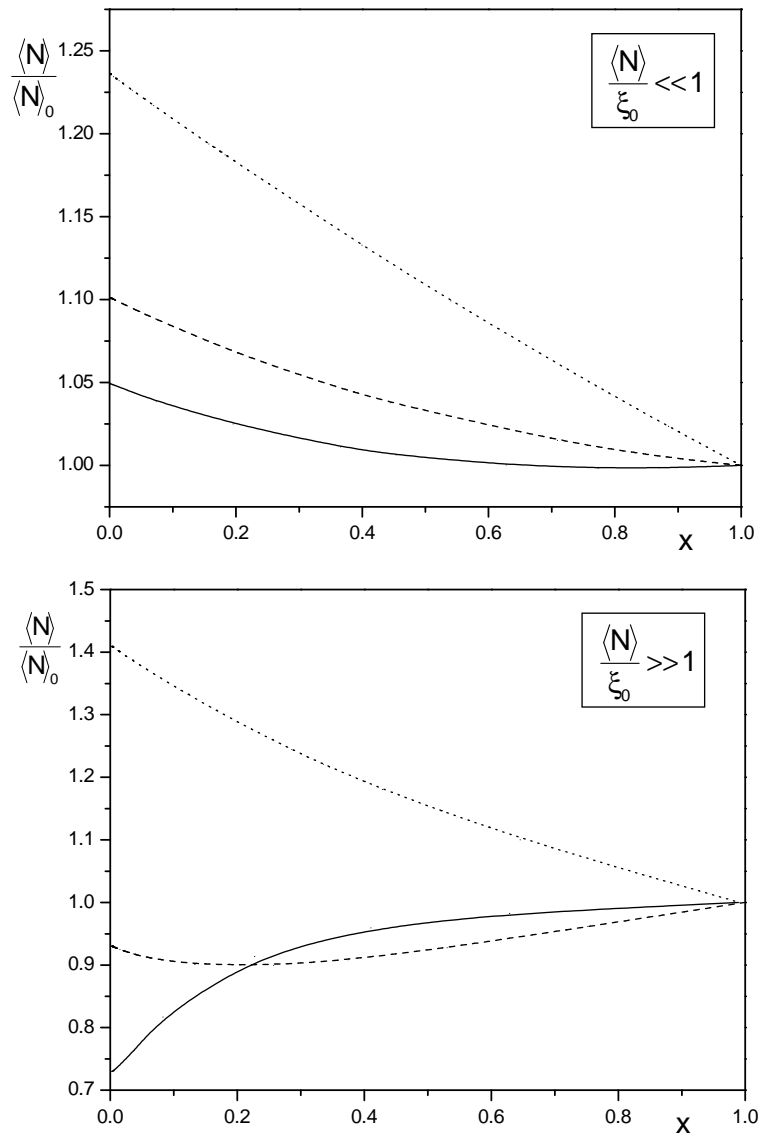
FIGURE 5.3: **top:** The relative mean aggregate size $\langle N \rangle / \langle N \rangle_0$ versus the fraction of chiral material x in the short-chain limit with $\phi \exp E = 1$, for $\sigma = 10^{-3}$ (drawn line), $\sigma = 0.1$ (dashed line) and $\sigma = 1$ (dotted line). **bottom:** As in the top figure, for the long-chain limit, with $\phi \exp E = 10^6$.

10^{-3}, 0.1 and 1), and we find that the composition influences the mean aggregate size by no more than a factor two in either limit.

5.5   Comparison to Experiment

We now compare the results of our theory with circular-dichroism measurements by Brunsveld and co-workers on mixtures of chiral and achiral discotic molecules dissolved in n-butanol and water at overall concentrations of 10^{-4} and 10^{-5} M. [18, 19] In both solvents a strong chirality amplification is found, especially so in n-butanol, where less than one per cent of chiral material is needed to induce a net helicity of half its maximum value measured. Again, this level of cooperativity is a remarkable find in self-assembled polymers, which are after all bound with fairly weak bonds. Interestingly, the net helicity in n-butanol is concentration dependent, whereas for the solution in water the curves for the two concentrations overlap. It appears that in the former solvent, the chirality amplification conforms to regime II, whilst in the latter it conforms to regime I.

It is important to stress at this point that if one measures the optical activity of a solution, one does not specifically measure the net helicity, but rather the chiral content of the sample, at least in principle. However, in the case of the experiments of refs [18, 19], it is not necessary to include a contribution from the free monomers. The reason is that in the discotic molecules studied in [18, 19], the chromophore and the chiral group are separated to such an extent that no Cotton effect is measured for a solution containing the homochiral monomers in a molecularly dispersed state. Therefore, circular dichroism only measures the *supramolecular chirality* (or the helicity) in this particular system.

However, as also discussed in Chapter 4, this does not mean that the measured Cotton effect is identical to the net helicity per bond as defined in eq (5.12). In fact, the strength of the Cotton effect measured in experiment is determined by the total amount of optically active material in a probe volume as well as by the optical properties of the two types (homochiral and achiral) of molecules. The former depends, e.g., on the concentration of dissolved material and on the optical path length. To account for this, we use the constant of proportionality α (as we did in Chapter 4) that links the theoretical net helicity per bond and the measured optical effect. For both sets of experiments, we have normalized the data of Brunsveld et al. [18, 19] to give a value of unity at the maximum in the curves, implying that we presume that full saturation of the Cotton effect takes place.

To properly deal with the optical properties of the molecules, one needs to realize that the measured effect may depend on the type of monomer and the type of bond it is involved in. Thus we again make use of the relative strength γ that distinguishes between contributions for a bond following a chiral monomer and one following an achiral monomer in an assembly, and assign this weighing factor to every bond that follows a chiral monomer, the fraction of which is $z(z+1)^{-1}$. We assign the weight 1 to bonds that follow an achiral monomer, the fraction of which equals $(z+1)^{-1}$. The mean net helicity obtained from experiment we denote by $\langle\eta\rangle'$, and it is plausibly given by a linear superposition of the two contributions

mentioned. Hence,

$$\langle \eta \rangle' = \alpha \langle \eta \rangle \left[1 + (\gamma - 1) \frac{z}{z+1} \right] \tag{5.18}$$

where γ and α are now treated as additional fitting parameters. It follows from eq (5.18) that if γ is smaller than unity (achiral monomers have a larger contribution to the net helicity than chiral ones), $\langle \eta \rangle'$ becomes a non-monotonic function of x. This is not so for $\gamma \geq 1$ in which case $\langle \eta \rangle'$ remains monotonic in x.

We first discuss the experiment that displays a concentration dependence, in which the solvent is n-butanol, and after that compare our theory to experimental results from the aqueous solutions. Since the chirality amplification is concentration dependent in the solvent n-butanol, we must reside within the short-chain regime, where $1 < \langle N \rangle < \xi_0$; it follows that $\sigma \approx \xi_0^{-2} \ll 1$. We have shown in Figure 5.1 that for these values of σ, the net helicity is insensitive to the value of σ. Therefore, the value of σ becomes arbitrary and we set $\sigma = 10^{-8}$. We now perform a fit at a single value of x, namely x_*, to find the proper value of $\phi \exp E$. For the concentration of 10^{-4} M this turns out to be at $\phi \exp E = 6 \cdot 10^4$, i.e., $\langle N \rangle \approx \langle N \rangle_0 \approx 250$.

We now plausibly assume that the bond energy $-E$ does not change with concentration. Then, if our assumption that $\langle N \rangle \ll \xi_0$ is valid, we should obtain good agreement with the measurements at 10^{-5} M if we use $\phi \exp E = 6 \cdot 10^3$ (a factor ten lower). Indeed, this turns out to be the case, indicating that our simple theory takes the concentration dependence into account in a proper way (see Figure 5.4). We can determine the reference free energy from the values of $\phi \exp E$, since ϕ is known.[2] This gives $-E = -19 \ k_B T$, which is close to the values of $-15 \ k_B T$ and $-16 \ k_B T$, obtained from measurements at similar concentrations of *homochiral* discotic molecules in the solvent n-butanol. [19, 24]

If we choose the values of $\phi \exp E$ mentioned above, we get good agreement over the entire range of fractions of chiral material, with the exception of the high-x regime, where a maximum is observed experimentally. As implied earlier, both here and in the previous Chapter, the presence of a maximum indicates that bonds following achiral molecules have a larger contribution to the helicity than do those following chiral ones and thus that the ratio between the contributions to the net helicity of chiral and achiral monomers γ must be smaller than unity. We perform a curve fit on the maximum in the curve and obtain good agreement for $\gamma = 0.9$ and $\alpha = 1$ for both concentrations (see Figure 5.4).

We now compare our theory to circular-dichroism measurements on mixtures of the same chiral and achiral discotic molecules in water, for which the chirality amplification is concentration independent for the concentrations studied. [18] This indicates that $\langle N \rangle \gg \xi_0$, and thus that the chirality amplification is an invariant of $\phi \exp E$ (see Figure 5.1). It turns

---

[2]To calculate the volume fraction from the molar concentration, a density for the discotic colecule of 1.3 g mL^{-1} was used. We obtained this number from X-ray measurements in the solid state. The molecular weight of the discotic lies around 3400 g mol^{-1}. We have neglected the difference in molar mass between the chiral and achiral molecules.
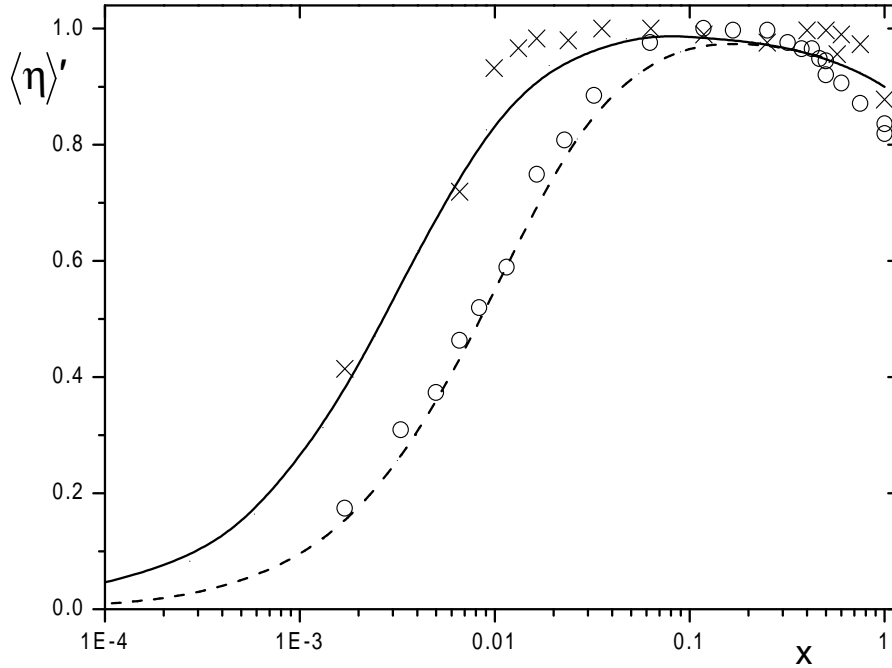
FIGURE 5.4: Fit of the theoretical net helicity $\langle\eta\rangle'$ versus x to experimental data of Brunsveld et al. [19] in n-butanol at two concentrations. (Circles: 10^{-5} M, crosses 10^{-4} M). Dashed line: curvefit for 10^{-5} M with fitting parameters $\phi\exp E = 6 \cdot 10^3$, $\sigma = 10^{-8}$, $\alpha = 1$ and $\gamma = 0.9$. Solid line: curvefit for 10^{-4} M with fitting parameters $\phi\exp E = 6 \cdot 10^4$, $\sigma = 10^{-8}$, $\alpha = 1$ and $\gamma = 0.9$.

out that the current theory reproduces our earlier fit in Figure 4.3 almost exactly (see Figure 5.5 and inset) if we use the same fitting procedure as before (fixing $\sigma = 6.4 \cdot 10^{-3}$ at the point x_*, and $\gamma = 0.65$ and $\alpha = 1.15$ from the maximum in the curve),[3] and set $\phi\exp E$ for both concentrations to be large (but obviously a factor 10 apart: we set $\phi\exp E = 10^7$ for 10^{-4} M and 10^6 for 10^{-5} M). This shows that the earlier approximate theory is indeed a special case of the current one, and is recovered in the infinite-chain limit, as it should be.

Our choice of $\phi\exp E$ here is arbitrary. As long as we choose a value that corresponds to the long-chain limit, we will obtain the proper concentration independence of the Cotton effect. Therefore, we cannot fix E from the circular-dichroism measurements. However, we are able to estimate a minimum value for this quantity if we determine the value of $\phi\exp E$ for which the chirality amplification becomes discernably concentration dependent,[4] for the

---

[3]Note that the value of $\alpha > 1$, necessary to obtain good agreement between theory and experiment, could indicate that the state of full one-handed helicity ($\langle\eta\rangle' = 1$) was not reached in experiment. Indeed, contrary to Figure 5.4, Figure 5.5 does not display a clear "plateau" of maximum helicity, but rather a sharp peak.

[4]We arbitrarily quantify the transition between concentration dependence and independence to take
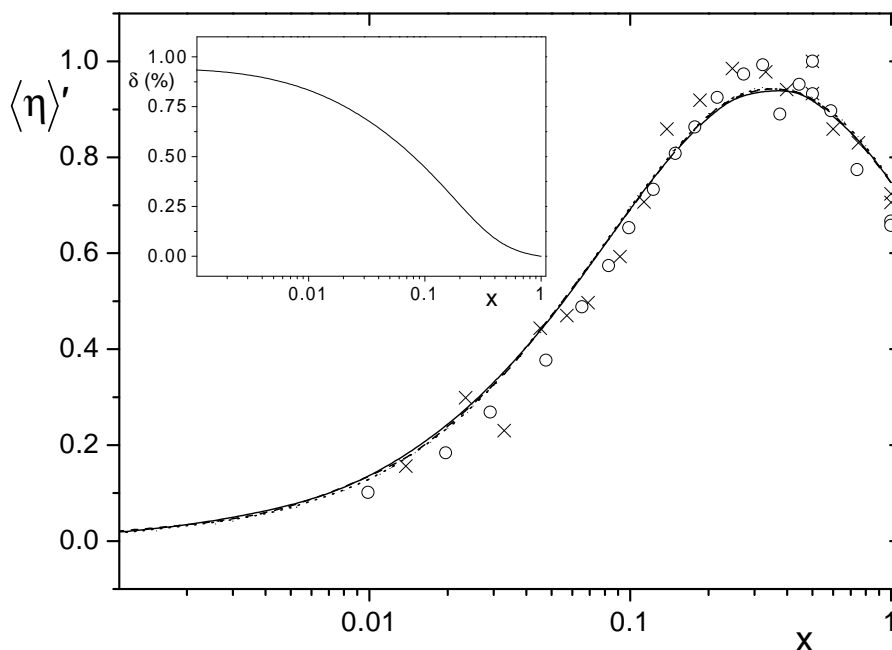
FIGURE 5.5:   Fit of the theoretical mean net helicity $\langle\eta\rangle'$ versus x to experimental data of Brunsveld et al. [18] in water at two concentrations. (Circles: 10^{-5} M, crosses 10^{-4} M). All three lines have the fit parameters $\sigma = 0.0064$, $\alpha = 1.15$ and $\gamma = 0.65$. Dashed line: curve fit for $\phi\exp E = 10^7$. Solid line: curve fit for $\phi\exp E = 10^6$. Dotted line: curvefit with the model from Chapter 4, valid in the long-chain limit. In the inset: The relative difference between the mean net helicity in the current model for $\phi\exp E = 10^6$ and that in the earlier model, in percent.

given value of $\sigma = 6.4\cdot10^{-3}$. For this particular system the transition between concentration dependence and independence occurs at $E = 18\ k_BT$, from which follows that E must be smaller than this value for a concentration dependence to occur for these molecules in water (with this σ) at these concentrations. Alternately, one might decrease ϕ and thus enter the concentration-dependent regime.

5.6   Conclusions

The one-dimensional, two-component Ising model, coupled to the theory of linear self-assembly as outlined in this Chapter, provides a good description of the concentration dependence of the sergeants-and-soldiers effect in helical supramolecular polymers. We find

---

place where a change in concentration of a factor ten induces a shift of 10% in the mean net helicity near the point where $\langle\eta\rangle = 1/2$.

that an increase of the penalty of a helix reversal leads to a larger chirality amplification in the long-chain limit, and that an increase of the solute concentration leads to an increase in the chirality amplification in the short-chain limit. However, we also find that, in the former limit, the strength of the sergeants-and-soldiers effect becomes insensitive to changes in the concentration, just as it becomes insensitive to the value of the free energy of a helix reversal in the latter limit. As a result, it may be difficult to determine the mean aggregate size from circular-dichroism experiments at high concentrations, and it may be equally difficult to determine the free energy of a helix reversal from measurements at low concentrations. The dependence of the chirality amplification on the (mean) chain length and the central role played by the cooperativity mirror conclusions of earlier work on conventional copolymers. [20] The theory we present shows quantitative agreement with circular-dichroism measurements of mixtures of chiral and achiral discotic molecules in the solvents water and n-butanol, for two concentrations that differ by a factor of ten. [18, 19] When we assume that chiral monomers have a lower contribution to the measured helicity than do achiral ones, we can reproduce the experimentally measured maximum in the Cotton effect as a function of the fraction chiral material. For long enough chains, the agreement between experiment and theory is identical to that obtained with our earlier, approximate treatment. In this regime, it is perhaps more convenient to use the earlier, less cumbersome, treatment.

Chapter 6

The Majority-Rules Principle in Long Chains

ABSTRACT

Apart from the sergeants-and-soldiers type we discussed in the previous two Chapters, chirality amplification can also occur in copolymers consisting of the two enantiomeric forms of the monomeric building blocks. We outline the first theoretical treatment of this so-called majority-rules type of chirality amplification in self-assembled aggregates. Our treatment, which is based on the one-dimensional, two-component Ising model, is analytical, and exact in the infinite-chain limit. We find a strong dependence of the strength of the chirality amplification on the free-energy penalty of a helix reversal, as well as on that of a mismatch between the preferred helical handedness of a monomer and the actual screw sense of the bond that follows it. The strength of the chirality amplification shows a monotonic increase with increasing helix reversal penalty, but a strongly non-linear and non-monotonic dependence on the mismatch penalty.

6.1   Introduction

As mentioned in the previous two Chapters, amplification of chirality is a well-known phenomenon in solutions of helical copolymers. [17, 20] Of the two classes of chirality amplification, the sergeants-and-soldiers type has been studied most extensively, while the majority-rules type is somewhat less well-known. The sergeants-and-soldiers principle is characterized by a strongly non-linear response of the optical properties of the (achiral) polymers to the addition of a small amount of homochiral material, [40] whereas the majority-rules principle represents a similar effect for chains consisting of both enantiomeric forms of the chiral monomers, one of which is present in (small) excess. [43] Both effects occur due to a shift in the balance between left- and right-handed helical bonds, which can be quite large.

Recently, strong chirality amplification of the sergeants-and-soldiers type was found in solutions of self-assembled helical aggregates by measurements of the optical activity. [18, 19] In Chapters 4 and 5, we found that the sergeants-and-soldiers principle in such self-assembled systems can be accurately described in terms of a one-dimensional, two-component Ising model. In this Chapter we modify this model to describe the majority-rules principle in long supramolecular polymers. The reason that a similar model may be used is that the same physical principles are at work in both the majority-rules and the sergeants-and-soldiers case. In both cases, the polymers consist of two types of monomer, which can be bound in two ways (either by a left-handed helical bond or by a right-handed one). In addition, both phenomena find their origin in the cooperativity of the helical aggregation. However, as we shall see below, for a description of the majority-rules type of chirality amplification we need two free-energy penalties, rather than one. This makes this treatment somewhat more involved than the one we applied in the previous Chapters.

Note that our treatment is not the first to describe the majority-rules effect. In a recent paper, [44] Selinger and Selinger investigated the majority-rules principle in conventional (covalently bound) polymers by applying a random-field Ising model. Unfortunately, the existing theory cannot be applied to supramolecular systems, at least not in principle, since the distribution of the two types of monomer along the chains is fixed in conventional polymers, whereas in supramolecular aggregates it is determined by the thermodynamic equilibrium. Our treatment is specifically suited to describe chirality amplification in supramolecular polymers, and is analytical and exact in the infinite-chain limit.

The remainder of this Chapter is organized as follows. In section 6.2 we outline our model for the majority-rules effect in dilute solutions of long supramolecular polymers, and in section 6.3 we calculate the net helicity (defined as the difference between the fractions of right- and left-handed bonds of a polymer) as a function of the enantiomeric excess (defined as the difference between the fractions of right-handed and left-handed chiral monomers). In section 6.4 we present our results and demonstrate that the amplification of chirality increases strongly with an increasing free-energy penalty on a helix reversal. We also

show the non-monotonic dependence of the chirality amplification on the free energy of a mismatch between the preferred screw sense of a monomer and the bond that follows it. Finally, in section 6.5 we summarize our findings and give a brief outlook.

6.2   The Single-Aggregate Partition Function

In our description we consider a dilute solution of aggregates, so that we may ignore inter-aggregate interactions. We assume that the aggregates are long and discard finite-size effects, allowing us to describe the configurational statistics of polymers with a relatively simple ground-state calculation. It seems reasonable to suggest that long-range intra-aggregate interactions are unimportant for the problem in hand. Presuming that the amplification of chirality is dominated by interactions on small length-scales, such as nearest-neighbor interactions, we can rely on a two-state Ising model in one dimension to properly describe the conformational state of the aggregates, as we also did in Chapters 4 and 5. [123]

We make a distinction between two types of monomer, a chiral monomer that has a preferred left-handed screw sense (which we shall abbreviate as a "−" monomer), and one that has a preferred right-handed screw sense (the "+" monomer). These monomers can be linked in two ways, one corresponding to a right-handed helical conformation and one corresponding to a left-handed one. These ways of bonding we refer to as the "+" bond, which is the bond type most compatible with the "+" monomer, and the "−" bond, which is most compatible with the "−" monomer. Furthermore, we introduce two free-energy penalties, R and W: the first penalizes a helix reversal along the chain, and the second penalizes a mismatch between the preferred screw sense of a monomer and the bonds near to it. The former penalty is invoked when two consecutive bonds have different conformations, and the latter is used whenever a "+" bond follows or precedes a "−" monomer, and vice versa. We apply the mismatch penalty twice when both monomers adjacent to a bond are of the type incompatible with that bond.

Our model corresponds to the following dimensionless Hamiltonian H for a chain of degree of polymerization N.

$$
\begin{aligned}
H \;=\; & \frac{1}{2}R\sum_{j=1}^{N-2}\left(-s_j s_{j+1}+1\right)+\frac{1}{2}P\sum_{j=1}^{N-1}\left(s_j+1\right) \\
& +W\sum_{j=1}^{N-1}\left[1-\frac{1}{2}\left(s_j n_j+s_j n_{j+1}\right)\right]-E(N-1)
\end{aligned}
\tag{6.1}
$$

Here, s_j gives the state of the jth spin (or bond), with $s_j=-1$ for a "down" spin (a "−" bond) and $s_j=+1$ for an "up" spin (a "+" bond), and n_j gives the type of the

jth monomer, with $n_j = -1$ for a "$-$" monomer and $n_j = +1$ for a "$+$" monomer. The description of the system is then a combination of two interacting sublattices, one that describes the monomers and one that describes the bonds. The quantity P corresponds to the magnetic-field strength in the Ising model and couples to the "up" spins, and $-E$ is the reference bond free energy. Note that the Hamiltonian (eq (6.1)) is only valid for chains of length $N \geq 3$, which is indeed the regime we wish to describe.

The (quasi grand canonical) partition function of a single aggregate now reads

$$\Xi(N) \equiv \left(\prod_{k=1}^{N} \sum_{n_k = \pm 1} \right) \exp \left[\mu_- \left(N - \frac{1}{2} \sum_{j=1}^{N} (n_j + 1) \right) + \frac{1}{2} \mu_+ \sum_{j=1}^{N} (n_j + 1) \right]$$
$$\times \left(\prod_{l=1}^{N-1} \sum_{s_l = \pm 1} \right) \exp -H \tag{6.2}$$

Here, the first and last bracketed terms are repeated sums, μ_- is the chemical potential of the "$-$" monomers, and μ_+ is that of the "$+$" monomers. We use a quasi-grand partition function here, in which the total number of monomers in the chain is kept fixed at N, while the chain composition can change. This partition function is evaluated with the aid of the well-known transfer-matrix method. The transfer matrix contains the statistical weights for all configurations of a monomer-bond pair, dependent on the monomer-bond pair preceding it. The matrix can be derived from the Hamiltonian (eq (6.1)) by standard methods. [82] For this, it turns out to be convenient to redefine the chemical potentials, so that we obtain a reference chemical potential (equal to μ_-) and an excess chemical potential, defined as $\mu \equiv \mu_+ - \mu_-$. We now define a fugacity $z \equiv \exp \mu$ that we introduce into the transfer matrix whenever a "$+$" monomer is considered. (See Chapter 5 for a formal derivation of a transfer matrix including these chemical potentials.) As mentioned before, the aggregate can be divided into two sublattices, one that contains the monomers (with states $+1$ and -1) and one that contains the bonds (also with states $+1$ and -1). Taking into account the interactions between the two sublattices, the transfer matrix becomes the sum of four matrices, one for each possible combination of monomers preceding and following the bond under consideration. It takes the final form

$$\mathbf{M} = \begin{pmatrix} (1+w)(zw+1) & (1+w)(zw+1)\sqrt{\sigma} \\ s\sqrt{\sigma}(1+w)(w+z) & s(1+w)(w+z) \end{pmatrix} \tag{6.3}$$

with $s \equiv \exp -P$ and $w \equiv \exp -W$ the Boltzmann factors of an "up" spin (over a "down" one), and that of a mismatch between a bond and a monomer, and $\sigma \equiv \exp -2R$ the square of the Boltzmann factor of a helix reversal. In the matrix representation we can rewrite the partition function $\Xi(N)$, eq (6.2), similar to how we did this in Chapter 5, giving

$$\Xi(N) = \exp \left[\mu_- N + E(N-1) \right] \tilde{\mathbf{u}} \cdot \mathbf{M}^{N-2} \cdot \tilde{\mathbf{u}}^+ \tag{6.4}$$

The quantities $\tilde{\mathbf{u}}$ and $\tilde{\mathbf{u}}^+$ are the vectors that describe the probability distribution over the states of the aggregate ends. Since our treatment is meant to describe the long-chain limit, we need not specify these.

6.3 Ground-State Approximation

To make the partition function explicit, we determine the eigenvalues of $\mathbf{M}$. These are $\lambda_{1,2} = \frac{1}{2}(1+w)\left(1 + zs + zw + sw \pm \sqrt{\psi}\right)$, where λ_1 is given by the plus sign and λ_2 by the minus sign. Here, $\psi = (zw + 1 - sw - sz)^2 + 4\sigma(zw + 1)(sw + sz)$. The partition function now becomes a sum of two terms, each including one of the eigenvalues. In the long-chain limit, the term which includes λ_1 is much larger than the one that contains λ_2. We can therefore use the so-called ground-state approximation and retain only this term. [24] The partition function then becomes

$$\Xi(N) \approx A(s,\sigma,w,z) \exp\left[\mu_0 N + E(N-1)\right] \lambda_1^N \tag{6.5}$$

Here, A is a prefactor that contains end-effects, and as such does not contribute in a significant way in the long-chain limit. Formally, equation (6.5) is only valid for $N \gg 1$, becoming exact in the infinite-chain limit, but we extrapolate it down to $N > 2$. This is allowed if the mean degree of polymerization, $\langle N \rangle \simeq \sqrt{\phi \exp \varepsilon}$, remains large; here ϕ is the volume fraction of aggregating molecules and $\varepsilon \equiv E - \ln A(s,\sigma,w,z)$ the free-energy penalty associated with the aggregate ends (the so-called end-cap energy). [24] In the long-chain regime, the mass distribution of the aggregates is fairly sharply peaked around $N = \langle N \rangle$. This means that we need not deal explicitly with the self-assembly, and we can represent the (concentration and temperature dependent) mean value $\langle N \rangle$ by N in the remainder of this Chapter.

From the partition function we can obtain the quantities which determine the strength of the chirality amplification, being the net helicity (the fraction right-handed minus the fraction left-handed helical bonds) and the enantiomeric excess x (the fraction of "+" monomers minus that of "−" monomers). These are given by

$$\eta \equiv -1 + 2\left(N-1\right)^{-1} \partial \ln \Xi(N)/\partial \ln s \sim -1 + 2\frac{s}{\lambda_1} \partial \lambda_1/\partial s \tag{6.6}$$

$$x \equiv -1 + 2N^{-1}\partial \ln \Xi(N)/\partial \ln z \sim -1 + 2\frac{z}{\lambda_1} \partial \lambda_1/\partial z \tag{6.7}$$

These limiting equations become exact for infinitely long chains. Since right-handed bonds are not intrinsically more or less favorable than left-handed ones, we now set $s = 1$ by symmetry, and simplify equations (6.6) and (6.7). The net helicity η and enantiomeric excess x become

$$\eta = \frac{(z-1)(1-w)}{\sqrt{\psi}} \tag{6.8}$$

$$x = \frac{(z-1)(1+w)\sqrt{\psi} + 4w\sigma(z^2-1) + (z^2-1)(1-w)^2}{\left[(z+1)(1+w) + \sqrt{\psi}\right]\sqrt{\psi}} \tag{6.9}$$

with ψ as defined earlier in this section. In principle, we can now eliminate z from equations (6.8) and (6.9) and express x in terms of η, σ and w. However, we find it more convenient
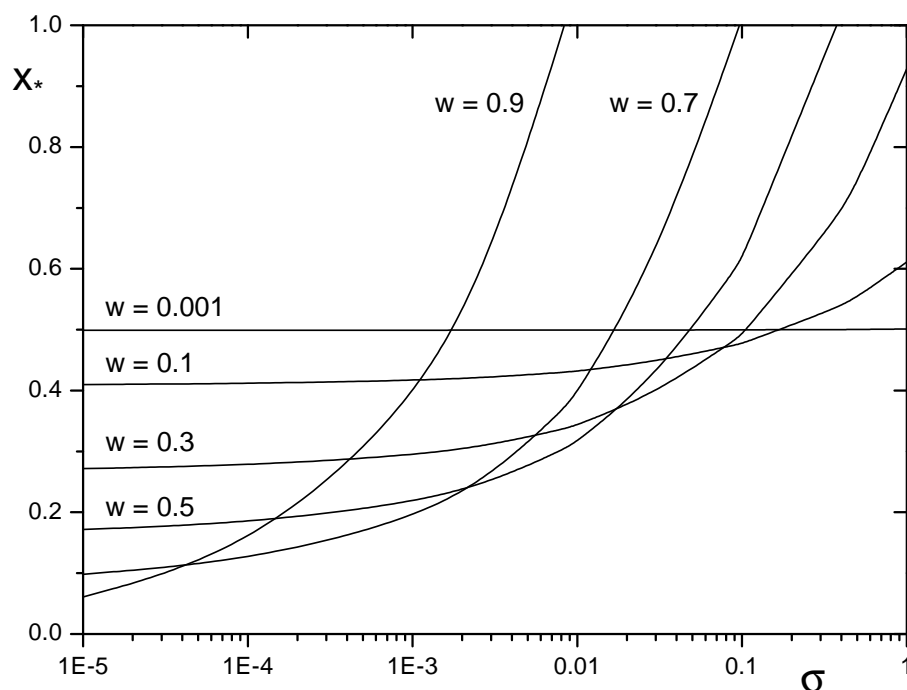
FIGURE 6.1:   The excess fraction of "+" chiral material needed to attain a net helicity of one-half, x_*, versus $\sigma = \exp -2R$, with R the free energy penalty of a helix reversal, for six values of the mismatch parameter w, as indicated.

to numerically solve z from equation (6.8) for fixed values of w, η and σ, and insert the obtained value for z back into equation (6.9) to obtain x. We discuss the results of this procedure in the next section. We limit our discussion to the regime where the fraction of "+" monomers is equal or larger than the fraction of "−" monomers. Since the majority-rules effect is symmetrical, the results for a majority of "−" monomers would be identical, albeit that η, as defined in eq (6.6), would become negative.

6.4   Results and Discussion

Let x_* be defined as the enantiomeric excess needed to induce a net helicity of one-half. It is a measure of the strength of the chirality amplification, in that the lower x_* is, the more monomers are influenced by a single "+" monomer. To investigate the impact of the various free-energy penalties on this quantity, we plot it in Figure 6.1, against the squared Boltzmann factor of a helix reversal σ, for different values of the Boltzmann factor w of a mismatch. The Figure shows that, for fixed low values of σ (and hence high values for the free energy of a helix reversal), the strength of the chirality amplification increases monotonically with an increasing value of the Boltzmann factor of a mismatch.
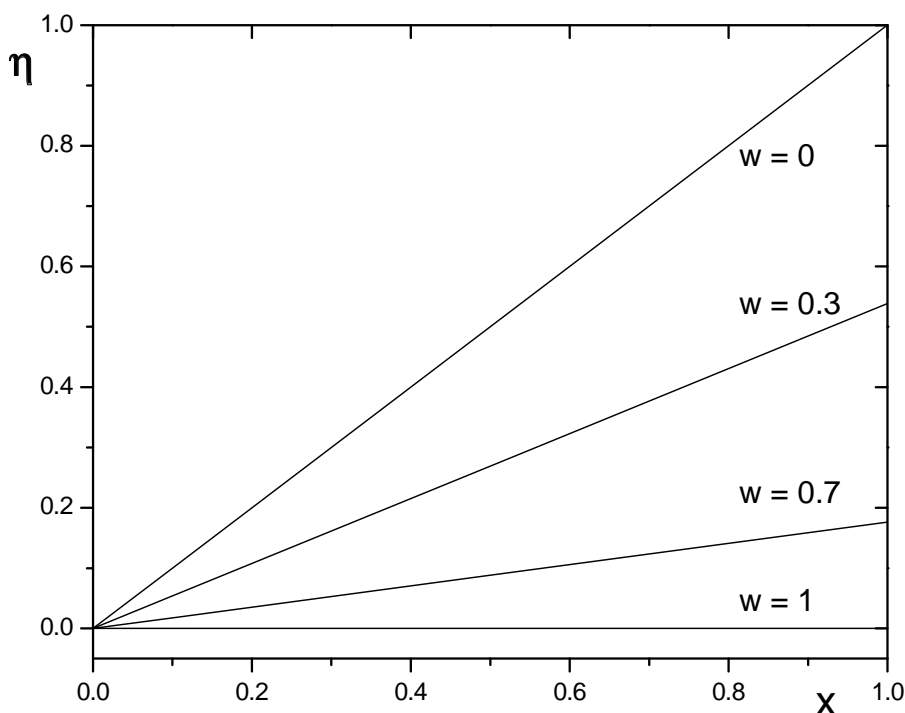
FIGURE 6.2:   The net helicity η as a function of the enantiomeric excess x, for different values of the mismatch parameter w as indicated, at a fixed value of the free energy of a helix reversal of zero ($\sigma = 1$).

This is because in this regime (where helix reversals are very unfavorable), the lower the mismatch free energy is, the more "$-$" monomers can be present in the aggregates without changing the net helicity. In this low-σ regime, the degree of chirality amplification becomes insensitive to the value of σ (especially for low w), as indicated by the horizontal curves. Apparently, the chirality amplification is dominated by the value of w here, whereas for higher values of σ, the free-energy penalty of a helix reversal becomes more important.

When we look at the high-σ regime, we observe that the amplification of chirality is lower than in the low-σ regime; for $\sigma = 1$ there is no longer any amplification of chirality. For values of w close to unity, it is even so that a net helicity of one-half cannot be reached, even if only "$+$" monomers are present.

We now look at the chirality amplification for two values of σ in more detail by taking vertical cuts through the diagram. To this end, we first consider the case $\sigma = 1$ (implying no penalty on helix reversals), see Figure 6.2. In this case, as may in fact already be concluded from Figure 6.1, we notice that there is indeed no chirality amplification. It follows from eqs (6.8) and (6.9) that

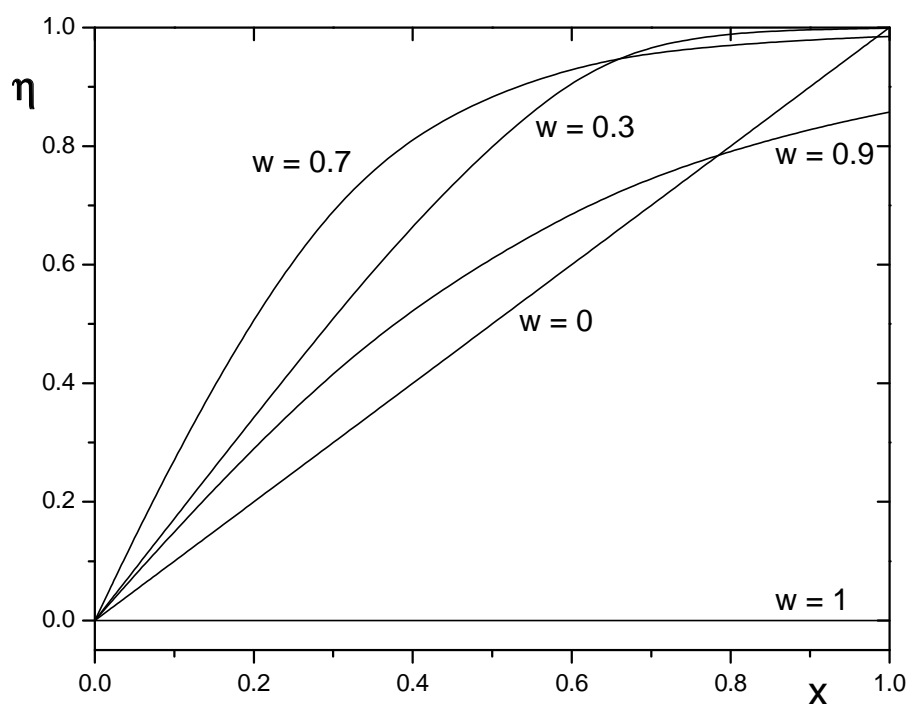$$\eta = \left(\frac{1 - w}{1 + w} \right) x \qquad (6.10)$$

FIGURE 6.3:   As Figure 1, at a fixed value of the free energy of a helix reversal of 3.5 k_BT, corresponding to $\sigma = 10^{-3}$.

This is a linear function of x, and an increase in w from zero to unity causes a monotonic decrease of the maximum net helicity. Two limiting cases present themselves: $w \to 0$ and $w \to 1$. In the first case, where the Boltzmann factor w goes to zero, $\eta \to x$. This in fact holds for all values of σ, as can be seen from eqs (6.8) and (6.9). The reason is that for $w = 0$, every "+" monomer must be followed by a "+" bond and every "−" monomer by a "−" bond. The σ-independence of the chirality amplification in this limit arises because our model does not allow for a helix reversal without a mismatch free energy being involved. In the second limit, $w \to 1$, the net helicity stays equal to zero over the entire range of x (and σ) values. There is then no longer a penalty on a mismatch between monomer and bond, and the chain conformation will be determined by entropy, leading to a state where half of the bonds have a "+" conformation and half a "−" conformation.

In Figure 6.3, we plot the net helicity as a function of the enantiomeric excess at a fixed helix reversal penalty of 3.5 k_BT, and we find that the chirality amplification changes in a strongly non-linear way with w for $\sigma \ll 1$. Strong chirality amplification occurs at values of w around 0.7 (corresponding to an energy penalty of 0.4 k_BT). When the value of w approaches unity, the maximum net helicity decreases, and the value $\eta = 1$ is no longer reached, not even in the case of aggregates that consist of only one type of enantiomer. This means that care must be taken in the interpretation of experimental data, as the

maximum obtained optical effect may not correspond to the state in which all bonds are of one type.

In the limit of infinite cooperativity ($\sigma \to 0$) we find from eqs (6.8) and (6.9) that η can only have two values, -1 or 1, dependent on whether z and w are smaller or larger than unity. This is because in this limit,

$$\eta \to \frac{(w-1)(z-1)}{\sqrt{(w-1)^2(z-1)^2}} \tag{6.11}$$

The numerator and denominator are identical, albeit that the sign of η varies with w and z. In other words, the aggregates are either fully right-handed or fully left-handed helical for all values of x. This may correspond to the discontinuous phase transition in the one-dimensional Ising model, which occurs under the same circumstances of infinite coupling constant and infinite chain length.

6.5   Conclusions and Outlook

We present an analytical treatment of the majority-rules type of chirality amplification in solutions of helical, self-assembled polymers, valid in the long-chain limit and exact in the infinite-chain limit. Contrary to our theory for the sergeants-and-soldiers principle, detailed in Chapters 4 and 5, this treatment requires two free-energy penalties, one on a helix reversal and one on a mismatch between a bond and the monomers near to it. We find that the chirality amplification becomes monotonically stronger with an increasing penalty on a helix reversal, but that it shows a strongly non-monotonic dependence on the mismatch penalty. Finally, we note that for low values of the mismatch penalty, fully right-handed or left-handed aggregates no longer form.

Since, to our knowledge, no experimental measurements have been performed on enantiomer mixtures in self-assembled polymers, we are at this time unable to check our theory against experiment. However, analogous experiments to the sergeants-and-soldiers measurements of Brunsveld and co-workers [18, 19] seem a logical choice for an experimental study of the majority-rules principle in supramolecular polymers, and these experiments are now in preparation. [130]

Our treatment is only valid for the long-chain limit, implying (see Chapter 5) that it can only be sensibly used to describe measurements performed in the concentration-independent regime. If one wishes to describe concentration dependence, an elaboration of our treatment is necessary, analogous to the one given in Chapter 5 to the ground-state treatment of the sergeants-and-soldiers case. This means that one should retain both eigenvalues of the transfer matrix and use the definitions eqs (6.6) and (6.7) to determine the chirality amplification.

Chapter 7

The Effect of Fields and Interactions on the Helical Transition in Linear Assemblies

ABSTRACT

Interaggregate interactions and external fields both potentially influence the size distribution of self-assembled polymers. To investigate the effect of interactions on *helical* supramolecular polymers, we combine a second-virial excluded-volume treatment with the theory of helical self-assembly. We find that interaggregate interactions can have a large effect on the mean size through a shift that occurs in the fraction of helical bonds, provided that the concentration of self-assembling particles is large enough, and provided that the difference in length between helical and non-helical bonds is relatively large. The mean aggregate size is also strongly dependent on the description of the aggregate ends. We also investigate the conformational state and mean aggregate size of helical aggregates in external dipole and quadrupole fields. For a so-called ordering field, for which the director is parallel to the axis of induced symmetry, we find enhanced growth of the polymers for certain ranges of angle between the director of the field and the aggregate axis. For a disordering field, the mean aggregate size decreases. The fraction of helical bonds also becomes dependent on the orientation of the aggregates. Here we find an increase in the fraction of the longer type of bond in an ordering field, and a decrease in a disordering one.

7.1   Introduction

The ideal-solution theory for helical self-assembly into linear aggregates, presented in the earlier Chapters, provides a good description for dilute solutions of linear aggregates, up to a volume fraction of approximately the mean reciprocal aspect ratio. [24, 60] However, for higher concentrations of aggregating material, interactions between the aggregates potentially play an important role, e.g., through a modified mass action [131] or through effects that stem from changes in the configurational statistics of the assemblies. [24] In the present Chapter we examine the conformational state of *helical* self-assembled polymers which do interact, either with other aggregates (which we treat via an excluded-volume theory) or with external fields of the quadrupole and dipole type.

Treatments have been put forward that deal with the effect of excluded-volume interactions and that of external fields on helical polymers and similar systems, [132, 133] as well as on self-assembled chains. [60, 108, 131, 134] Here, we consider the effect of fields and interactions on polymers that have both properties, i.e., helical supramolecular polymers. Since interactions have been predicted to influence the mean size of non-helical aggregates, both rod-shaped ones and flexible coils, [60, 108, 135] it stands to reason that a similar effect may also occur in helical self-assembled aggregates. Moreover, because there is a strong coupling between the size and the conformational state of helical aggregates, the degree of helicity of the chains may also be affected by interactions or fields.

To investigate the effect of interaggregate interactions, we treat the aggregates as rigid rods, and apply Onsager's excluded-volume theory. [136] This theory takes repulsive two-particle interactions between such rodlike particles into account, on the basis that they cannot occupy the same space. [136, 137] The smaller the angle between the rods, the lower the free energy of interaction between them. We consider only the long-aggregate limit here, and ignore factors that stem from interactions between the cylindrical part of an aggregate and the ends of another, as well as between two aggregate ends.

It is well-known theoretically that the size distribution of aggregates can also react to external fields, such as electric or magnetic fields. [134] In fact, elongated micelles subject to a mechanical shear field have been predicted to undergo a gelation transition in the semi-dilute regime. [138] We present a treatment for self-assembled aggregates coupled to external fields that can be described by a potential in a statistical-mechanical theory (such as electric fields or certain types of elongational flow field), for the case where the self-assembled aggregates exhibit a helical transition. As we shall see, ordering fields (which are fields with a director that is parallel to the axis of induced symmetry) tend to increase the mean aggregate size, and disordering fields tend to decrease it. The fraction of helical bonds also changes with the type of field, as well as with the angle between the field director and the aggregate axis. We find that the longer type of bond is preferentially formed in an ordering field, and the shorter type in a disordering field.

This Chapter is organized as follows: in section 7.2 we study how the interaggregate interactions in long, rigid aggregates affect the helical transition. We find that the aggregate size can increase drastically under the influence of the interactions, dependent on the difference in length between the helical and non-helical bonds, the concentration of aggregating monomers, and the boundary conditions we enforce. In section 7.3, we incorporate the effect of external fields on the growth and the helical transition of the aggregates, and find that boundless growth of the aggregates can occur in certain types of orienting field. Perhaps not entirely surprising, we also find that the fraction of helical bonds in these aggregates is determined by the relative lengths of the helical and non-helical bonds. In section 7.4, we provide a brief outlook and discussion, focusing on the problems that occur in treatments of helical polymers in elongational flow and the methods needed to rectify these. We also discuss the phenomenon of boundless micellar growth in external orienting fields. Finally, in section 7.5, we summarize our findings. Unlike in previous Chapters, we cannot confront our theory with experimental results. This is because, to our knowledge, the effects of external fields and interaggregate interactions on helical supramolecular polymers have not been experimentally studied.

7.2   Interaggregate Interactions

Consider an isotropic solution of long rodlike aggregates, i.e., aggregates with a very large persistence length compared to the aggregate size, which are presumed to be rigid and smooth. In order to calculate the effect of interaggregate interactions between aggregates of lengths L and L' we apply a second-virial approximation. This approximation is valid if the mean length of the aggregates is much larger than their transverse dimension. [136, 137, 139] This implies large aggregation numbers, in particular if the aggregates have a large transverse dimension (such as those consisting of discotic molecules).

The excluded volume of two rods with lengths L and L' is, to leading order, equal to $2LL'd|\sin\gamma|$, with d the width of the rods and γ the angle between them. [137, 140] The correction terms of order Ld^2 and d^3, corresponding to the interaction of an aggregate end with the cylindrical part or with the end of the other aggregate, are small at sufficiently low concentrations. The former term, however, does renormalize the dimensionless scission energy (the energy required to break an aggregate in two) by a factor of $\kappa\phi$, with κ a constant of order unity and ϕ the volume fraction of material in solution, defined below in eq (7.10). [140] The dimensionless scission energy is often of order 10, so we ignore this renormalization here (see also below). In isotropic solution, we can average the excluded volume over all angles, which gives $\frac{\pi}{2}LL'd$. [109, 137]

The length of a self-assembled rod can be expressed as

$$L(N) = ND + (N-1)l \tag{7.1}$$

with N the number of monomers comprising the aggregate, l the (mean) bond length, and D the monomer thickness along the aggregate axis. We now presume that there are two types of bond, helical and non-helical, that may be unequal in length. If we take this into account, we can write

$$l = l_1\theta + l_2(1 - \theta) = l_1(\theta + q - \theta q) \tag{7.2}$$

where l_1 is the length of a helical bond, l_2 the length of a non-helical bond, $q \equiv l_2/l_1$, and θ the "instantaneous" fraction of helical bonds in the aggregate. Other definitions of the aggregate length are possible, but give the same results.

We now invoke a mean-field approximation to describe the conformational properties of the aggregates, and replace the length and fraction of helical bonds of the aggregates surrounding a test aggregate by their mean values. Within this approximation, the free energy of interaction of the test aggregate with the other rods is, at the level of a second-virial approximation, given by half the excluded volume times the number density of rods, and becomes

$$U = \frac{\pi}{4}L(N)\langle L\rangle d\rho \tag{7.3}$$

Here, ρ is the (dimension-bearing) number density of the aggregates, and $\langle L\rangle = \langle N\rangle D + (\langle N\rangle - 1)\langle l\rangle$ is the mean length of these aggregates, averaged over all conformations of the aggregates, as well as over the size distribution. In this expression, $\langle N\rangle$ is the mean degree of polymerization (averaged over the size distribution of the aggregates) and $\langle l\rangle = l_1(\langle\theta\rangle + q - \langle\theta\rangle q))$ the mean length of a bond in these aggregates, averaged over all conformations of the chains. Here, $\langle\theta\rangle$ is the mean fraction of helical bonds in the solution, also averaged over all chain conformations.

This gives

$$U = \frac{\pi}{4}\phi d\nu^{-1}[ND + (N-1)l]\left[D + \langle l\rangle - \frac{\langle l\rangle}{\langle N\rangle}\right] \tag{7.4}$$

with ν the volume of a monomer. In eq (7.4), the first term describes the length of the aggregate under consideration, and the second that of the others (scaled to $\langle N\rangle$).

We now combine eq (7.2) with eq (7.4), and note that $\theta = (2N-2)^{-1}\sum_{i=1}^{N-1}(s_i+1)$ with $s_i = \pm 1$ a quantity that gives the state of a bond (+1 for a helical bond, and -1 for a non-helical one), as in the Hamiltonian of eq (2.4). We find that we obtain a term with the same form as the one describing the coupling of an external magnetic field on the spins in an Ising system (see Chapter 1). This means that the interactions renormalize the excess free energy of a helical bond over a non-helical one, which becomes

$$P' = P + \frac{\pi\phi dl_1^2(1-q)}{4\nu}\left[q\frac{D}{l_1} + \langle\theta\rangle + q - \langle\theta\rangle q\right] \tag{7.5}$$

where P is the bare excess free energy of a helical bond, and P' the renormalized one. We have dropped the last term from eq (7.4), since it is small in the long-chain limit $\langle N\rangle \gg 1$. Note that, in eq (7.5), P' depends on the mean fraction of helical bonds. As we shall see

later, this fraction also depends on P', which implies that the problem has to be solved self-consistently.

With the renormalization of the helical-bond energy described, the canonical partition function $Q(N)$ takes a form similar to that in Chapters 2 and 3, and obeys, in the ground-state approximation, valid if $N \gg 1$,

$$Q(N) = (\lambda_+ \exp E')^N \exp -E_{cap} \tag{7.6}$$

where E' is given by

$$E' = E - \frac{\pi \phi d l_1^2}{4\nu} \left(\frac{D}{l_1} + q \right) \left(\frac{D}{l_1} + \langle\theta\rangle + q - \langle\theta\rangle q \right) \tag{7.7}$$

and

$$E_{cap} = E - \ln y + 2\ln\lambda_+ - \frac{\pi \phi d l_1^2}{4\nu} \left(q\frac{D}{l_1} + \langle\theta\rangle + q - \langle\theta\rangle q \right) \tag{7.8}$$

is the end-cap or scission energy. Here, $-E$ is the reference free energy in the absence of a helical transition and interactions, y is a prefactor which depends on the boundary conditions set (see Chapter 2, but note that in the equation for y here, s has been replaced by s'), and $\lambda_+ = \frac{1}{2} + \frac{1}{2}s' + \frac{1}{2}\sqrt{(s'-1)^2 - 4s'\sigma}$ is the largest eigenvalue of the so-called transfer matrix. In this expression, $s' \equiv \exp -P'$ is the Boltzmann factor associated with the excess free energy of a helical bond. As before, in Chapters 2 and 3, the parameter $\sigma \equiv \exp -2R$ is the square of the Boltzmann factor of an interface between a helical and a non-helical region along the polymer (with free energy R). This parameter we assume unchanged by the interactions.

We find that the renormalization of E given in eq (7.7) depends on the fraction of helical bonds. Away from the helical transition, E would be rescaled with a factor $-\pi\phi d(l_2 + D)^2/4\nu$, which is of the same order of magnitude as the factors that arise from terms proportional to Ld^2 that we ignored (as mentioned earlier). It turns out that the corrections to E due to interaggregate interactions are small (typically of the order of 0.2 $k_B T$ on a free energy of order 20 $k_B T$), unless the product $\phi q d l_1^2/\nu$ is very large. This being unlikely, we can reasonably ignore the corrections entirely and write $E' \approx E$, and $E_{cap} \approx E - \ln y + 2\ln\lambda_+$. Apparently, the coupling between interactions and self-assembly predominantly occurs through the renormalization of the excess helical bond energy, eq (7.5).

From equation (7.5), we deduce that there must be two regimes, one where the mean bond length is much larger than the thickness of a monomer, $\langle l\rangle \gg D$, and one where the opposite is the case, $D \gg \langle l\rangle$. We focus attention on the case where the bond length dominates and set $D/l_1 = 0$ in eqs (7.5), (7.7) and (7.8). We describe how the lengths of the bonds and the concentration influence the fraction of helical bonds, as well as the mean aggregate size. At the end of this section, we give a brief summary of the results in the limit where $D \gg \langle l\rangle$.
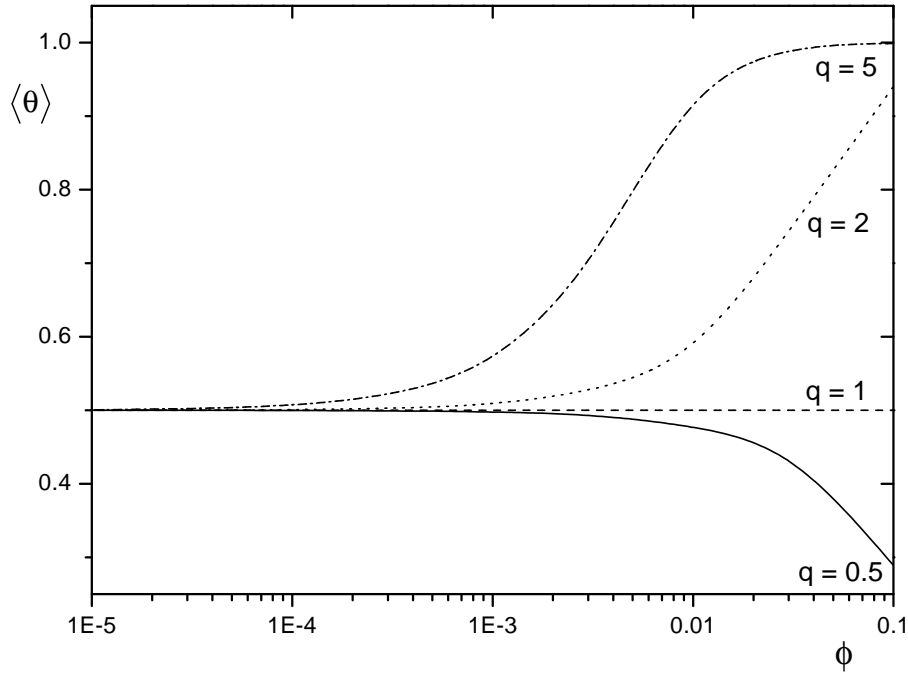
FIGURE 7.1:   The mean fraction of helical bonds $\langle \theta \rangle$ as a function of the volume fraction ϕ of assembling monomers, for $\sigma = 10^{-3}$, $s = 1$ and four values of the ratio of the lengths of a non-helical and a helical bond, q, as indicated. For dl_1^2/ν we choose a value of unity.

The strength of the coupling between the helical transition and the interaction is determined by the product of ϕ and the dimensionless volume $\pi dl_1^2/4\nu$ (see eq (7.5)). The numerical value of the latter depends on the geometry of the monomers. In the case of the discotic molecules of Meijer and co-workers, [9] ν is of the order $\pi Dd^2/4$, and the dimensionless volume $\pi dl_1^2/4\nu$ is likely of the order of magnitude of 0.1. As we shall show later, even if we set this volume to unity (increasing the effect of interactions), the interactions have a modest effect on the mean size of the aggregates, unless the volume fraction of assembling material is very high, and $\phi \to 1$. On the other hand, the impact on the helical transition can be quite substantial.

From the partition function we can calculate the mean fraction of helical bonds by taking the derivative of $\ln Q$ with respect to $\ln s'$. This gives in the long-chain limit [24, 32]

$$\langle \theta \rangle = \frac{1}{2} + \frac{1}{2}(s' - 1) \left[(s' - 1)^2 + 4\sigma s' \right]^{-1/2} \tag{7.9}$$

Note, as mentioned above, that s' is a function of the mean fraction of helical bonds (through $\langle l \rangle$), and that we therefore need to solve this equation self-consistently with eq (7.5). Results of our calculations can be seen in Figure 7.1. There, we plot the fraction of helical bonds $\langle \theta \rangle$ as a function of the volume fraction of self-assembling material ϕ,

for $\sigma = 10^{-3}$ and several values of the ratio between the lengths of a non-helical and a helical bond, q. For convenience, we have chosen the dimensionless volume $\pi dl_1^2/4\nu$ equal to unity.[1]

As can be seen from Figure 7.1, $\langle\theta\rangle > 1/2$ for $q > 1$. This means that more helical bonds form if a non-helical bond is longer than a helical one. The condition $q = 1$ corresponds to the case where both types of bond have the same length, and gives the same results as the model in which there are no interactions, since P is not changed in this case. For $q > 1$, we find an increase in the fraction of helical bonds. This makes sense, because the excess free energy due to the excluded-volume interaction scales with the square of the length of the aggregates. The longer the aggregates, the higher this excess free energy. [136] Therefore, the shorter bond is preferentially formed if $q > 1$ and the assemblies interact appreciably.

We conclude that interaggregate interactions can indeed have a large effect on the conformational state of the aggregates, if the concentration of dissolved material and the difference in bond lengths are both large enough. We can make an estimate of the concentration for which the helical transition is significantly influenced by the interaggregate interactions, and find that this is the case for $\phi \geq 4\nu\sqrt{\sigma}/dl_1^2|1-q^2|$ (see also Figure 7.1). It appears that the value of the dimensionless volume and that the cooperativity parameter σ both play important roles. If the cooperativity is low, or dl_1^2 is small compared to the reference volume, a high concentration is required for the interactions to have a significant impact on the fraction of helical bonds.

In realistic polymers, such as the aggregates consisting of discotic molecules that we consider throughout the thesis, the ratio q presumably has a value larger than unity, since the bond strength of a helical bond should be larger than that of a non-helical one. On the other hand, it seems likely that q is not larger than, say, two, due to the details of the molecular architecture. [141] In this case, the interactions have only a minor effect, unless the concentration is very high. For this reason we shall focus in the remainder of our discussion on values of q between 0.8 and 2. The behavior at low concentrations, where the effect of the interactions is small, unless q becomes very large, validates our approach in Chapters 2 and 3, in which we neglected interactions in the dilute regime.

The mean size of the aggregates can be calculated by dividing the volume fraction of aggregating material,

$$\phi = \sum_{N=1}^{\infty} N\rho(N)\nu \tag{7.10}$$

by the dimensionless number density of aggregates $\rho = \sum_{N=1}^{\infty} \rho(N)$, where $\rho(N)$ is given by $\rho(N) = \nu^{-1}Q(N)\exp\mu N$. In this expression, μ is the chemical potential of the assembling monomers and $Q(N)$ is the partition function of a helical aggregate. (See also Chapter 2,

---

[1]The choice to fix the length of a helical bond in this way causes the asymmetry between values of $q > 1$ and $q < 1$ in Figure 7.1, since a non-helical bond for $q = \alpha > 1$ has a much larger impact on the total length of the aggregate than for $q = 1/\alpha < 1$.
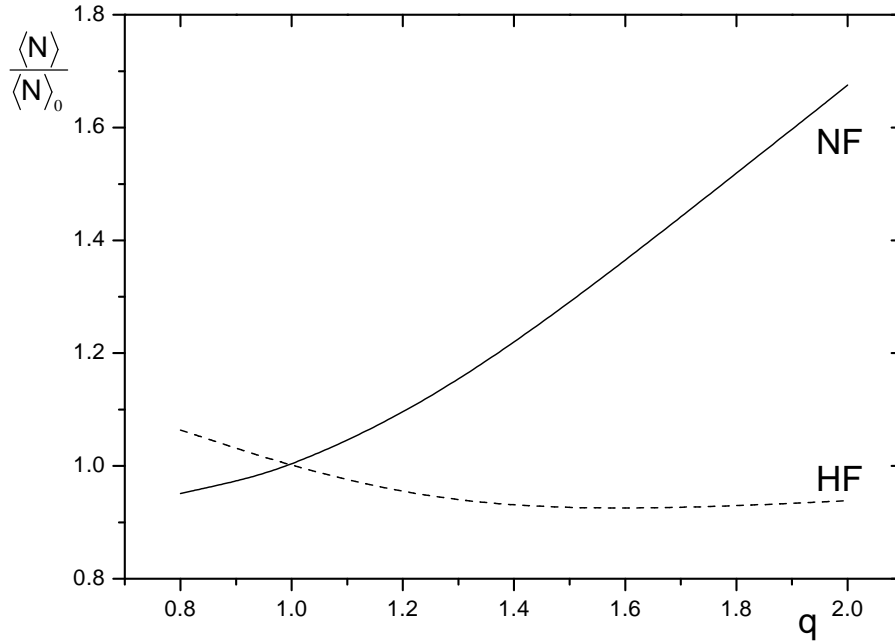
FIGURE 7.2:   The ratio $\langle N \rangle / \langle N \rangle_0$ between the mean aggregate sizes with and without interactions versus the ratio between the lengths of a non-helical and a helical bond, q, for two different boundary conditions: one with one end fixed to be non-helical and the other free (NF) and one with one end fixed to be helical and the other free (HF), as indicated. Here, $E' = 20\ k_B T$, $s = 1$, $\sigma = 10^{-3}$, $\phi = 0.1$, and $dl_1^2/\nu = 1$.

but note that $\rho(N)$ is dimension-bearing here, whereas it was dimensionless in the earlier Chapters.) Solving the summations gives $\phi = y\lambda_+^{-2}(\lambda_+ \exp -\mu')(1 - \lambda_+ \exp -\mu')^{-2} \exp -E$ and $\rho = y\lambda_+^{-2}(\lambda_+ \exp -\mu')\ (1 - \lambda_+ \exp -\mu')^{-1} \exp -E$. The mean size becomes

$$\langle N \rangle = (1 - \lambda_+ \exp -\mu')^{-1} \tag{7.11}$$

with $\mu' = -\mu - E'$ a function of the free energy of a helical bond and of the chemical potential of the assembling monomers. To solve eq (7.11), we determine the value of μ' from the law of conservation of mass, eq (7.10).

The dependence on q of the ratio $\langle N \rangle / \langle N \rangle_0$ between the mean degree of polymerization with and without interactions that follows, is shown in Figure 7.2, for $E' \approx E = 20\ k_B T$, $s = 1$, $\sigma = 10^{-3}$, $\phi = 0.1$, and $dl_1^2/\nu = 1$. Here, $\langle N \rangle_0$ is the mean aggregate size in the absence of interaggregate interactions. As we mentioned earlier, for $q = 1$ we regain the theory for aggregates without interactions (apart from a small change in E due to end effects, which we ignore here), and, therefore, the mean aggregate sizes with and without interactions are identical at this point.

It turns out that the mean aggregate size strongly depends on the boundary conditions

imposed through the quantity y. The impact of two different boundary conditions is shown in Figure 7.2. Clearly, the theory predicts a qualitatively different behavior as a function of q for the boundary condition in which one end is helical and one is free (HF), and that with one end non-helical and one free (NF). This again demonstrates the sensitivity of the size of the (long) aggregates to the state of the ends, which we also saw in Chapter 2.

For $q > 1$, the helical bond forms more readily than the non-helical one. The larger q, the more helical bonds will form. However, in the case of the boundary conditions with one end free and one end fixed non-helical, NF, the first bond of an aggregate is always non-helical. This type of bond is unfavorable and the system tends to form as few of these as possible, hence the increase in the aggregate size for this set of boundary conditions. For the boundary conditions HF (one end free and one helical) there is hardly any effect in the regime $q > 1$, for the same reason. For $q = 1$ and $s = 1$, the values of y for the two sets of boundary conditions become identical. It can be seen that the mean size of the aggregates can be affected quite strongly by the value of q at relatively high concentrations, and thus by the shift in the fraction of helical bonds. At a volume fraction of 0.01 this is no longer the case, and the mean aggregate size changes at most by a factor 1.06 over the range of q from zero to two.

We now briefly address the case that the bond length is much shorter than the thickness of a monomer ($D \gg \langle l \rangle$). The effect of interactions on the mean aggregate size and the fraction of helical bonds is much smaller, although the trends are the same. This is because in this case, the renormalized free energy of a helical bond does not depend on the fraction of helical bonds. This means that the problem is no longer a self-consistent one, and that the coupling between the helicity and the interactions becomes passive. We can again estimate the value of the concentration needed for the interactions to change the net helicity and we find that this is the case for $\phi \geq 2\sqrt{\sigma}\nu/dl_1^2|1-q|$. This resembles the result for the case $D \ll \langle l \rangle$, albeit that the dependence on q is weaker here, and therefore, at the same value of q, a higher concentration is needed to obtain the same shift in the helicity.

7.3   External Fields

To describe the conformational state of helical supramolecular aggregates under the influence of an external perturbation, we presume that the solution of aggregates is dilute, and that the particles are rodlike. We focus on external perturbations that can be described in terms of a potential, and on systems where a steady state has been reached, so that it is possible to describe the chains with equilibrium statistical mechanics. [142, 143]

The dimensionless free-energy density, F, of a solution of aggregates in an external field

can be written as

$$F = \int d\mathbf{u} \sum_{N=1}^{\infty} \rho(N, \mathbf{u})[\ln \rho(N, \mathbf{u}) - 1 - \ln \widetilde{Q}(N, \mathbf{u})] \tag{7.12}$$

with $\rho(N, \mathbf{u})$ the dimensionless number density of aggregates and $\widetilde{Q}(N, \mathbf{u})$ the canonical partition function of an aggregate in the external field, to be specified below. Here, $\mathbf{u}$ is a unit vector describing the direction of the main aggregate axis. The partition function includes information not only on the conformational state of the bonds, but also on the field-aggregate interaction. The equilibrium distribution $\rho(N, \mathbf{u})$ minimizes the free-energy (eq (7.12)), and reads

$$\rho(N, \mathbf{u}) = \widetilde{Q}(N, \mathbf{u}) \exp \mu N \tag{7.13}$$

with μ a Lagrange parameter that takes the role of the (dimensionless) chemical potential of the assembling monomers, fixed by the conservation of mass

$$\phi = \int d\mathbf{u} \int N\rho(N, \mathbf{u})dN \tag{7.14}$$

As before, ϕ denotes the volume fraction of assembling material in solution.

We restrict ourselves to the cases in which the interaction with the field couples to the aggregate size as $U(\mathbf{u})N^{\alpha}$. For an electric or magnetic field, $\alpha = 1$, [144] while for the torsional component of an elongational flow field, $\alpha = 3$, at least if the rods are not entangled. [108, 131] We first give a description of polarizable helical rodlike aggregates in a quadrupole field, and after that discuss that of a dipole field, both for $\alpha = 1$. The coupling with $\alpha = 1$ is easy to describe, yet gives some non-trivial results. The case where $\alpha = 3$ is touched upon in section 7.4.

For a quadrupole field, we write the total effect of the field on the aggregate as a sum of two terms: $U(\mathbf{u}) = K(1 + \delta\theta)\cos^2 \gamma$, where γ denotes the angle between the field and the aggregate axis, and K is the coupling constant between the field and the aggregate, which is a function of the polarizability of the monomers, as well as the magnitude of the external field. $K\delta\theta$ describes the additional coupling due to the difference in polarizability of monomers in a helical and non-helical conformation; θ is the "instantaneous" fraction of helical bonds of a configuration. The constants K and δ can be positive or negative; $K < 0$ indicates an ordering field, and $K > 0$ indicates a disordering one. A value of $\delta < 0$ indicates that monomers in a helical conformation have a lower polarizability than those in a non-helical conformation. For $\delta > 0$, the opposite is true.

For $\alpha = 1$, [144] we can calculate the effect of the field on a single bond of the helical or non-helical type in a similar way as we did in section 7.2. Incorporating the field into the Hamiltonian of a single chain (see Chapter 2), we find that the values of the helical and non-helical binding free energies are shifted, and that the excess free energy of a helical bond becomes $\widetilde{P}(\mathbf{u}) \equiv P + K\delta\cos^2 \gamma$. The partition function now takes the (ground-state) form

$$\widetilde{Q}(N, \mathbf{u}) = \widetilde{y}\widetilde{\lambda}_{+}^{N-2} \exp E(N - 1) \tag{7.15}$$

where $\widetilde{\lambda}_+ = \widetilde{\lambda}_+(\mathbf{u}) = w(\frac{1}{2} + \frac{1}{2}\widetilde{s} + \frac{1}{2}\sqrt{(1 - \widetilde{s})^2 + 4\widetilde{s}\sigma})$ again has a form similar to the well-known Zimm-Bragg eigenvalue, with $w = w(\mathbf{u}) \equiv \exp(-K\cos^2\gamma N)$ and $\widetilde{s} = \widetilde{s}(\mathbf{u}) \equiv \exp{-\widetilde{P}(\mathbf{u})}$. [36] The term $\widetilde{y} = \widetilde{y}(\mathbf{u})$ is a function of the boundary conditions imposed (see also Table 2.2) and contains the non-extensive terms that remain after the coupling between the field and the aggregate has been absorbed into the eigenvalue.

When we insert eq (7.15) into eq (7.13), we obtain for the equilibrium size distribution

$$\rho(N, \mathbf{u}) = \widetilde{y}\widetilde{\lambda}_+^{N-2} \exp\left[\mu N + E(N-1)\right] = \widetilde{y}\widetilde{\lambda}_+^{-2}\left(\widetilde{\lambda}_+ \exp{-\widetilde{\mu}}\right)^N \exp{-E} \qquad (7.16)$$

where $\widetilde{\mu} \equiv -E - \mu$ is a shifted chemical potential. This quantity we fix by multiplying eq (7.16) by the degree of polymerization N, integrating over the variables $x \equiv \cos\gamma$ and N, and invoking eq (7.14),

$$\begin{aligned}
\phi &= 4\pi \exp{-E} \int_0^1 \widetilde{y}\widetilde{\lambda}_+^{-2} dx \int_0^\infty N\left(\widetilde{\lambda}_+ \exp{-\widetilde{\mu}}\right)^N dN \\
&= 4\pi \exp{-E} \int_0^1 \widetilde{y}\widetilde{\lambda}_+^{-2}(\widetilde{\mu} - \ln\widetilde{\lambda}_+)^{-2} dx \qquad (7.17)
\end{aligned}$$

To make headway, we use a Taylor expansion of $\widetilde{y}\widetilde{\lambda}_+^{-2}$, as well as λ_+, for small values of $|K\delta x^2| \ll 1$. (This is justifiable because $|K|$ must be small in order to obtain reasonable values for the mean aggregate size, as we shall show later.) It is easy to show that the leading-order term $B \equiv \lim_{K\delta x^2 \to 0} \widetilde{y}\widetilde{\lambda}_+^{-2}$ dominates in the expansion of $\widetilde{y}\widetilde{\lambda}_+^{-2}$. This reduces eq (7.17) to

$$\phi = 4\pi \langle N\rangle_0^2 B \int_0^1 \left[1 + (1 - C\delta)\langle N\rangle_0 Kx^2\right]^{-2} dx \exp{-E} \qquad (7.18)$$

where $\langle N\rangle_0 = (\widetilde{\mu} - \ln\widetilde{\lambda}_+^0)^{-1}$ is the mean size of an aggregate in the absence of the field, $\widetilde{\lambda}_+^0 = \frac{1}{2} + \frac{1}{2}s + \frac{1}{2}\sqrt{(s-1)^2 + 4\sigma s}$ the eigenvalue of the transfer matrix in the absence of a field (cf. eq (2.10)), and $C = s(-1 + \lambda_+ + 2\sigma)/(2\lambda_+ - 1 - s)$. Note that we need not specify B, as it does not influence the mean aggregate size, nor the mean fraction of helicity, as we shall see below.

If we solve the integral (7.18), we obtain for $K > 0$

$$\phi = 2\pi \langle N\rangle_0^2 B h^{-1/2}\left(\frac{\sqrt{h}}{1+h} + \arctan\sqrt{h}\right) \exp{-E} \qquad (7.19)$$

with $h \equiv K(1 - C\delta)\langle N\rangle_0$. Note that for $h \ll 1$, there is no coupling of the field to the aggregates and $\langle N\rangle = \langle N\rangle_0$. For $K < 0$ we get

$$\phi = 2\pi \langle N\rangle_0^2 B (-h)^{-1/2}\left(\frac{\sqrt{-h}}{1+h} + \frac{1}{2}\ln\frac{1+\sqrt{-h}}{1-\sqrt{-h}}\right) \exp{-E} \qquad (7.20)$$

In the latter case, a singularity occurs for $\sqrt{-h} = 1$ (or $K \langle N \rangle_0 = (-1 + C\delta)^{-1}$).

The total number density of aggregates can be calculated in a similar fashion, giving

$$\rho = 4\pi \langle N \rangle_0 B h^{-1/2} \arctan \sqrt{h} \exp -E \tag{7.21}$$

for $K > 0$, and

$$\rho = 2\pi \langle N \rangle_0 B (-h)^{-1/2} \ln \frac{1 + \sqrt{-h}}{1 - \sqrt{-h}} \exp -E \tag{7.22}$$

for $K < 0$. The singularity for $K \langle N \rangle_0 \to -(1 - C\delta)^{-1}$ for negative values of K, persists in the mean aggregate size, which follows from $\langle N \rangle \equiv \phi/\rho$. This gives

$$\langle N \rangle = \frac{1}{2} \langle N \rangle_0 \left[1 + 2 \frac{\sqrt{-h}}{1+h} \left(\ln \frac{1 + \sqrt{-h}}{1 - \sqrt{-h}} \right)^{-1} \right] \tag{7.23}$$

for $K < 0$. For $K > 0$, where there is no singularity, we obtain

$$\langle N \rangle = \frac{1}{2} \langle N \rangle_0 \left[1 + \frac{\sqrt{h}}{1+h} \left(\arctan \sqrt{h} \right)^{-1} \right] \tag{7.24}$$

From equations (7.23) and (7.24), we see that $\langle N \rangle / \langle N \rangle_0$ is a natural function of $K \langle N \rangle_0$. Note also that the mean aggregate size becomes independent of the boundary conditions set, contrary to what we found for the coupling of the helical aggregation to the molecular field in section 7.2.

Equation (7.23) contains a divergence for $h \to -1$, which implies that the theory predicts boundless growth for this value. As to be discussed in section 7.4, this phenomenon has been predicted earlier for solutions of aligned micelles, and is often interpreted in terms of a gelation transition. [131, 138, 145] On the other hand, we deduce from reference [146] that the divergence can be removed by allowing for a finite bending flexibility, and must therefore be regarded as spurious.

It is instructive to see how the mean aggregate size depends on the angle between the aggregate axis and the field. An angle-dependent aggregate size may be defined as

$$\langle N \rangle (\mathbf{u}) \equiv \frac{\phi(\mathbf{u})}{\rho(\mathbf{u})} = (\widetilde{\mu} - \ln \widetilde{\lambda}_+)^{-1} \tag{7.25}$$

with $\rho(\mathbf{u}) \equiv \int \rho(N, \mathbf{u}) dN$, and $\phi(\mathbf{u}) \equiv \int N\rho(N, \mathbf{u}) dN$. Note that the mean aggregate size becomes independent of the boundary conditions, again unlike what we observed in earlier Chapters. It is obvious from eq (7.25) that boundless aggregate growth occurs if $\widetilde{\mu} = \ln \widetilde{\lambda}_+$, which is only possible for $K < 0$. The angle at which infinite growth takes place can be easily determined, and equals $x_* = \cos \gamma_* \approx 1/\sqrt{(1 - C\delta)K \langle N \rangle_0}$. For angles smaller than x_* the mean aggregate size becomes negative, which is obviously unphysical.
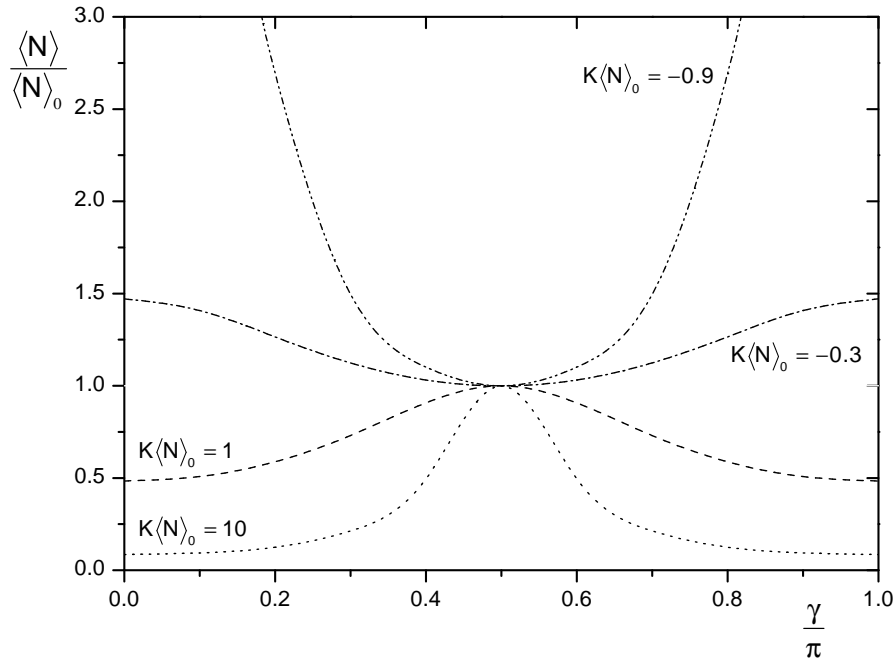
FIGURE 7.3: The ratio $\langle N \rangle / \langle N \rangle_0$ of the mean aggregate size with and without an external field versus the angle between the aggregate axis and the external field, γ, for several values of $K \langle N \rangle_0$, as indicated, with fixed $s = 1$, $\delta = -0.1$, and $\sigma = 10^{-3}$.

Results are presented in Figure 7.3, where we show the ratio of the mean aggregate size in the presence of the field, $\langle N \rangle$, and that in its absence, $\langle N \rangle_0$, versus the angle γ, for several values of the effective field strength $K \langle N \rangle_0$, at fixed $s = 1$, $\sigma = 0.001$, and $\delta = -0.1$. Our choice for δ implies that the monomers have a lower polarizability when they are in a helical conformation than when they are in a non-helical one. For values of $K \langle N \rangle_0$ below $-1/(1 - C\delta)$, we indeed find aggregation numbers that go to infinity for angles close to zero. Furthermore, we can see that the effect of the field on the aggregate size increases with increasing field strength. The effect of an orienting field ($K < 0$) is to increase the mean aggregate size for angles other than $\pi/2$, where the rod is oriented perpendicular to the field and for which the aggregates are not affected by the field. A disorienting field has the opposite effect, namely to decrease the mean aggregate size.

Since helical structures have an inherent direction, it is not unlikely that a helix may carry a permanent dipole. In this case the interaction of the polymer with the field is described by a dipolar field. This situation is very similar to that of a polarizable rod in a quadrupolar field, albeit that the angle dependence becomes Kx rather than Kx^2. [144] In this case, we find infinitely long aggregates (after integration over all aggregate sizes and angles) for $K \langle N \rangle_0 \geq \pm 1/(1 - C\delta)$, so both for positive and negative values of K. If we plot the renormalized mean aggregate size as a function of the angle γ (see Figure 7.4), we see that, for both positive and negative values of $K \langle N \rangle_0$, an increase in the aggregate size
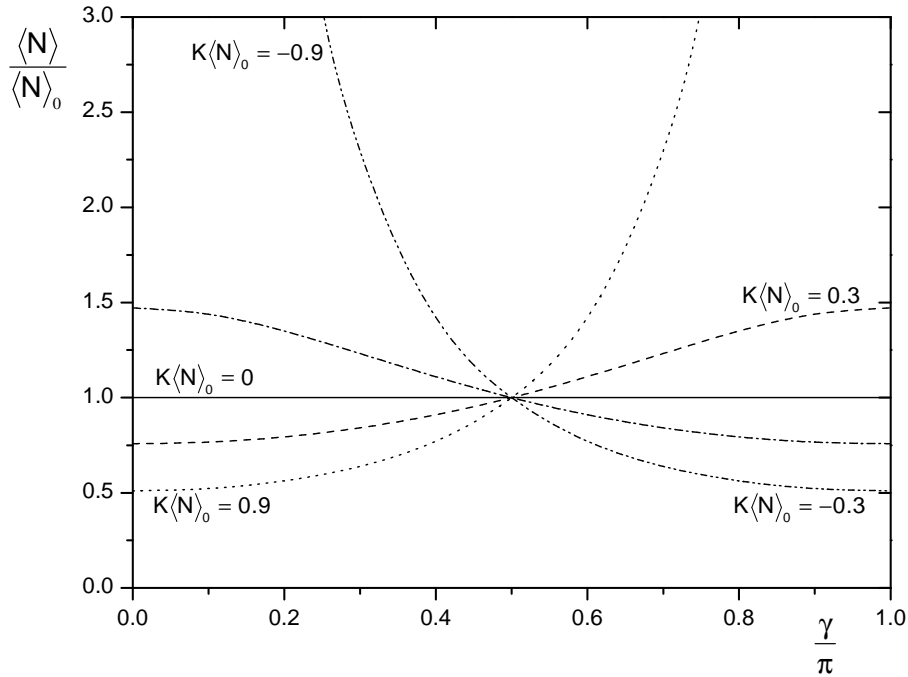
FIGURE 7.4:   As Figure 7.3, but for a dipolar field.

is observed for a certain range of angles. We note that the aggregates are now smallest not when they are perpendicular to the field, but when they are parallel to the field, but the dipole moment is in the direction opposite to that of the field director.

We conclude that the mean size of a helical aggregate depends strongly on the presence of an external field. Whether the same is true for the conformational state of the aggregate we can check by calculating the fraction of helical bonds, averaged over all internal configurations $\langle \theta \rangle (\mathbf{u})$ of an aggregate, as a function of the angle between the aggregate and the field. In the ground-state approximation this equals (cf. eq (7.9)) [144]

$$\langle \theta \rangle (\mathbf{u}) \approx \frac{\partial \ln \widetilde{\lambda}_+}{\partial \ln \widetilde{s}} = \frac{1}{2} + \frac{1}{2}(\widetilde{s} - 1) \left[(\widetilde{s} - 1)^2 + 4\sigma\widetilde{s} \right]^{-1/2} \tag{7.26}$$

In Figure 7.5 we show the dependence of the helicity on the angle γ between the axis of the aggregate and the field, for several values of $K \langle N \rangle_{0}$,[2] and $s = 1$, $\sigma = 0.001$, and $\delta = -0.1$.

Dependent on the sign of the field, rods inclined at large angles have either a larger or a smaller degree of helicity than those nearly parallel to the field. This can be explained by realizing that if $K < 0$, the field induces monomers to adopt a non-helical conformation, since non-helical monomers have a stronger interaction with it. This gives a decrease in θ. For $K > 0$, the opposite is the case, and the mean helicity increases. The larger the

---

[2]We used the values $E = 10$ and $\phi = 0.01$ to calculate the value of $\langle N \rangle_0$, since there is no direct coupling to $\langle N \rangle_0$ in eq (7.26). For this choice, $\langle N \rangle_0 \approx 50$. If we set $E = 20$, we obtain $\langle N \rangle_0 \approx 1800$
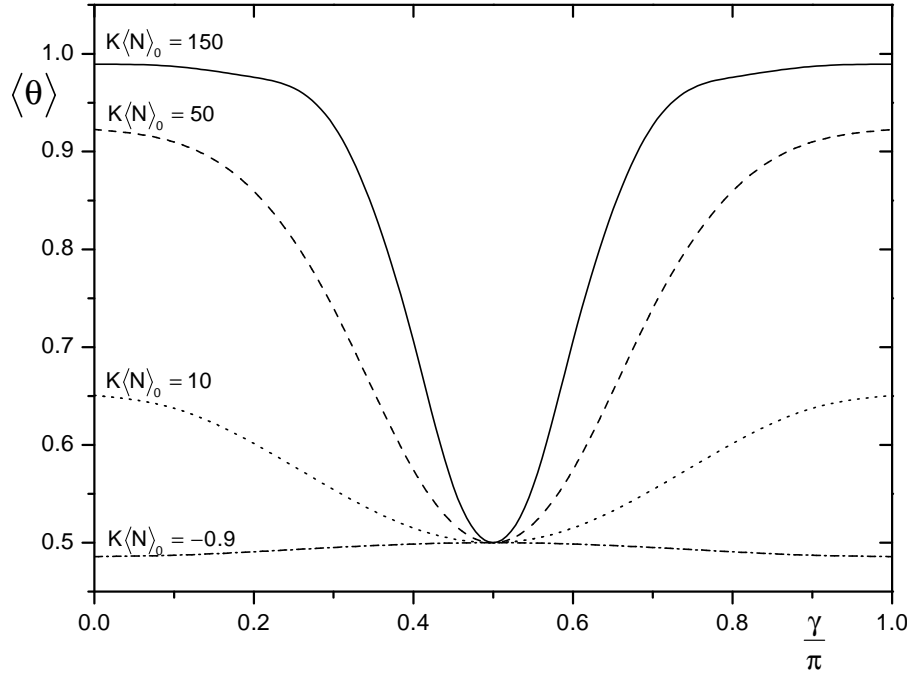
FIGURE 7.5: The fraction of helical bonds in an aggregate as a function of the angle between the aggregate axis and the external field, for fixed $s = 1$, $\sigma = 0.001$, and $\delta = -0.1$. Indicated are four different values of $K \langle N \rangle_0$.

coupling to the field is, the stronger the effect on the helicity. We conclude that very large values of $K \langle N \rangle_0$ are necessary to induce a significant effect in the helicity for these values of σ and δ. We did not study the helicity for values of $K \langle N \rangle_0$ below -0.9 because of the spurious boundless aggregate growth for $K \langle N \rangle_0 \to -1$.

In Figure 7.6, we vary some of the other parameters, while fixing $K \langle N \rangle_0$ at 150. If we examine an aggregate in which the helical transition is less cooperative ($\sigma = 0.1$ instead of 0.001), we see that the dependence of the helicity on the angle becomes broader and less pronounced. This implies that we can also obtain a stronger effect of the field on the helicity at somewhat lower values of $K \langle N \rangle_0$ if we choose σ small enough. If we differentiate the helical and non-helical bonds further by increasing the absolute value of δ, we see an increase in the peak sharpness: helical bonds are so short that they are even more favorable than before (in the disordering field), and as such the preference for them becomes stronger, even for values of γ quite close to $\pi/2$.

Another way to influence the balance between helical and non-helical bonds is by changing the Boltzmann factor s, effectively changing the bare excess free energy of the helical bond (in the absence of a field). Even a small change has a large effect on the helicity curve (Figure 7.6): the range over which the aggregates are almost fully non-helical increases in
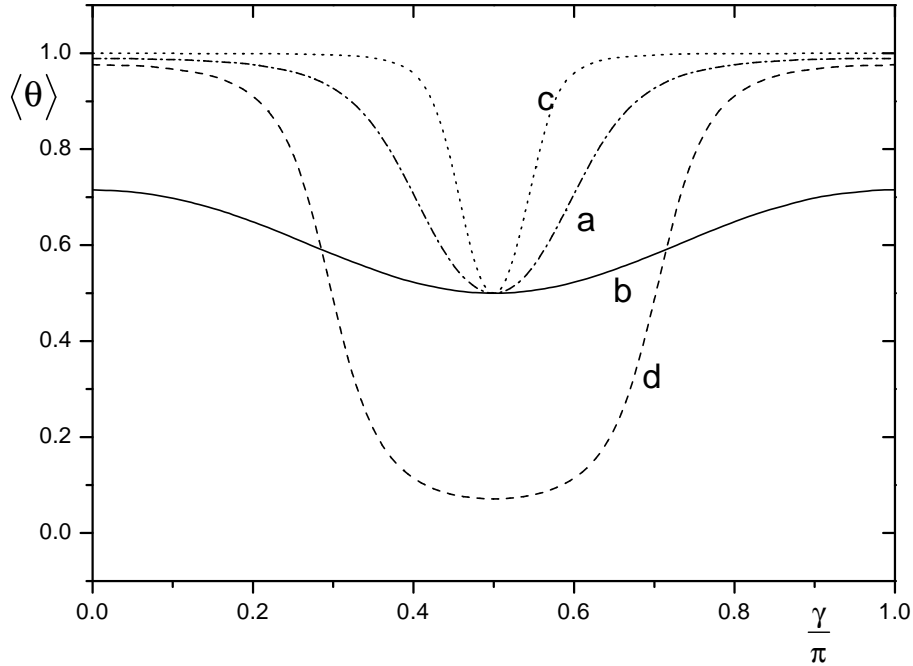
FIGURE 7.6:   As Figure 7.5, but for fixed: **a.** $s = 1$, $\sigma = 0.001$, and $\delta = -0.1$; **b.** $s = 1$, $\sigma = 0.1$, and $\delta = -0.1$; **c.** $s = 1$, $\sigma = 0.001$, and $\delta = -0.5$, and **d.** $s = 0.9$, $\sigma = 0.001$, and $\delta = -0.1$. $K \langle N \rangle_0 = 150$ in all cases.

size when we decrease the value of s. Only for aggregates that lie almost parallel to the field does the difference in polarizability between helical and non-helical bonds play a role.

7.4   Discussion

As we mentioned in the previous section, boundless growth can occur in helical aggregates for certain angles, dependent on the type of field. Theories describing rigid, self-assembled structures in external as well as molecular fields are known to predict such infinite growth. [131, 145] It occurs because of a positive feedback between the aggregate size and the alignment of the aggregates: the larger the aggregate is (in the direction parallel to the field), the larger the orienting effect of the field on it becomes, and the more it will grow. [145] This phenomenon is also well known in the context of liquid crystallinity of self-assembled polymers. [109, 146, 147] Whether or not the unbounded aggregate growth can be directly linked to the gelation transition predicted in some micellar systems is not altogether clear at this point, due to a lack of experimental data on aggregates in external fields. [131] Only in shear flow, which cannot be described by a simple potential, is there

any experimental evidence (from viscosity measurements) that suggests a change in the size of the aggregates. [131]

As we already announced in the previous section, it proves possible, however, to avoid the boundless growth in some of the theoretical descriptions, implying it is a mathematical anomaly. Two techniques have been proposed to achieve this. First, the infinite growth can be suppressed by introducing a finite flexibility of the chains, as was done by van der Schoot in the description of liquid crystalline ordering of linear micelles, [146] and second, it can (in principle) be suppressed by including a stretching term into the potential. [131, 134]

Ideally, we would like to describe the conformational state and properties of helical aggregates in elongational flow, rather than only in fields of the type described above. If we apply an external field of the elongational type, and assume the so-called fast-reaction regime to apply [131], the elongational flow can be described with a term that scales like $U(\mathbf{u})N^3$, as already mentioned in section 7.1. The third power with N makes it impossible to use the method we used for the coupling with the electric field, and insert the polymer-field coupling into the Hamiltonian of the helical chain. Instead, one should calculate the influence of the field on an entire aggregate, rather than per bond. [131, 142] We have not been able to find an expression for the mean size of the helical aggregates in elongational flow.

Nevertheless, it is obvious that for an elongational flow field there is a singularity, now for all angles γ, since the coupling to the field scales with N^3, which grows much faster than the linear term. To suppress the infinite growth, we can again attempt to introduce flexibility or use a term for the component of the flow parallel to the rod, i.e., a stretching term, into the expression for the free energy. [131, 134] This term has the form $[P_2(\cos\gamma)]^2 N^5$. Since the prefactor is never smaller than zero, this term cannot increase the anomalous growth. However, this term becomes zero for $\cos\gamma = 1/\sqrt{3}$, so that it cannot suppress the infinite growth for this angle. Therefore, it does not solve the problem of infinite growth for all angles, and upper limits on the allowed aggregate size have to be manually inserted. [131, 134] The treatment of elongational flow and the effect of flexibility and chain stretching deserve further study.

Another interesting object for study is the possible effect of external fields and interactions on the chirality amplification in aggregates formed from monomer mixtures. We speculate that, since the right-handed and left-handed helical bond are symmetrical, they have the same length, and the coupling of the interaggregate interactions should be the same for both types of bond. This would mean that there is no effect on the chirality amplification itself. Due to symmetry, we imagine that the polarizability of the left-handed and right-handed helical monomers are equal in magnitude as well, and hence there is likely no effect for external fields.

7.5   Conclusions

We have demonstrated that interaggregate interactions, taken into account on the second-virial level, change the mean size and the conformational state of self-assembled helical aggregates. We find that the helical transition can couple strongly to the interaggregate interactions, and that the shift in the helicity due to the interactions can cause a large change in the aggregate size, if the concentration is high enough. Dependent on the ratio q between the lengths of a helical and a non-helical bond, the formation of a helical bond becomes relatively more or less favorable. The boundary conditions imposed have a large influence on the qualitative picture of the aggregate size as a function of q.

The effect on helical supramolecular polymers of external fields with a quadrupole and dipole character has been described. Apart from the known factors that regulate the conformational state of the aggregates in the absence of a field, it now also depends on the polarizability of the monomers in the helical and non-helical bond states, as well as on the sign and magnitude of the field. For an ordering field, the longest of the bond types is favored, all other things being equal, and the mean size of the aggregates increases. In the case of a disordering field, the opposite is the case and the aggregates become shorter.

Bibliography

[1] Poland, D.; Scheraga, H. A. *Theory of Helix-Coil Transitions in Biopolymers*; Academic Press: New York, 1970.

[2] Friedhoff, P.; von Bergen, M.; Mandelkow, E.-M.; Davies, P.; Mandelkow, E. *Proc. Natl. Acad. Sci. USA* **1998**, *95*, 15712.

[3] Watts, N. R.; Misra, M.; Wingfield, P. T.; Stahl, S. J.; Cheng, N.; Trus, B. L.; Steven, A. C.; Williams, R. W. *J. Struct. Biol.* **1998**, *121*, 41.

[4] Oosawa, F.; Asakura, S. *Thermodynamics of the Polymerization of Protein*, 1st ed.; Academic Press: London, 1975.

[5] Oosawa, F. *Biophys. Chem.* **1993**, *47*, 101.

[6] Korn, E. D. *Physiol. Rev.* **1982**, *62*, 672.

[7] Klug, A. *Angew. Chem. Int. Ed. Engl.* **1983**, *22*, 565.

[8] Brunsveld, L.; Folmer, B. J. B.; Meijer, E. W. *MRS Bulletin* **2000**, *25*, 49.

[9] Brunsveld, L.; Zhang, H.; Glasbeek, M.; Vekemans, J. A. J. M.; Meijer, E. W. *J. Am. Chem. Soc.* **2000**, *122*, 6175.

[10] Hirschberg, J. H. K. K.; Brunsveld, L.; Ramzi, A.; Vekemans, J. A. J. M.; Sijbesma, R. P.; Meijer, E. W. *Nature* **2000**, *407*, 167.

[11] Van Nostrum, C. F.; Bosman, A. W.; Gelinck, G. H.; Schouten, P. G.; Warman, J. M.; Kentgens, A. P. M.; Devillers, M. A. C.; Meijerink, A.; Picken, S. J.; Sohling, U.; Schouten, A.-J.; Nolte, R. J. M. *Chem. Eur. J.* **1995**, *1*, 171.

[12] Yoshida, N.; Harata, K.; Inoue, T.; Ito, N.; Ichikawa, K. *Supramol. Chem.* **1998**, *10*, 63.

[13] Gallivan, J. P.; Schuster, G. B. *J. Org. Chem.* **1995**, *60*, 2423.

[14] Lovinger, A. J.; Nuckolls, C.; Katz, T. J. *J. Am. Chem. Soc.* **1998**, *120*, 264.

[15] Fenniri, H.; Mathivanan, P.; Vidale, K. L.; Sherman, D. M.; Hallenga, K.; Wood, K. V.; Stowell, J. G. *J. Am. Chem. Soc.* **2001**, *123*, 3854.

[16] Engelkamp, H.; Middelbeek, S.; Nolte, R. J. M. *Science* **1999**, *284*, 785.

[17] Green, M. M.; Park, J.-W.; Sato, T.; Teramoto, A.; Lifson, S.; Selinger, R. L. B.; Selinger, J. V. *Angew. Chem. Int. Ed. Engl.* **1999**, *38*, 3138.

[18] Brunsveld, L.; Lohmeijer, B. G. G.; Vekemans, J. A. J. M.; Meijer, E. W. *Chem. Commun.* **2000**, 2305.

[19] Brunsveld, L.; Lohmeijer, B. G. G.; Vekemans, J. A. J. M.; Meijer, E. W. *J. Incl. Phenom. Macrocycl. Chem.* **2001**, *41*, 61.

[20] Teramoto, A. *Prog. Polym. Sci.* **2001**, *26*, 667.

[21] Terech, P.; Weiss, R. G. *Chem. Rev.* **1997**, *97*, 3133.

[22] Van Nostrum, C. F. *Adv. Mater.* **1996**, *8*, 1027.

[23] Oosawa, F.; Kasai, M. *J. Mol. Biol.* **1962**, *4*, 10.

[24] van der Schoot, P.; Michels, M. A. J.; Brunsveld, L.; Sijbesma, R. P.; Ramzi, A. *Langmuir* **2000**, *16*, 10076.

[25] Flory, P. J.; Miller, W. G. *J. Mol. Biol.* **1966**, *15*, 284.

[26] Engel, J.; Schwarz, G. *Angew. Chem.* **1970**, *82*, 468.

[27] Vogl, O.; Jaycox, G. D. *Polymer* **1987**, *28*, 2179.

[28] Okamoto, Y.; Nakano, T. *Chem. Rev.* **1994**, *94*, 349.

[29] Schellman, J. A. *J. Phys. Chem.* **1958**, *62*, 1485.

[30] Bixon, M.; Lifson, S. *Biopolymers* **1966**, *4*, 815.

[31] Bloomfield, V. A. *Am. J. Phys.* **1999**, *67*, 1212.

[32] Grosberg, A. Yu.; Khokhlov, A. R. *Statistical Physics of Macromolecules*; AIP Press: New York, 1994.

[33] Montroll, E. W.; Goel, N. S. *Biopolymers* **1966**, *4*, 855.

[34] Leung, M. L. C.; Tong, B. Y.; Wu, F. Y. *Phys. Lett.* **1975**, *54A*, 361.

[35] Peng, Y.; Hansmann, U. H. E. *Biophys. J.* **2002**, *82*, 3269.

[36] Zimm, B. H.; Bragg, J. K. *J. Chem. Phys.* **1959**, *31*, 526.

[37] Ising, E. *Z. Phys.* **1925**, *31*, 253.

[38] Applequist, J. *J. Chem. Phys.* **1963**, *38*, 934.

[39] Goodby, J. W. *J. Mater. Chem.* **1991**, *1*, 307.

[40] Green, M. M.; Reidy, M. P.; Johnson, R. J.; Darling, G.; O'Leary, D. J.; Willson, G. *J. Am. Chem. Soc.* **1989**, *111*, 6452.

[41] Selinger, J. V.; Selinger, R. L. B. *Phys. Rev. E* **1997**, *55*, 1728.

[42] Carlini, C.; Ciardelli, F.; Pino, P. *Makromol. Chem.* **1968**, *119*, 244.

[43] Green, M. M.; Garetz, B. A.; Munoz, B.; Chang, H.; Hoke, S.; Cooks, R. G. *J. Am. Chem. Soc.* **1995**, *117*, 4181.

[44] Selinger, J. V.; Selinger, R. L. B. *Phys. Rev. Lett.*, **1996**, *76*, 58.

[45] Ben-Shaul, A.; Rorman, D. H.; Hartland, G. V.; Gelbart, W. M. *J. Phys. Chem.* **1986**, *90*, 5277.

[46] Jensen, P. J.; Bennemann, K.-H. *J. Chem. Phys.* **1985**, *83*, 6457.

[47] Tobolsky, A. V.; Owen, G. D. T. *J. Polym. Sci.* **1962**, *59*, 329.

[48] Gitterman, M. *J. Phys. A: Math. Gen.* **2000**, *33*, 8373.

[49] Cardy, J. *Scaling and Renormalization in Statistical Physics*, Cambridge University Press: Cambridge, 1996.

[50] Morgenstern, I.; Binder, K.; Baumgärtner, A. *J. Chem. Phys.* **1978**, *69*, 253.

[51] Ciferri, A. *Prog. Polym. Sci.* **1995**, *20*, 1081.

[52] Moore, J. S. *Curr. Opin. Colloid Interface Sci.* **1999**, *4*, 108.

[53] Lawrence, D. S.; Jiang, T.; Levett, M. *Chem. Rev.* **1995**, *95*, 2229.

[54] Reinhoudt, D. N.; Crego-Calama, M. *Science* **2002**, *295*, 2403.

[55] Lehn, J.-M. *Supramolecular Chemistry: Concepts and Perspectives*, VCH: Weinheim, 1995.

[56] Whitesides, G. M.; Mathias, J. P.; Seto, C. T. *Science* **1991**, *254*, 1312.

[57] Greer, S. C. *Annu. Rev. Phys. Chem.* **2002**, *53*, 173.

[58] Ben-Shaul, A.; Gelbart, W. M. In *Micelles, Membranes, Microemulsions, and Monolayers*; Gelbart, W. M., Ben-Shaul, A., Roux, D., Eds.; Springer Verlag: New York, 1994.

[59] Ciferri, A. (editor) *Supramolecular Polymers*, Marcel Dekker Inc: New York, 2000.

[60] Brandt, H. C. A.; Hendriks, E. M.; Michels, M. A. J.; Visser, F. *J. Phys. Chem.* **1995**, *99*, 10430.

[61] Van Roij, R. *Phys. Rev. Lett.* **1996**, *76*, 3348.

[62] Scott, R. L. *J. Phys. Chem.* **1965**, *69*, 261.

[63] Tobolsky, A. V.; Eisenberg, A. *J. Am. Chem. Soc.* **1960**, *82*, 289.

[64] Missel, P. J.; Mazer, N. A.; Benedek, G. B.; Young, C. Y.; Carey, M. C. *J. Phys. Chem.* **1980**, *84*, 1044.

[65] Porte, G. *J. Phys. Chem.* **1983**, *87*, 3541.

[66] Cates, M. E.; Candau, S. J. *J. Phys.: Condens. Matt.* **1990**, *2*, 6869.

[67] Taylor, M. P.; Herzfeld, J. *J. Phys.: Condens. Matt.* **1993**, *5*, 2651.

[68] Odijk, T. *Curr. Opin. Colloid Interface Sci.* **1996**, *1*, 337.

[69] Lehn, J.-M. *Proc. Natl. Acad. Sci. USA* **2002**, *99*, 4763.

[70] Wheeler, J. C.; Pfeuty, P. *Phys. Rev. A* **1981**, *24*, 1050.

[71] Cabani, S.; Paci, A.; Rizzo, V. *Biopolymers* **1976**, *15*, 113.

[72] Qian, H.; Schellman, J. A. *J. Phys. Chem.* **1992**, *96*, 3987.

[73] Hairyan, Sh. A.; Mamasakhlisov, E. Sh.; Morozov, V. F. *Biopolymers* **1995**, *35*, 75.

[74] Takano, M.; Nagayama, K.; Suyama, A. *J. Chem. Phys.* **2002**, *116*, 2219.

[75] ten Brinke, G.; Karasz, F. E. *J. Chem. Phys.* **1983**, *79*, 2065.

[76] Domb, C. *The Critical Point*, Taylor & Francis: London, 1996.

[77] de Jongh, L. J.; Miedema, A. R. *Experiments on Simple Magnetic Model Systems*, Taylor & Francis Ltd: London, 1974.

[78] Newell, G. F.; Montroll, E. W. *Rev. Mod. Phys.* **1953**, *25*, 353.

[79] Lee, T. D.; Yang, C. N. *Phys. Rev.* **1952**, *87*, 410.

[80] Hill, T. L., *Statistical Mechanics*, McGraw-Hill Book Company: New York, 1956.

[81] Chandler, D. *Introduction to Modern Statistical Mechanics*, Oxford University Press: New York, 1987.

[82] Goldenfeld, N. *Lectures on Phase Transitions and the Renormalization Group*, Addison-Wesley: Amsterdam, 1992.

[83] Kramers, H. A.; Wannier, G. H. *Phys. Rev.* **1941**, *60*, 252.

[84] Tanaka, T.; Suzuki, M. *J. Chem. Phys.* **1973**, *59*, 3795.

[85] Ben-Naim, A. *Statistical Thermodynamics for Chemists and Biochemists*, Plenum Press: New York, 1992.

[86] Flory, P. J. *Macromolecules* **1974**, *7*, 381.

[87] Flory, P. J. *Statistical Mechanics of Chain Molecules*, Hanser Publishers: New York, 1989.

[88] Volkenstein, M. V. *Configurational Statistics of Polymeric Chains*, Interscience Publishers, John Wiley & Sons: London, 1963.

[89] Wu, F. Y. *J. Appl. Phys.* **1984**, *55*, 2421.

[90] Mitchell, D. J.; Ninham, B. W. *J. Chem. Soc., Faraday Trans. 2* **1981**, *77*, 601.

[91] Reiss, H.; Bowles, R. K. *J. Chem. Phys.* **1999**, *111*, 7501.

[92] Kegel, W. K.; Reiss, H., *Ber. Bunsenges. Phys. Chem.* **1996**, *100*, 300.

[93] Van der Schoot, P. *Europhys. Lett.* **1997**, *39*, 25.

[94] Henderson, J. R. *Phys. Rev. E* **1997**, *55*, 5731.

[95] Schäfer, L. *Phys. Rev. B* **1992**, *46*, 6061.

[96] Wittmer, J. P.; Milchev, A.; Cates, M. E. *J. Chem. Phys.* **1998**, *109*, 834.

[97] Wang, Z.-G.; Costas, M. E.; Gelbart, W. M. *J. Phys. Chem.* **1993**, *97*, 1237.

[98] Dudowicz, J.; Freed, K. F.; Douglas, J. F. *J. Chem. Phys.* **1999**, *111*, 7116.

[99] Petschek, R. G.; Pfeuty, P.; Wheeler, J. C. *Phys. Rev. A* **1986**, *34*, 2391.

[100] Wittmer, J. P.; van der Schoot, P.; Milchev, A.; Barrat, J. L. *J. Chem. Phys.* **2000**, *113*, 6992.

[101] Duyndam, A.; Odijk, T. *Langmuir* **1996**, *12*, 4718.

[102] Brunsveld, L.; Meijer, E. W.; Prince, R. B.; Moore, J. S. *J. Am. Chem. Soc.* **2001**, *123*, 7978.

[103] Henderson, J. R. *J. Chem. Phys.* **2000**, *113*, 5965.

[104] DuPré, D. B. *Biopolymers* **1990**, *30*, 1051.

[105] Sijbesma, R. P.; Beijer, F. H.; Brunsveld, L.; Folmer, B. J. B.; Hirschberg, J. H. K. K.; Lange, R. F. M.; Lowe, J. K. L.; Meijer, E. W. *Science* **1997**, *278*, 1601.

[106] Corbin, P. S.; Zimmerman, S. C. *Hydrogen-bonded Supramolecular Polymers* in: Ciferri, A. (editor) *Supramolecular Polymers*, 1st ed.; Marcel Dekker: New York, 2000.

[107] Niranjan, P. S.; Forbes, J. G.; Greer, S. C.; Dudowicz, J.; Freed, K. F.; Douglas, J. F. *J. Chem. Phys.* **2001**, *114*, 10573.

[108] Gelbart, W. M.; Ben-Shaul, A.; McMullen, W. E.; Masters, A. *J. Phys. Chem.* **1984**, *88*, 861.

[109] Van der Schoot, P.; Cates, M. E. *Langmuir* **1994**, *10*, 670.

[110] Palmans, A. R. A.; Vekemans, J. A. J. M.; Fischer, H.; Hikmet, R. A.; Meijer, E. W. *Chem. Eur. J.* **1997**, *3*, 300.

[111] Palmans, A. R. A.; Vekemans, J. A. J. M.; Havinga, E. E.; Meijer, E. W. *Angew. Chem. Int. Ed. Engl.* **1997**, *36*, 2648.

[112] Brunsveld, L., *private communication.*

[113] Zhang, J.; Moore, J. S. *J. Am. Chem. Soc.* **1992**, *114*, 9701.

[114] Ecoffet, C.; Markovitsi, D.; Jallabert, C.; Strzelecka, H.; Veber, M. *J. Chem. Soc. Faraday Trans.* **1992**, *88*, 3007.

[115] Sheu, E. Y.; Liang, K. S.; Chiang, L. Y. *J. Phys. France* **1989**, *50*, 1279.

[116] Boden, N.; Bushby, R. J.; Hardy, C.; Sixl, F. *Chem. Phys. Lett.* **1986**, *123*, 359.

[117] Malthête, J.; Jacques, J.; Tinh, N. H.; Destrade, C. *Nature* **1982**, *298*, 46.

[118] Gedde, U. W. *Polymer Physics*, 1st ed.; Chapman and Hall: London, 1995.

[119] Ramzi, A.; Brunsveld, L.; Meijer, E. W. to be published.

[120] Mruk, R.; Zentel, R. *Macromolecules* **2002**, *35*, 185.

[121] Gu, H.; Sato, T.; Teramoto, A.; Varichon, L.; Green, M. M. *Polym. J.* **1997**, *29*, 77.

[122] Lifson, S.; Andreola, C.; Peterson, N. C.; Green, M. M. *J. Am. Chem. Soc.* **1989**, *111*, 8850.

[123] Lee, F. T.; Montroll, E. W.; Yu, L. *J. Stat. Phys.* **1973**, *8*, 309.

[124] Kawatra, M. P.; Kijewski, L. *J. Phys. Rev.* **1969**, *183*, 291.

[125] Chiang, M. F.; Wu, F. Y. *Phys. Lett.* **1970**, *31A*, 189.

[126] van Gestel, J.; van der Schoot, P.; Michels, M. A. J. *Langmuir,* **2003**, *19*, 1375.

[127] van Gestel, J.; van der Schoot, P.; Michels, M. A. J. *J. Phys. Chem. B* **2001**, *105*, 10691.

[128] Toyoda, S.; Fujiki, M. *Macromolecules* **2001**, *34*, 640.

[129] Farina, M. *Topics in Stereochem.* **1987**, *17*, 1.

[130] Palmans, A. R. A., *private communication.*

[131] Gelbart, W. M.; Ben-Shaul, A.; Wang, S.-Q.; Bruinsma, R. *Surfactants in Solution* **1991**, *11*, 113.

[132] Kim, Y. H.; Pincus, P. *Biopolymers* **1979**, *17*, 2315.

[133] Matsuyama, A.; Kato, T. *J. Chem. Phys.* **2001**, *114*, 3817.

[134] Wang, S.-Q.; Gelbart, W. M.; Ben-Shaul, A. *J. Phys. Chem.* **1990**, *94*, 2219.

[135] Ben-Shaul, A.; Gelbart, W. M. *J. Phys. Chem.* **1982**, *86*, 316.

[136] Onsager, L. *Ann. N. Y. Acad. Sci.* **1949**, *51*, 627.

[137] Vroege, G. J.; Lekkerkerker, H. N. W. *Rep. Prog. Phys.* **1992**, *55*, 1241.

[138] Bruinsma, R.; Gelbart, W. M.; Ben-Shaul, A. *J. Chem. Phys.* **1992**, *96*, 7710.

[139] Khokhlov, A. R.; Semenov, A. N. *Physica* **1981**, *108A*, 546.

[140] van der Schoot, P.; Cates, M. E. *Europhys. Lett.* **1994**, *25*, 515.

[141] Sijbesma, R. P., *private communication.*

[142] Marrucci, G.; Ciferri, A. *J. Polym. Sci., Polym. Lett. Ed.* **1977**, *15*, 643.

[143] Kramers, H. A. *J. Chem. Phys.* **1946**, *14*, 415.

[144] van der Schoot, P.; Cates, M. E. *J. Chem. Phys.* **1994**, *101*, 5040.

[145] Turner, M. S.; Cates, M. E. *J. Phys.: Condens. Matt.* **1992**, *4*, 3719.

[146] van der Schoot, P. *J. Phys. II France* **1995**, *5*, 243.

[147] Odijk, T. *J. Phys. France* **1987**, *48*, 125.

Summary

In biomacromolecules, the conformational transition of a random coil into a helix and the self-organization of molecules into supramolecular aggregates are two important processes that usually occur in separate systems but can also be found to occur sequentially (or simultaneously) in a single system. Recently, some types of synthetic molecule have also been shown to display both transitions.

The type of molecule we focus on is one that assembles into linear supramolecular aggregates, bound by physical interactions, such as electrostatic or solvophobic interactions, or hydrogen bonds. Furthermore, these aggregates can undergo a helical-type conformational transition in solution under the influence of a change in, e.g., concentration or temperature. To describe the properties of such aggregates we combine a model for the configurational transition (that is an extension of the one-dimensional Ising model) with the theory of linear self-assembly.

The combination of the theories of self-assembly and the helical transition can be pursued rigorously, and we find that there are essentially two regimes, one where the polymerization transition and the helical transition are separate, and one where they coincide. In both regimes, we find that the growth and the conformation of the aggregates are strongly coupled, leading to a growth spurt of the aggregates in the regime where the helical form dominates. It turns out that the conformation and mean size of the aggregates depend strongly on our choice of description of the aggregate ends. We can choose to restrict the aggregate ends (the first and last bond of the aggregate) to be helical or non-helical, or choose not to restrict them at all. In so varying the boundary conditions, we observe that three distinct classes of behavior manifest themselves. Comparison of the theory with experimental measurements shows that only one of these classes can account for the experimental results.

Experiments, in which mixtures of chiral and achiral versions of the self-assembling monomers were used, show a strong change in the optical properties with the fraction of homochiral material, even for small fractions of this material. This phenomenon also occurs in conventional (covalently-bound) polymers, and is known as the sergeants-and-soldiers type of chirality amplification. We combine the theory of self-assembly with a two-component Ising-like model in order to describe the sergeants-and-soldiers principle in

self-assembled polymers. We find two regimes, in accordance with experimental measurements: one in which the chirality amplification increases with the concentration, and one which shows no concentration dependence. Apart from the mass action, the free-energy penalty of a helix reversal can also strongly influence the chirality amplification. We find that mass action dominates when the aggregates are short, and that the free-energy penalty of a helix reversal dominates in long polymers.

We use a similar, if somewhat more elaborate, theory to describe the so-called majority-rules type of chirality amplification in mixed aggregates. This type of chirality amplification occurs when the polymers consist of the two enantiomeric forms of the monomers, one in slight excess over the other. Apart from a dependence on the free energy of a helix reversal, we also find a strongly non-linear dependence on the free-energy penalty of a mismatch between the preferred screw sense of a monomer and the handedness of the bond following it.

Inspired by possible applications of the helical supramolecular polymers, such as in novel gelators, we investigate the behavior of these aggregates at higher volume fractions, taking interaggregate interactions into account. We also study the effect of external fields on the conformational state of the assemblies. We find that both external fields (of the dipole and quadrupole types) and interaggregate interactions (for which we use a second-virial type description) can have an effect on the conformational state and size of the aggregates. We find, in accordance to what is known for (non-helical) self-assembled aggregates, that for some values of the external-field strength and for some angles between the aggregate axis and the field director, unbounded growth of the aggregates is predicted.

Throughout this work, we place special emphasis on comparing our theory with experimental measurements on aggregates of discotic molecules whenever available, and obtain quantitative agreement in all cases.

Outlook

Judging from the comparison to experiment, we have succeeded in giving an accurate description of the helical transition and the sergeants-and-soldiers principle in self-assembled polymers in dilute solution. However, some obvious routes of investigation are still open. Our treatment of the majority-rules principle, for instance, has not yet been compared to measurements of the optical activity due to a lack of experimental data. Also, we have not yet explicitly extended this approach to include all chain lengths.

A theory for the behavior of helical aggregates which interact was outlined by us in Chapter 7. This study was not exhaustive and many other effects, such as liquid-crystal formation, have yet to be described. Also in the theory of the effect of fields on the aggregates, we

have detailed only a few cases. Flow fields in particular remain an interesting object for further study.

Samenvatting

Twee belangrijke processen die optreden in de natuur zijn de conformationele overgang tussen een helische toestand en een kluwen in biopolymeren en de zelfassemblage van supramoleculaire aggregaten uit monomere eenheden door de vorming van fysische bindingen. Deze twee processen komen afzonderlijk van elkaar voor, maar er zijn ook systemen bekend waarin beide voorkomen, soms los van elkaar, maar soms ook tegelijkertijd. Recentelijk zijn er ook synthetische moleculen ontwikkeld die beide overgangen vertonen.

We concentreren ons hier op het type molecuul dat lineaire aggregaten vormt, die worden samengehouden door fysische wisselwerkingen, zoals waterstofbruggen of electrostatische of solvofobe interacties. Bovendien kunnen de aggregaten waarin we geïnteresseerd zijn een conformationele overgang ondergaan van een wanordelijke toestand naar een helische structuur onder invloed van bijvoorbeeld een verandering in temperatuur of concentratie. Om de eigenschappen van deze aggregaten te beschrijven combineren we een model voor de helische overgang (een uitbreiding op het bekende één-dimensionale Ising model) met een beschrijving van de lineaire zelfassemblage.

Het is mogelijk om de theorieën van de zelfassemblage en de helische overgang te combineren tot een exacte beschrijving van de helische zelfassemblage. We hebben gevonden dat er twee regimes bestaan, één waar de polymerisatie en de helische overgang gescheiden zijn en één waar ze samenvallen. In beide regimes bestaat een sterke koppeling tussen de zelfassemblage en de helische overgang, wat tot uitdrukking komt in het feit dat de voorspelde aggregaatgrootte sterk toeneemt in het gebied waar de helische vorm domineert. Bovendien blijkt dat de gemiddelde grootte en de configuratie van de aggregaten sterk afhangen van de beschrijving van de uiteinden van de aggregaten. Dit kunnnen we testen door de eerste en/of laatste binding van in het aggregaat helisch of niet-helisch te kiezen of door ze vrij te laten. We vinden op deze manier drie klassen van gedrag. Slechts één van deze klassen geeft een goede overeenstemming met meetresultaten.

In mengsels van chirale en achirale monomeren wordt, zelfs voor lage concentraties aan chiraal materiaal,een sterke verandering in de optische eigenschappen van de aggregaten gemeten, ten opzichte van geheel achirale aggregaten. Dit fenomeen treedt ook op in conventionele (covalent gebonden) polymeren en is bekend als het sergeants-and-soldiers principe van chiraliteitsversterking. We combineren de zelfassemblage-theorie met een

Ising-achtig model voor twee-componenten systemen om dit sergeants-and-soldiers principe in supramoleculaire polymeren te beschrijven. In overeenstemming met experimenten vinden we twee regimes, één waar de chiraliteitsversterking toeneemt met de concentratie en één waar geen concentratie-afhankelijkheid optreedt. Buiten het effect van de concentratie kan ook de vrije energie van een verandering in de draairichting van de helix langs de keten een grote invloed hebben op de mate van chiraliteitsversterking. We voorspellen dat het concentratie-effect domineert voor korte aggregaten, terwijl voor lange aggregaten de vrije energie van een helix-omdraaiing het belangrijkst is.

We gebruiken een soortgelijke, zij het wat uitgebreidere, theorie om het zogenaamde majority-rules principe van chiraliteitsversterking in gemengde aggregaten te beschrijven. Dit is een soort chiraliteitsversterking die optreedt in polymeren die opgebouwd zijn uit de twee enantiomere vormen van de monomeren, de één in een kleine overmaat ten opzichte van de andere. Afgezien van de afhankelijkheid van de vrije energie van de helixomdraaiing vinden we hier ook een, sterk niet-lineaire, afhankelijkheid van de vrije energie die optreedt als een rechtsdraaiende binding een monomeer volgt dat een linksdraaiende binding prefereert, en vice versa.

Geïnspireerd door mogelijke toepassingen van de helische aggregaten in bijvoorbeeld gelatoren, hebben we het gedrag van deze ketens bij hogere concentraties onderzocht. Hiervoor nemen we wisselwerkingen tussen aggregaten mee in onze beschrijving. Tevens bekijken we het effect van uitwendige velden op de toestand en lengte van de aggregaten. Uit de theorie volgt dat zowel uitwendige quadrupool- en dipoolvelden als interacties tussen aggregaten een groot effect kunnen hebben op de grootte en toestand van de ketens. Voor bepaalde waarden van de veldsterkte en de hoek tussen de director van het veld en de aggregaat-as vinden we, in overeenstemming met wat bekend is voor cylindrische micellen, een in principe ongelimiteerde groei van de polymeren. Het is mogelijk dat deze groei overeenkomt met een geleringsovergang. De oneindige groei is echter waarschijnlijk te remmen door de polymeren in ons model een eindige flexibiliteit te geven.

In dit proefschrift wordt voortdurend veel nadruk gelegd op de vergelijking tussen onze theorie en experimenten die uitgevoerd zijn aan oplossingen van bepaalde schijfvormige moleculen. In alle gevallen vinden we een kwantitatieve overeenkomst tussen theorie en experiment.

Vooruitzicht

De vergelijking tussen theorie en experiment geeft aan dat onze beschrijving voor de zelf-geassembleerde helische structuren en het sergeants-and-soldiers principe in verdunde oplossing een goede is. Enkele voor de hand liggende onderzoeksonderwerpen blijven echter open. Zo is er geen vergelijking met experiment uitgevoerd voor onze beschrijving van het

majority-rules principe, door een gebrek aan experimentele gegevens. Ook hebben we deze theorie nog niet uitgebreid, voorbij de lange-keten limiet.

In Hoofdstuk 7 hebben we een theorie besproken voor de helische aggregatie met inter-aggregaat-interacties. Deze beschrijving was niet uitputtend en er blijven vele effecten onbeschreven, zoals bijvoorbeeld het ontstaan van vloeibaar kristallijne fasen. Ook in de theorie van het effect van velden op helische aggregaten hebben we maar enkele gevallen bestudeerd. In het bijzonder het effect van stromingsvelden blijft een interessant onderwerp dat nog niet in detail is beschreven voor deze systemen.

Dankwoord

Op deze plaats wil ik de mensen bedanken zonder wie dit proefschrift niet tot stand zou zijn gekomen. Een aantal van hen wil ik bij naam noemen.

In eerste instantie wil ik graag noemen mijn promotor Thijs Michels. Buiten zijn hulp op het professionele vlak wist hij ook nog tijd te vinden om me, wanneer nodig, een motiverend steuntje in de rug te geven. Mijn co-promotor Paul van der Schoot kan hier ook niet ontbreken. Met zijn bevlogenheid, kennis van zaken en perfectionisme heeft hij mij en mijn werk naar een hoger niveau geduwd. Daarnaast heeft hij ook op het persoonlijke vlak een indruk op me gemaakt die ongetwijfeld onuitwisbaar zal blijken.

Verder kan ik natuurlijk mijn kamergenoot Nazar Sushko niet vergeten, die met zijn hartelijkheid en vriendschap de sfeer in onze kamer altijd goed hield en bovendien over handige wiskunde- en computerkennis beschikte. Tevens wil ik mijn tijdelijke kamergenoten, Peter Prinsen en Tanya Nimalasuriya, bedanken voor de gezellige gesprekken over wetenschappelijke en niet-wetenschappelijke onderwerpen. Ook de rest van de vakgroep heb ik ervaren als een prettige en open groep mensen, met name collega-AiO's Frank Pasveer en Vladimir Stojanovic, die altijd klaarstonden om deze chemicus een stapje verder te helpen met een natuurkundig of wiskundig probleem.

Voor hun inzet op experimenteel gebied en hun bereidheid om de discussie aan te gaan over hun resultaten ben ik Luc Brunsveld, Rint Sijbesma en Bert Meijer zeer erkentelijk.

Tot slot wil ik de mensen achter de schermen bedanken, diegenen die het belangrijkst voor me zijn in mijn leven buiten de faculteit natuurkunde. Hiermee doel ik natuurlijk op mijn ouders, mijn broer Bas en mijn vrienden. Ik ben jullie oneindig veel dank verschuldigd voor alles wat jullie voor me gedaan hebben en alles wat jullie voor me betekenen.

Curriculum Vitae

Jeroen van Gestel is geboren op 21 december 1975 te Tilburg. Na de VWO-opleiding aan het Theresia Lyceum te Tilburg cum laude voltooid te hebben, is hij in 1994 aan de studie Scheikundige Technologie aan de Technische Universiteit Eindhoven beginnen. Na een stageperiode bij ATO-DLO in Wageningen in de laatste maanden van 1998 werd in augustus 1999 het afstudeerproject binnen de vakgroep Anorganische Chemie en Katalyse (Prof. Dr. R.A. van Santen) voltooid. Per oktober 1999 heeft hij in de groep Polymeerfysica in de faculteit Technische Natuurkunde aan de Technische Universiteit Eindhoven aan zijn promotieonderzoek gewerkt, onder leiding van Prof. Dr. M.A.J. Michels en Dr. Ir. Paul van der Schoot. De belangrijkste resultaten van dit onderzoek, uitgevoerd met experimentele ondersteuning vanuit de groep Macromoleculaire en Organische Chemie van Prof. Dr. E.W. Meijer, eveneens aan de Technische Universiteit Eindhoven, staan beschreven in dit proefschrift.

Jeroen van Gestel was born in Tilburg on the 21st of December, 1975. After obtaining his VWO (pre-university education) degree with honors at the Theresia Lyceum in Tilburg, he studied Chemical Engineering at the Technische Universiteit Eindhoven from September 1994 to August 1999. During this period he worked on a project in ATO-DLO in Wageningen, before starting his undergraduate project in the laboratory of Inorganic Chemistry and Catalysis (under Prof. Dr. R.A. van Santen). In October 1999, he started as a Ph. D. student in the Polymer Physics group of the faculty of Applied Physics of the Technische Universiteit Eindhoven, under the supervision of Prof. Dr. M.A.J. Michels and Dr. Ir. Paul van der Schoot. The most important results of this work, which was performed with experimental support from the laboratory of Macromolecular and Organic Chemistry at the Technische Universiteit Eindhoven (Prof. Dr. E.W. Meijer), are described in this thesis.

List of Publications

Helical Transition of Polymer-like Assemblies in Solution
J. van Gestel, P. van der Schoot, and M.A.J. Michels
J. Phys. Chem. B **105**, 10691 (2001)

Role of End Effects in Helical Aggregation
J. van Gestel, P. van der Schoot, and M.A.J. Michels
Langmuir **19**, 1375 (2003)

Amplification of Chirality in Helical Supramolecular Polymers
J. van Gestel, P. van der Schoot, and M.A.J. Michels
accepted for publication in Macromolecules.

Amplification of Chirality in Helical Supramolecular Polymers beyond the Long-Chain Limit
J. van Gestel, P. van der Schoot, and M.A.J. Michels
submitted for publication to J. Chem. Phys.

Chirality Amplification in Helical Supramolecular Polymers: the Majority-Rules Principle
J. van Gestel
submitted for publication to Macromolecules.

STELLINGEN

behorende bij het proefschrift

Theory of Helical Supramolecular Polymers

van

Jeroen van Gestel

Eindhoven, 30 september 2003

I

Een vrije energie van slechts een paar $k_B T$ kan er voor zorgen dat een groot aantal bindingen in een helisch polymeer eenzelfde conformatie aanneemt. Het is opmerkelijk dat dit effect in zelf-geassembleerde ketens even sterk kan zijn als in conventionele polymeren, ondanks het feit dat de monomeren een grotere onderlinge afstand en een geringere bindingssterkte hebben.

Dit proefschrift.

II

Het één-dimensionale Ising-model is niet het schijnbaar puur academische model waarvoor het vaak wordt aangezien, maar heeft wel degelijk toepassingen in reële, drie-dimensionale systemen.

Dit proefschrift.

D. Poland, H.A. Scheraga, Theory of Helix-Coil Transitions in Biopolymers, Academic Press, New York (1970).

T.L. Hill, Statistical Mechanics, McGraw-Hill Book Company, New York (1956).

III

In de beschrijving van wanordelijke systemen wordt het verschil tussen zogeheten ingevroren wanorde en evenwichtswanorde te weinig benadrukt.

Dit proefschrift, hoofdstuk 4.

M.L.C. Leung, B.Y. Tong, F.Y. Wu, Physics Letters, 54A, 361 (1975).

N. Goldenfeld, Lectures on Phase Transitions and the Renormalization Group, Addison-Wesley, Amsterdam (1992).

IV

Het is op zijn minst twijfelachtig om eindige polypeptiden te behandelen met een theorie die geldig is voor oneindig lange ketens en hierbij bovendien een oneindig grote vrije energie per lengte-eenheid in te vullen. Conclusies over de aard van de helix-kluwen-overgang die uit een dergelijke werkwijze volgen, en tegenspreken wat

er al bekend is op dit gebied, dienen dan ook met een korrel zout te worden genomen.

Y. Peng, U.H.E. Hansmann, N.A. Alves, Journal of Chemical Physics, 118, 2374 (2003) en referenties hierin.

V

Het gebruik van dichterlijke taal in een wetenschappelijke publicatie, zelfs door vooraanstaande wetenschappers, leidt niet altijd tot een verhoogde leesbaarheid.

J.-M. Lehn, Proceedings of the National Academy of Sciences of the USA, 99, 4763 (2002).

VI

Niet alleen in de wetenschap en natuur is coöperativiteit belangrijk, maar ook muziek en 'sequentiële kunst' zijn het mooist als het waargenomen geheel meer is dan de som van de delen.

VII

Door te spreken in pretentieuze termen als 'grafische literatuur' en 'sequentiële kunst' proberen stripliefhebbers zich af te zetten tegen de consensus dat strips geen serieuze literatuur zijn.

VIII

Het toepassen van 'trial-and-error' methoden om diagnoses te stellen in de medische praktijk is verontrustend.

IX

De neiging van fysici om systemen te beschrijven aan de hand van algemene modellen die vaak gestoeld zijn op volstrekt andere systemen, verschilt sterk van de werkwijze

van chemici, die fenomenen vaak op een meer individuele basis behandelen. Hoewel dit kan leiden tot een wat stroeve communicatie, vullen de twee zienswijzen elkaar aan.

X

Dit proefschrift bevat geen drukbouten.